

Food Distribution in Ant Colonies: Trophallaxis and Self-Organization

Dissertation

for the award of the degree
“Doctor rerum naturalium”
of the Georg-August-Universität Göttingen

within the doctoral program
Physics of Biological and Complex Systems
of the
Georg-August University School of Science (GAUSS)

submitted by

Johannes Gräwer

from Lüneburg

Göttingen 2017

Thesis Committee

Prof. Eleni Katifori, PhD

Department of Physics and Astronomy, University of Pennsylvania, Philadelphia

Prof. Dr. Florentin Wörgötter

Department of Computational Neuroscience, Third Institute of Physics - Biophysics /
Bernstein Center for Computational Neuroscience, Georg-August-Universität Göttingen

Dr. Marco G. Mazza

Research Group Nonequilibrium Soft Matter, Department Dynamics of Complex Fluids,
Max Planck Institute for Dynamics and Self-Organization, Göttingen

Members of the Examination Board

First Referee: Prof. Eleni Katifori, PhD

Department of Physics and Astronomy, University of Pennsylvania, Philadelphia

Second Referee: Prof. Dr. Florentin Wörgötter

Department of Computational Neuroscience, Third Institute of Physics - Biophysics /
Bernstein Center for Computational Neuroscience, Georg-August-Universität Göttingen

Further members of the Examination Board

Dr. Marco G. Mazza

Research Group Nonequilibrium Soft Matter, Department Dynamics of Complex Fluids,
Max Planck Institute for Dynamics and Self-Organization, Göttingen

Prof. Dr. Reiner Kree

Institute for Theoretical Physics, Georg-August-Universität Göttingen

apl. Prof. Dr. Ulrich Parlitz

Research Group Biomedical Physics, Max Planck Institute for Dynamics and Self-Organization, Göttingen

Dr. Karen Alim

Research Group Biological Physics and Morphogenesis, Max Planck Institute for Dynamics and Self-Organization, Göttingen

Date of oral examination: June 01, 2017

Contents

I	Introduction	7
1	Preface	9
1.1	Motivation	9
1.2	Thesis aims	12
1.3	Thesis organization	13
2	Biology of Trophallaxis	17
2.1	Ant trophallaxis	18
2.2	Biological significance	19
2.3	Review of selected experimental work	20
3	Physics of Trophallaxis	23
3.1	Ant colonies as complex systems	23
3.2	Trophallaxis as a universal self-organized distribution mechanism	24
3.3	Challenges of analytic trophallaxis models	25
3.4	Review of related theoretical and computational work	26
3.4.1	Macroscopic models	26
3.4.2	Microscopic models	27
3.4.3	Interaction network models	28
3.4.4	Epidemic models	29
4	Agent-Based Trophallaxis Simulation	31
4.1	Simulation model	31
4.1.1	Agent motion	31
4.1.2	Food intake from the source	33
4.1.3	Food exchange between agents	34
4.2	Simulation parameters	35
4.2.1	Dimensional parameters	36
4.2.2	Dimensionless parameters	36
4.3	Simulated scenarios	38
4.3.1	1D without explicit motion	39
4.3.2	2D without explicit motion	40

4.3.3	2D with explicit motion	41
4.4	Observables	41
4.4.1	Global measures	42
4.4.2	Spatial measures	43
4.4.3	Individual measures	45
II Trophallaxis without Explicit Motion		47
5	Mean-field Limit	49
5.1	Mean-field model	49
5.1.1	Governing equation	49
5.1.2	Average food concentration	51
5.2	Binary food concentration approximation	51
5.2.1	Average food concentration	52
5.2.2	Food concentration variance	52
5.3	Comparison of simulations and analytic predictions	52
5.3.1	Results with system wide interaction range	52
5.3.2	Results with intermediate interaction ranges	54
6	Diffusive Limit	57
6.1	Diffusion approximation derivation	57
6.1.1	Comparison of 1D and 2D spatial simulation results	58
6.1.2	Continuum variables	58
6.1.3	Governing equation	61
6.2	Diffusion approximation solutions	64
6.2.1	Food source as a boundary condition	65
6.2.2	Food source as a source term	67
6.3	Comparison of simulations and analytic predictions	71
6.3.1	Average food concentration	71
6.3.2	Mean squared food distance	72
6.3.3	Food concentration variance	73
6.3.4	Global food intake time scale	75
7	Master Equation Description	77
7.1	Basic equation without carrying capacity and source term	77
7.1.1	Governing equation	78
7.1.2	Formal analytic solution	80
7.2	Full equation with carrying capacity and source term	80
7.2.1	Carrying capacity	81
7.2.2	Source term	82

7.2.3	Governing equation	83
7.3	Comparison of simulations and analytic predictions	84
7.3.1	Total food	84
7.3.2	Mean squared food distance	84
III	Trophallaxis with Explicit Motion	87
8	Discrete Space Simulation Results	89
8.1	Comparison of simulations and experimental work	89
8.2	Distribution of food among individual ants	90
9	Continuous Space Simulation Results	93
9.1	Ant velocity and interaction range interplay	93
9.1.1	Transition between diffusive and mean-field dynamics	94
9.1.2	Ant velocity scaling relation	96
9.1.3	Interaction range scaling relation	98
9.1.4	Slow motion limit case	100
9.2	Ant velocity and food exchange ratio interplay	101
9.2.1	Transition between diffusive and mean-field dynamics	102
9.2.2	Food exchange ratio scaling relation	106
9.2.3	Inverted food exchange ratio dependency regime	106
9.3	Heterogeneous case study	109
9.3.1	Simulation model extensions	109
9.3.2	Comparison of heterogeneous and standard simulations	111
IV	Epilogue	113
10	Summary and Discussion	115
10.1	Simulation model	115
10.2	Mean-field model	116
10.3	Diffusion model	117
10.4	Master equation model	118
11	Outlook	119
11.1	Experiments	119
11.2	Simulation	120
11.3	Theory	121
12	Concluding Remarks	123

Contents

Appendix	125
A Active Brownian Motion	127
B Mean Squared Interaction Distance	131
C Solving the Diffusion Approximation	135
C.1 Food source as a boundary condition	135
C.2 Food source as a source term	136
D Figures	139

Part I

Introduction

1 Preface

1.1 Motivation

Ants are fascinating. Their ecological success is overwhelming [1, 2]. For each human on this planet there are around one million ants. If one lined up all the ants, they would cover the distance light travels in one day.

Except for the polar regions, ants can be found all over the world. They exhibit a tremendous biological diversity in thousands of species with completely different ways of living (Fig. 1.1). In just one square meter of the Amazon rainforest one can find more ant species than all the primate species of the world.

Probably the most fascinating thing about ants is their ability to form colonies that act as one social entity, sometimes called superorganisms [3]. Depending on species and habitat, a single ant colony can consist of as little as ten or as many as hundreds of millions of ants, occupying an area of a few square centimeters or several square kilometers [2]. But what has led to this impressive level of social organization?

Roughly one hundred million years ago, some solitary insect species evolved social interactions that enabled the formation of colonies. A main reason for this advance was their ability to feed each other with previously ingested food (Fig. 1.2). Among other things, this allowed them to develop the well-known division of labor: groups or castes of individuals specializing in certain tasks. This social organization



Figure 1.1: Examples of ant nests. Left: Tree nest of weaver ants *Oecophylla* (by Robin Klein, CC BY-SA 2.0). Right: Needle mound of red wood ants *Formica rufa* (by Thue, public domain).



Figure 1.2: Liquid food exchange (trophallaxis) among Argentine ants *Linepithema humile* (by Dave Kirkeby, CC BY-SA 4.0).

reached its climax in the evolution of non-reproductive castes, sacrificing their own reproduction to the benefit of the colony [2, 4]. The mutual feeding technique that supported this social evolution is called ‘trophallaxis’.

This thesis is based on the question how ant colonies use trophallaxis to supply their members with food. As it gave them significant evolutionary advantages, trophallaxis became and still is the dominant food distribution mechanism in ant colonies [5]. Given its biological importance, surprisingly little is known about how this food distribution mechanism actually works.

One thing is certain though. An ant colony cannot be understood by looking at a single ant. Not even the observation of a very special individual, such as the queen, can explain the colony’s behavior. It is the ants’ interactions that run the colony in a self-organized way [6, 7]. This also holds for the food distribution mechanism. There is no central control which manages the distribution of food via trophallaxis.

This thesis investigates the physical aspects of trophallaxis self-organization. This is imperative, as no satisfying fundamental description of the physics behind trophallaxis exists. All the existing work lacks essential aspects of the problem. Fundamental theoretical groundwork is needed, and this thesis makes the first steps towards a complete description.

Along the way of trying to learn about ants, one can expect to also learn from ants. Their ability to collectively solve problems that are insurmountable to a single ant makes them an ideal source of inspiration for the design of artificial

self-organizing systems, sometimes called ‘ant algorithms’ (Fig. 1.3) [8]. In this sense, the mechanisms underlying the self-organization of food distribution in ant colonies that mark the main subject of this thesis are an object of interest itself. The knowledge obtained by their analysis will most certainly influence future bio-inspired engineering work.



Figure 1.3: Social cooperation of weaver ants *Oecophylla*. Top: Load transportation of *O. longinoda* (by Axel Rouvin, CC BY-SA 3.0). Bottom: Nest construction of *O. smaragdina* (by Sean Hoyland, public domain).

1.2 Thesis aims

To the best of our knowledge, there exists no biophysically motivated simulation model or analytic description of trophallaxis that includes all its essential features. The main goal of this thesis is to fill this gap. In our view, the essential properties of the physical mechanisms behind the food distribution in ant colonies are:

- the finite nature of the colony size (both in terms of ant numbers and geometry);
- the inherent time dependency of the food spreading that cannot be reduced to the consideration of steady states;
- the continuous and finite nature of the individual food transfers (ants can exchange variable amounts of food until they are full) that cannot be simplified to a binary approach (fed or unfed ants);
- the locally conservative nature of the food spreading (no food is lost or generated when it is transferred from one ant to another)¹, which constitutes an important difference to other spreading processes (like disease or information transfer);
- the relevance of mesoscopic interaction ranges (ants do not stand still and simply feed from or to their immediate neighbors, but they can also not interact with every other colony member at any time).

We will explain the important points listed above in more detail in the remaining chapters of the introduction (see Sections 2.1, 3.3 and 4.1).

Given these characteristics of trophallaxis, our aim is to understand the collective properties of food dispersion with the simplest possible computational and analytic models. Therefore we intentionally aim to design models that do not include a food distribution strategy of the ants, information transfer between ants, or any specific biological details like behavioral models, complex motion patterns, or division of labor (e.g. foragers that venture outside the nest versus workers that stay inside). This choice allows the use of our models as benchmarks to compare to the behavior of real ant colonies or less reduced models, and to assess to what extent the observed performance is due to complex strategies or information transfer among ants, and how much they stem from the collective properties of a stochastic system.

After finding an appropriate theoretical description of trophallaxis, we want to qualitatively study this model system, and ask: How does the most basic individual behavior (i.e. how much food is exchanged and what distances ants travel between

¹This is to be understood with respect to the time scale relevant to the food spreading. Eventually, the food will of course serve its purpose to be digested. As we will explain further in Section 2.1, this consumption of food by the ants however is negligible for its spreading, because it takes much more time [9, 10].

food exchanges) influence the global dynamics (i.e. how fast and how well is food distributed in the colony)? Can we predict the model macroscopic colony behavior based on simple microscopic properties?

The discovered relationships between individual behavior and global food distribution dynamics can then hopefully provide microscopic explanations of experimental observations and phenomenological theories that are still missing (see Section 3.4).

At last, a secondary objective of this thesis is to provide a so far hardly explored connection between the physics of food transport in ant colonies and established physical theories of transport.

1.3 Thesis organization

This thesis is subdivided into four parts:

- I Introduction,
- II Trophallaxis without Explicit Motion,
- III Trophallaxis with Explicit Motion, and
- IV Epilogue.

The rest of Part I contains a chapter on the biology of trophallaxis that further explains what trophallaxis is and how it works. It also gives an overview of the empirical knowledge about trophallaxis obtained from experiments (Chapter 2). This is followed by a chapter on the physics of trophallaxis that explains the basic ideas of why we chose to study ants with physics. It also discusses recent advances in the theoretical and computational work on trophallaxis (Chapter 3). Finally, we present a novel agent-based simulation model of trophallaxis in Chapter 4 that will prove to achieve this thesis' main goal: to provide a description of trophallaxis that includes all its essential features.

Part II then derives three separate analytical models, each predicting trophallaxis dynamics in different behavioral regimes, and compares them to the results of our simulation. In order to keep the analytical modeling manageable, we do not explicitly include the ants' motion in all of the work presented in Part II (cf. Section 4.3). Instead, we define an interaction region around every ant that implicitly models its motion in the following way. Real ant colonies exhibit so called spatial fidelity zones [11, 12]. Those are small overlapping areas, distributed over the nest, one for each ant, in which the ants preferably move. They only interact with another ant, if their spatial fidelity zones overlap. Our interaction regions can therefore be used to describe real ant colonies with moving ants, if their spatial fidelity zones match our interaction region.

The three analytical approaches we present in Part II model:

- a well-mixed colony, where every ant has the chance to interact with every other ant at all times, described with a mean-field theory (Chapter 5);
- a colony with small spatial fidelity zones, where ants only exchange food within their local neighborhood, described with a diffusion equation (Chapter 6); and
- the intermediate case of a colony with large overlapping spatial fidelity zones, described with a master equation like probabilistic model (Chapter 7).

In Part III, we proceed with the qualitative study of our trophallaxis simulation results, including the explicitly simulated motion of every ant. First we present some proof of concept results in Chapter 8, obtained from a simplified simulation model where the ants perform a simple random walk on a two-dimensional grid. Chapter 9 then contains the majority of our simulation findings, using an active random motion in continuous space.

Part IV finally summarizes and discusses the main results of the thesis (Chapter 10), gives an outlook (Chapter 11) and some last concluding remarks (Chapter 12).

Collaborative contributions

The analytic work of the mean-field model (Chapter 5) and parts of the analytic work of solving the diffusion model (Sections 6.2.1 and 6.2.2) was done in collaboration with Eleni Katifori. The derivation of the diffusion model (Section 6.1.3) and the analytic work of the master equation model (Chapter 7) was done in collaboration with Henrik Ronellenfitsch.

Related publications

The agent-based simulation model (Chapter 4), the mean-field model (Chapter 5), and the diffusion model (Chapter 6) are content of the following publication:

J. Gräwer, H. Ronellenfitsch, M. G. Mazza, and E. Katifori, *Trophallaxis inspired model for distributed transport between randomly interacting agents*, Physical Review E, under review (2017).

(preprint available at: <https://arxiv.org/abs/1607.06055>)

A second publication of the authors J. Gräwer, M. G. Mazza, and E. Katifori, containing the simulation results with explicit motion (Chapter 9) is in preparation.

Acknowledgments

First of all, I am thankful for the time all the members of my examination board (Eleni Katifori, Florentin Wörgötter, Marco Mazza, Reiner Kree, Ulrich Parlitz, and Karen Alim) spent on evaluating my work. Special thanks go to the members of my thesis committee (Eleni Katifori, Florentin Wörgötter, and Marco Mazza) for guiding my work.

I am deeply grateful for the way Eleni Katifori and Marco Mazza co-supervised me: inspiring, constructive, and always sympathetic. Eleni Katifori gave me all the freedom I wanted and only the push I needed. Marco Mazza welcomed me with open arms, when my previous research group dissolved. Both of which is anything but granted.

Another person of great importance to this thesis is Henrik Ronellenfitsch. His sage counsel has helped me countless times. Among all the other people whose perspective has helped me in scientific discussion, I would like to mention Jana Lasser, Jonathan Dawson, Soumyajyoti Biswas, and Jérémy Vachier.

Finally, I would like to express my gratitude to all the people who sacrificed their time to read and comment this thesis: Henrik Ronellenfitsch, Jana Lasser, Jérémy Vachier, Soumyajyoti Biswas, Fabian Schwarzendahl, Eleni Katifori, and Marco Mazza.

License

The content of this thesis is licensed under the terms of the Creative Commons Attribution-ShareAlike license (CC BY-SA 4.0). The full license text can be found at <https://creativecommons.org/licenses/by-sa/4.0/>.

In addition, this thesis contains attributed reproductions of works under the CC BY-SA 2.0/3.0/4.0 and CC BY-NC 3.0 licenses. The full license texts for the original images can be found at

<https://creativecommons.org/licenses/by-sa/2.0/>,

<https://creativecommons.org/licenses/by-sa/3.0/>,

<https://creativecommons.org/licenses/by-sa/4.0/>,

and <https://creativecommons.org/licenses/by-nc/3.0/>.

Image source links are provided in the List of Figures.

2 Biology of Trophallaxis

About one hundred years ago, in 1918, the leading expert on social insects of his time, North American entomologist William Morton Wheeler, proposed the term ‘trophallaxis’ to describe the mutual exchange of liquid food between social insects (Figs. 1.2 and 2.1) [13, 14]. He derived it from the Greek words *τροφή* (nourishment) and *ἀλλάττειν* (to exchange). It replaced the formerly used ‘oecotrophobiosis’ successfully up to the present.

Wheeler described two variants of trophallaxis: mouth-to-mouth (stomodeal) and anus-to-mouth (proctodeal) food transfer [15]. Social hymenopterans (i.e. ants, bees, and wasps) mainly show stomodeal trophallaxis [5], which is why we focus on this variant in this chapter.

Since this work studies the food distribution in ant colonies, we first briefly explain how trophallaxis works in ants in Section 2.1. Section 2.2 then gives a broader view of why and how trophallaxis is relevant in general. Finally, Section 2.3 sketches the development of experimental work on trophallaxis from its origins to the current state.



Figure 2.1: Liquid food exchange (trophallaxis) among carpenter ants *Camponotus* (by Rakesh Kumar Dogra, CC BY-SA 3.0).

2.1 Ant trophallaxis

The intestinal tract of ants consists of three compartments, connected in series: the crop (also social or storage stomach), the midgut, and the rectum (see Fig. 2.2). Ingested food enters the intestinal tract through the crop, where it can be temporarily stored. Ants can store food with a weight comparable to their own body weight inside their crop. [16].

At some point, the stored food from the crop is either further digested onto the midgut and the rectum, or regurgitated to the mouth. The regurgitated food can then be passed on to other ants. This exchange of food from one ant to another is the phenomenon Wheeler called trophallaxis (Figs. 1.2 and 2.1). It is important to note that the digestion of food typically takes much longer than the process of regurgitating and feeding to nest mates [9, 10].

Trophallaxis among ants is initiated and accompanied by complex tactile interactions between the participants' antennas, forelegs and mouthparts [5, 2]. Bert Hölldobler and Edward Osborne Wilson, leading ant experts of our time, have compared the food release of the donating ant with a gag reflex [2], triggered by a tactile stimulus of its labium. The labium is a central mouthpart of insects that



Figure 2.2: Schematic drawing of the food exchange between two ants (trophallaxis). Food is transferred from the right ant to the left (as indicated by the arrows). The intestinal tract compartments are shown: crop (K), midgut (M), and rectum (R). (by Turid Hölldobler-Forsyth [5]. Supplied by courtesy of the German National Library of Science and Technology, Hannover.)

ants use for the actual transfer of liquid food from one ant's mouth to another's [5].

The ants' reflexive donation of food can be triggered by many other arthropods, imitating the tactile signals and thus causing ants to give away food [5]. Hölldobler even successfully triggered the food donation manually using a hair [2].

2.2 Biological significance

Social ants heavily make use of their ability to store, distribute and share liquid food. Foraging ants can collect food from sources outside their colony's nest and deliver it to non-foraging colony members inside the nest (Fig. 2.3). These then distribute the food further inside the nest, until every member of the colony, including the larvae and the queen, is fed [2, 13, 5]. This way, only a fraction of the colony has to spend time on foraging, and the rest can focus on other tasks like brood care or nest building. Entomologists consider the advantages of this food distribution through trophallaxis to be one of the most central features of insect eusociality, if not its origin [2, 17, 18, 7, 14].¹ It is fundamental to division of labor and thus forms the basis of social organization [19] and ultimately the worldwide ecological success of ants [1, 2].



Figure 2.3: Meat ants *Iridomyrmex purpureus* feeding on honey (by Fir0002/Flagstaffotos, CC BY-NC 3.0).

¹Eusociality is the highest level of social organization in animals that includes cooperative brood care, the division of labor into reproductive and non-reproductive castes, and overlapping generations within one colony. An extensive introduction can be found in [1].

Apart from some exceptional cases (e.g. in the subfamilies *Myrmeciinae* and *Ponerinae*), trophallaxis is the main distribution mechanism of liquid food within the colony for all ant species, despite their huge diversity [5].

Trophallaxis is not only of great significance for ants, but also for other eusocial insects like bees [18], or even other animals, such as bats [20], spiders [21] and birds [22].

2.3 Review of selected experimental work

The origins of experimental research on trophallaxis date back to the 19th century. In 1879, the important Swiss myrmecologist Auguste-Henri Forel for the first time experimentally proved that worker ants exchange food, using dyed liquid food [23]. Through dissecting or simply crushing the ants after the food exchange, dye traces could be found to indicate the food transfer. A similar method was developed later, through mixing starch into the food and detecting it with iodine [24]. Alternatively, poison was fed to single ants, allowing for an investigation of the spread of food among members of the colony, by observing how many of them died [24].

The next big methodical improvement was the use of radioactive isotopes to trace the food. This was successfully applied for the first time with bees in 1952 [25], and with ants in 1954 [26]. It allowed a more accurate measure of the amounts of food exchanged and in vivo observation. For example, Pendleton and Grundmann could trace a radioactive liquid they injected in a plant, passing through aphids feeding on the plant into ants feeding on the aphids' secretions (honeydew) [26]. Using radioactive tracers allowed biologists to answer many questions raised by earlier researchers like Wheeler and Forel since the 1950s.

One of the major successes in the experimental work on trophallaxis was the identification of a 'chain of demand' mechanism that drives the foraging of food and its distribution in the colony via trophallaxis. In a nutshell, the larvae and the queen demand food from the nest-workers, which then demand food from the foragers, whose activities are thus controlled by the colony's collective needs [27, 28].

The food distribution mechanism has also been found to be sensitive and directed with respect to the food's nutrient content. Food containing large amounts of carbohydrates for example is more likely delivered to workers, whereas amino acids are preferably delivered to larvae and queens. Oils are equally distributed [24, 29]. Overall, the speed and extent of food distribution varies with environmental factors (e.g. temperature and humidity), colony size, individual ant physiology, and social structure of the colony [5].

Experimental trophallaxis research has not only focused on the colony level, but also on the individual level. It has been found that the majority (about 90

percent) of trophallactic food exchanges are initiated by the receiving ant [30, 5]. Nevertheless, foragers returning to the nest with a full crop are actively looking for food exchange partners [5]. Also, the willingness (or probability) of an ant to give away food increases with the amount of food stored inside its crop. Likewise, the intensity of contacting other ants to beg for food has been observed to decrease with the amount of food an ant carries [5]. The motivation to initiate trophallaxis does however not only depend on the crop content, but also on the social status and physiology of the individual ant [24, 5].

Furthermore, the duration of a trophallactic food exchange has been found to correlate with the amount of food transferred. The more food is exchanged, the longer the exchange takes [31], but with a non-linear dependency [10].

There is no doubt anymore that trophallaxis is not only about the mere exchange of food. For example, it has been found that glandular secretions of the donating ant are mixed with the exchanged food and passed on to the receiving ant [24], leaving room for speculations about a chemical information transfer during trophallaxis. In general, experiments showed that trophallaxis can mediate a uniform colony odor, enabling members of a colony to identify each other [32]; and it confers social immunity against pathogens [33].

In the 1980s, the ants' antennal communication during trophallaxis was found to transmit only very limited information [34]. Recent experimental evidence published in 2016 suggests that the exchange of food itself can indeed serve as a communication channel for ant colonies [35], which has already been shown for bees in the 1990s [36].

Further improvement in the experimental accuracy of measuring the food distribution in ant colonies has lately been achieved by Buffin *et al.* in 2009 [19] and Greenwald *et al.* in 2015 [10]. Buffin *et al.* used scintigraphy, a medical imaging method, to monitor the spatio-temporal distribution of food inside an artificial nest for the first time, allowing for a resolution of 10×10 cm in space and 30 seconds in time. Since this resolution was still not good enough to monitor food exchanges at the individual level, Greenwald *et al.* developed a new approach, using fluorescently labeled food. In addition with a barcode-based identification system, this allowed them to measure the full spatio-temporal dynamics of food distribution at the individual level.

Although the experimental methods to study trophallaxis have improved tremendously over the last century, the research on the biology of trophallaxis is far from being completed. Some questions that remain open for example are: Do individuals actively choose their food exchange partners? If so, on what grounds? Similarly, what determines the amount of food exchanged? Is it purely based on the local information of an individual; based on more global information, including

2 *Biology of Trophallaxis*

the needs of other individuals; or simply not actively decided at all? Do the food trophallaxis partners exchange information about their crop contents at some point before, during or after the food exchange? Answering these and alike questions will shed further light on the intriguing mechanisms behind the self-organized food distribution of social insects.

3 Physics of Trophallaxis

This thesis explores the physical mechanisms and concepts of trophallaxis, not its biology. In this chapter, we explain what that means, and make a case for why this approach is useful. Furthermore, we integrate our work into the scientific context of previous work.

Section 3.1 starts off with showing that many aspects of ant colonies are successfully understood through the concepts of complex systems, and presents selected previous scientific achievements in this field.

Section 3.2 then shows that the physical mechanisms underlying trophallaxis are of a universal character which raises interesting questions about self-organized distribution and nonequilibrium transport theory. This universal character also makes the results of our work applicable to areas other than the food distribution in ant colonies. Some examples are given in Section 3.2 as well.

Section 3.3 follows with a short description of the fundamental challenges this and other works inevitably face when building analytic models of trophallaxis. These challenges also constitute the physical essence of trophallaxis.

A review of related work using similar approaches to study trophallaxis or closely related systems finally shows that there is still a great need for theoretical groundwork on the matter, both analytically and computationally (Section 3.4).

3.1 Ant colonies as complex systems

In the context of physics, complex systems are often thought of as systems whose complexity emerges from the direct or indirect interactions of its parts [37, 38]. Although these parts themselves (and possibly even their interactions) might be simple and predictable, their collective behavior is not. This concept is purposely very general and applies equally to animate as well as inanimate systems.

Among biological systems, ant colonies constitute an example of complex systems, if not the prime example. The behavior of a single ant appears to be relatively simple and rather limited [2]. With a brain as small as one tenth of a cubic millimeter, a single ant can only make elementary decisions based on local stimuli that confer very small amounts of information [39]. However, despite the apparent simplicity of their individual members and the absence of central control, insect

societies as a whole exhibit a surprising degree of complexity and can perform complicated tasks such as foraging, brood care, nest building, and - of course - food distribution that would be infeasible for a single individual [2, 6, 40].

The notion of complex systems is closely connected to the concept of self-organization [37]: the emergence of order or organization in a (complex) system without external or central control. A substantial amount of work has been performed, using complex systems methodologies, to study the self-organization of ecological systems [41], social behavior [42], social insects in general [43], and ant colonies in particular [44].

Presumably the most prominent example of self-organization in social insect colonies is not their food distribution system, but their division of labor [45]. The adaptive and decentralized allocation of tasks to individuals leading to a failure robust division of labor has successfully been studied theoretically with agent-based simulations and analytic response threshold models [46], and experimentally confirmed as well [47, 48].

Another example of social self-organization in insect societies is their ability to make collective decisions like food source or nest site selection. The underlying symmetry breaking has also successfully been studied computationally [49] and experimentally [50, 51, 52] with a complex system framework.

Social insect colonies have been a fruitful source of inspiration for the design of artificial multi-agent systems, optimization algorithms, and robots in their capacity as self-organized problem solvers [53, 54, 55, 8]. They are evolutionary optimized, balancing constraints and prove to be robust against individual failure [40]. For example, the mechanisms of trophallaxis have inspired a novel algorithm for swarm searching [56], and a division of labor model from eusocial wasps has been applied to agent-based simulations of a well performing adaptive task allocation algorithm [57, 58].

3.2 Trophallaxis as a universal self-organized distribution mechanism

From a physical point of view, the self-organization exhibited by ants in the distribution of food in the colony is independent from the specific biological features of ants and that the quantity being distributed is liquid food. The same underlying mechanism could be used to distribute any kind of exchangeable quantity (be it matter, energy or information) among any kind of interacting units (e.g. humans, animals, or artificial devices like computers or robots).

This universality has not been exploited extensively up to the present. The field of

self-organized robot engineering is one example of using the generic mechanisms of trophallaxis. Artificial swarms of robots (e.g. for search and rescue missions) have been designed to self-organize using a trophallaxis strategy for the exchange of information [59, 60] or electric energy [61, 62]. Also, multiple unmanned aerial vehicles have successfully performed formation flights through trophallaxis mechanisms [63].

Interesting theoretical questions can arise from comparing the physics of trophallaxis with well-known transport phenomena studied in theoretical physics: Is trophallaxis a regular diffusion process? What role does the active motion of the quantity exchanging units play? How does trophallaxis relate to nonequilibrium transport systems [64]? One aim of this thesis is to lay the groundwork for answering these questions, because a sufficient analytical investigation of trophallaxis has not yet been performed.

3.3 Challenges of analytic trophallaxis models

There are some properties inherent to trophallaxis that render its analytic description challenging. First of all, any real system using trophallaxis as a resource distribution system is finite in space and in the number of motile units, agents or individuals. A description of finite trophallaxis systems of a biologically realistic size is likely to show finite size effects. In other words, finite size effects have to be realistically incorporated in any attempt of theoretical modeling.

Second, not only the space and the number of individual participants is finite, but also the participants capacity to carry the exchanged quantity (food or other) is limited. Ants can only store a finite amount of food in their crop, robots can only carry a finite amount of batteries, interacting agents can only hold finite information, and so forth. As can be seen in the analytical approach we present in Chapter 7, this can introduce nonlinearities in the systems dynamics.

Third, trophallaxis systems are open, in a thermodynamic or systems theory sense. In ant colonies, for example, food that is distributed in the colony first has to enter the nest. Modeling fluxes of food into trophallactic systems is crucial, but not necessarily straightforward, as they are typically time dependent and coupled to the internal system state. Starving colonies could for example increase their foraging efforts, and hence the flow of food into the nest. As a consequence, trophallaxis systems are also inherently out of equilibrium, so that their analytic descriptions cannot resort to steady-state analysis.

Finally, modeling the interaction between trophallactic exchange partners may require intermediate range descriptions. Depending on the context, trophallaxis could be performed over short distances (like the ants' food exchange), large distances (supposable for information exchange), or anything in between. Even

in the biological context of real ant colonies, interaction ranges larger than the ants' immediate vicinity might be relevant, when ants are actively looking for food exchange partners or communicate chemically. Different analytical approaches can therefore be necessary to cover all relevant interaction ranges.

3.4 Review of related theoretical and computational work

The theoretical and computational work on trophallaxis (and closely related cases) is surprisingly limited. As we show below, there exists no biophysically motivated analytic description or simulation model of trophallaxis that includes all its essential features. Particularly, none of the existing models includes a description of the continuous amounts of food carried by each individual, and exchanged between them.

We present the existing work in the following categories: macroscopic models, describing the global food dynamics at the colony level (Section 3.4.1); microscopic models that include the description of individual behavior (Section 3.4.2); interaction network models, that use network theory to study the network of trophallactic interactions (Section 3.4.3); and epidemic models, originally designed to describe disease or excitation spreading (Section 3.4.4).

3.4.1 Macroscopic models

In a first, simple approach macroscopic models have been proposed to analytically describe the dynamics of food transport into the whole colony. The advantage of this approach is that these models can easily be compared to experiments, because precise measurements of individual food exchanges are not necessary. This allowed a comparison between analytic models and experiments with now outdated experimental methods like scintigraphy [19] (cf. Section 2.3).

All macroscopic analytic models that have been proposed so far predict an exponential saturation dynamics of the form $f(t) \sim 1 - e^{-\gamma t}$, either for the total amount of food taken up by the colony [10, 19], or for the number of ants that have been fed [65, 66]. Buffin *et al.* [19] and Sendova-Franks *et al.* [66] relate the global saturation rate γ to a combination of the number of foragers bringing food into the nest, the amount of food a single ant can carry, and the average rate at which two ants encounter each other, but give no detailed microscopic description of the food dissemination process. Our models will provide further insight into this (cf. Chapters 5, 6 and 9). In particular, we will go beyond the mean-field assumption that all previous macroscopic models used: that ants meet with the same probability everywhere and anytime.

Buffin *et al.* [19, 67] also described the spatial distribution of food observed in their scintigraphy experiments analytically with a phenomenological differential equation for the growth dynamics of the radioactive area; again no link to the individual behavior was established.

3.4.2 Microscopic models

In order to fully understand the self-organized food distribution in ant colonies, microscopic models are indispensable. Since organization on the collective level is expected to emerge from the interaction of individuals, a good description at the individual level is the key element.

Surprisingly, no microscopic analytical description of trophallaxis in ants has been published so far. The work that came closest is a diffusion model by Blonder and Dornhaus, constructed to capture the information flow in an ant colony, not the food flow [68]. They use antenna-body interactions between ants as a proxy for communication and study the distribution of information in the colony, mediated through these physical interactions. This information spreading resembles food distribution through trophallaxis to a large degree (cf. Section 3.2). Their microscopic model can therefore also serve as an important starting point for trophallaxis modeling.

Using a 2D ideal gas model for the ants motion and a SI epidemic model (see [69] for a review) for their interaction dynamics, they derive a logistic growth prediction as an upper bound for the number of informed individuals inside the nest. Their experiments show that in real ant colonies information flows significantly slower than predicted at large time scales and faster than predicted at short time scales. The analytic model by Blonder and Dornhaus connects the macroscopic flow of information to the number of individuals, the size of the nest, the average interaction radius of individuals, and their average speed. We use a similar approach in both our analytical and our computational work in this thesis, and extend this description to also cover the exchange of continuous amounts of food instead of the binary status informed or not informed.

Motivated by the already mentioned engineering of self-organized robots, Ngo and Schiøler derived a probabilistic model for the expected individual battery resources of energy exchanging robot swarms [61]. They use integro-differential equations, an approach we also make use of in Chapter 7. In addition, they present a computational model, simulating the technical aspects of energy exchanging robots. It shares similarities with the more biophysically motivated simulation model we present in Chapter 4.

Other examples of simulation models designed to describe robot swarms self-organizing through trophallaxis mechanisms are the work of Kubo and Melhuish [62]

or Shamsuddin *et al.* [70].

The last related microscopic model that should be mentioned here, is the worker-larva feeding interaction simulation from Cassil *et al.* [27]. This simulation led to the discovery of the ‘chain of demand’ mechanism which drives the food distribution in ant colonies (see Section 2.3). The model of Cassil *et al.* pursues a different goal than our work. It rather aims at a detailed biological description than at modeling the physical distribution mechanisms, including as much as twelve different parameters describing various attributes of worker ants and larvae. This approach makes it more difficult to assess the self-organizing character of food distribution in ant colonies, but in turn has the advantage of a transparent biological interpretation.

3.4.3 Interaction network models

When a foraging ant brings back food to its nest, it often feeds multiple nest mates with one crop load [5]. Each of the ants that received food can then again give food to multiple other ants, creating a network of trophallactic interactions. These networks, made of individuals as nodes and food exchanges between pairs of individuals as edges, have been the subject of extensive investigation in the last decade, not only for ants [10], but also for other social insects [40, 71].

In general, tools from network theory have successfully advanced the field of behavioral ecology and furthered our understanding of the dynamics, selection pressures, development, and evolution of complex social systems [72, 73]. For ants in particular, the work of Sendova-Franks *et al.* used the trophallactic interaction network to show how an increased spatial mixing can cause an increased speed of food distribution after starvation [66].

Not only the exchange of food, but also the exchange of information or other substances (e.g. pathogens) can form an interaction network (cf. Section 3.2). The work of Blonder and Dornhaus also studied the structure of the network created by physical interactions [68]. Combining this network approach with their analytic diffusion model allowed them to link the interaction network structure to microscopic parameters, like the speed or interaction range of individual ants. The structural properties of these physical interaction networks have been shown to regulate the colony behavior in a self-organized fashion [6, 74, 75].

A characteristic quality of social insect interaction networks is the nature of their time dependency. They are dynamic, because their edges only exist for short time intervals. In fact, at any given instant of time, only a small number of isolated edges will exist in the network, because not all individuals interact at the same time. Additionally, the chronological order of these time framed edges matters, since an individual can for example only pass something on to another after it has received it and not vice versa. Excellent reviews of these so-called ‘temporal’ or

‘time-ordered’ networks can be found in [76, 77].

While this network approach has yielded remarkable success, providing invaluable insight into the food distribution process and the strategies ants employ to achieve it, the quantitative study of very basic trophallactic properties is still in its infancy. The time scales of food distribution and saturation and their relation to individual behavior are unknown. Especially the connection between the motion patterns of individuals and the resulting interaction network structure needs further investigation [78]. Again, this thesis, along with works like the study of Blonder and Dornhaus [68], attempts to provide the first steps towards these goals.

3.4.4 Epidemic models

Theoretic descriptions of trophallaxis like the models we present also bear some connection to epidemic models of the type found in [79, 80, 81]. In fact, an epidemic might actually spread in the colony through the trophallaxis of poisonous food.

However, whereas disease spreading models are usually locally non-conservative in the quantity spread (the disease can pass from one agent to the next without the original donor agent getting cured of the disease), trophallaxis is a conservative process. The agents only distribute the food they carry and cannot locally generate more food. Also, they exchange continuous quantities instead of the binary status of being infected or not infected (similar to the information spreading models, cf. Section 3.4.2 and [68]). Finally, the boundary conditions of a trophallactic system are typically different than the ones encountered in disease spreading models.

4 Agent-Based Trophallaxis Simulation

This chapter presents the core of this thesis: the agent-based simulation model of self-organized food transport in ant colonies. It begins with a description of the model itself (Section 4.1), followed by a discussion of the model’s parameters (Section 4.2). An explanation of the different simulated scenarios, their initial conditions and parameter values follows (Section 4.3), before a section defining all observables used in this thesis closes the chapter (Section 4.4).

4.1 Simulation model

We consider a simple stochastic model of food exchanging, self-propelled agents, confined to a finite nest chamber. A graphical representation of how we model the trophallaxis process is shown in Fig. 4.1. The nest chamber is modeled as a square area of size $L \times L$ with a food source located at the center of one boundary, modeling the nest entrance (see Fig. 4.1 (a)). The N agents (that is, the ant colony)¹ iteratively try to perform three basic actions: moving, collecting food from the source, and exchanging food with each other. We proceed to describe the details of these actions in the rest of this section.

4.1.1 Agent motion

We model the agents’ random movement as active Brownian motion of point-like particles (ABPs, see [82] for a review) moving with a constant speed v and a random unit orientation vector \hat{e}_i , so that the discretized equations of motion for agent i are:

$$\vec{x}_i(t + \Delta t) = \vec{x}_i(t) + \Delta t v \hat{e}_i(t) \quad (4.1)$$

$$\hat{e}_i(t + \Delta t) = \hat{e}_i(t) + \sqrt{2D_r \Delta t} \hat{\xi}_{\perp_i}(t) + \Delta t \alpha(t) \hat{e}_i(t) , \quad (4.2)$$

where $\vec{x}_i(t) \in [0, L]^2 \subset \mathbb{R}^2$ is the agent’s position at time t ; Δt is the discretization time step; D_r is the rotational diffusivity, controlling the average rate of change in

¹We do not always use the word ‘agent’, to describe the abstract representation of an ant in our simulation model, but also simply refer to the simulation agents as ‘ants’ or ‘simulated ants’ in other contexts.

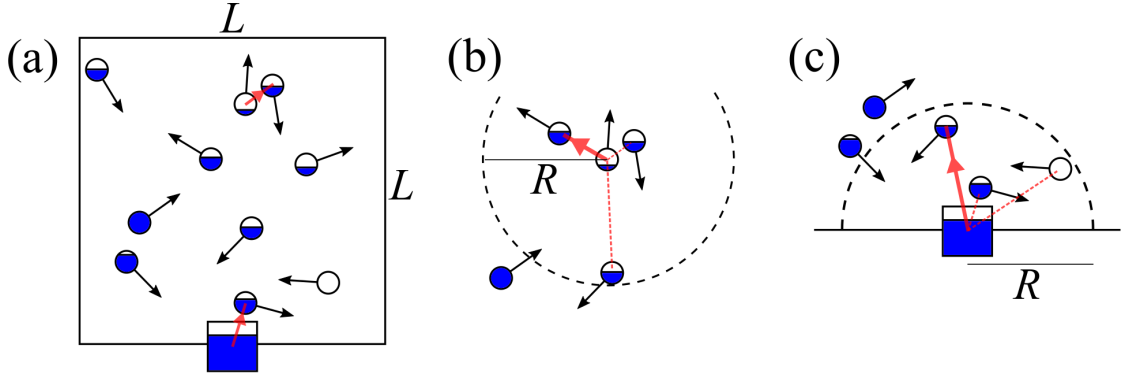


Figure 4.1: Illustration of the simulation model.

(a) Sketch of the entire system. The blue color represents the amount of food carried by each agent (circles). An agent is solid blue when filled at capacity ($c_i(t) = c_{\max}$). The red arrows stand for trophallactic interactions, and the direction of the arrow represents the direction of food transfer. The black arrows signify the direction of agent movement $\hat{e}_i(t)$. The source is depicted as a square at the middle of the bottom system wall.

(b) Trophallactic interaction between two agents. The donor agent, at the center of the dotted circle, selects one partner at random from the agents inside the interaction radius R (dotted circle) and transfers food. The potential receiver agents are indicated with red dashed lines.

(c) One agent that is within distance R from the source and not yet completely full is selected at random to pick up food from the source. The agent picks up a quantity $(c_{\max} - c_i)$ from the source to fill up completely.

orientation; $\hat{\xi}_{\perp i}(t)$ is the component orthogonal to $\hat{e}_i(t)$ of a uniformly distributed random vector on the unit circle $\hat{\xi}_i(t)$; and $\alpha_i(t)$ is a Lagrangian multiplier, chosen such that $|\hat{e}_i(t)| = 1$ for all times and agents. A more detailed description and derivation of Eqs. (4.1) and (4.2) from time continuous equations can be found in Appendix A, along with explanatory sketches (Figs. A.1 and A.2).

Note that there are no forces between the pointlike agents. Each agent's motion is independent of the other agents' motion. In order to confine the agents inside the nest chamber, we apply hard reflective boundary conditions at the system boundaries.

This random movement obviously is a gross oversimplification of the complex and occasionally directed motion of ants in real colonies. Also, real ants are more likely to walk along walls than to back away from them, as studied in [78]. However, for the purpose of this simulation model, active Brownian particles serve as a sufficient starting point, because real ants show diffusive mixing behavior in a confined environment like a nest chamber to some extent [83, 12].

4.1.2 Food intake from the source

Each agent i can carry a concentration $c_i(t) \leq c_{\max}$ of food, up to the carrying (or crop) capacity c_{\max} , which is the same for all agents.² At $t = 0$, no food is inside the system

$$c_i(0) = 0 \quad \forall i, \quad (4.3)$$

and enough food to fill every agent

$$f_{\max} = N c_{\max} \quad (4.4)$$

exists at the food source of the system. The source is located at the middle of one boundary at

$$\vec{x}_{\text{source}} = \left(\frac{1}{2}L, 0 \right) \quad (4.5)$$

(cf. Fig. 4.1 (a)). The agents have a finite interaction radius R that limits the spatial interaction range, i.e. the distance to the partner with whom they can exchange food. Whenever an agent randomly locates the food source, such that the position of the source \vec{x}_{source} is within the agent's interaction range ($|\vec{x}_i(t) - \vec{x}_{\text{source}}| \leq R$), it attempts to pick up food from the source (see Fig. 4.1 (c)). Food only enters the system through these uptake events. Once food has entered the system, it cannot leave the system, as no food sinks exist. Together, the total amount of food in all the ants and the food remaining at the source is conserved.³

In order to temporally resolve the food flow into the system, we do not model these food intake events as instantaneous, but consider them to last a time T , called interaction refractory period. Therefore, every $T/\Delta t$ time steps, one of the available agents that are within range of the source ($|\vec{x}_i(t) - \vec{x}_{\text{source}}| \leq R$) and not at their carrying capacity ($c_i(t) < c_{\max}$) is chosen with equal probability, and its food concentration is set to the maximum value $c_i(t) = c_{\max}$. Agents that are at capacity do not attempt to pick up food at the source, so they are ignored even if they are within range of the source. Both the source and the agent that picked up food are then in a refractory state for the next $T/\Delta t$ time steps. During this period, the refractory agent is not allowed to partake in any food exchanges and no other agent can pick up food from the refractory source. Agents thus pick up food

²With $c_i(t)$ we denote the concentration of food in agent i at time t , where concentration is to be understood as amount of food per agent. Summing over the food concentrations of all agents thus gives $F(t)$, the total amount of food, not a per agent concentration.

³This neglects the digestion of food. As explained before (Section 2.1), for the purpose of simulating food dissemination this is reasonable though, because food is distributed much faster in the colony than consumed by individual ants [9, 10].

from the source one at a time.⁴ The agent that just picked up food from the source continues to move in its refractory period though, so that every agents always moves. This is again chosen for simplicity, so as to decouple the food exchange events (whether an agent is refractory or not) from the random motion.

The exact location of the food source is not important for this model. The model can be modified by moving the source outside the nest, labeling the ants that reach and subsequently exit the nest entrance as foragers, and adjusting the characteristic time between source visits (in our model equal to the refractory period) to account for the extra time needed to reach the source.

4.1.3 Food exchange between agents

The core of our model is the exchange of food between agents, the trophallactic interaction. Little is known about the specific details of trophallaxis on the individual level in real animal societies [2, 10]. Therefore, we propose a minimal set of interaction rules that reproduce basic trophallaxis dynamics. Agents that acquired food can randomly choose a food exchange partner within their finite interaction radius R and try to exchange a fixed percentage σ of the food that they are carrying (see Fig. 4.1 (b)). We will call this percentage σ ‘food exchange ratio’ from now on. The specific interaction rules are:

1. Every agent i that currently
 - has food ($c_i(t) > 0$),
 - is not refractory (its last food exchange or intake from the source was more than $T/\Delta t$ time steps ago), and
 - has at least one other agent j in its interaction range ($|\vec{x}_i(t) - \vec{x}_j(t)| \leq R$) that is also not refractory
 is selected in a random order.⁵
2. The selected agent i randomly chooses one of the non-refractory agents j in its interaction range.

⁴It should be noted that real ants can and do feed in parallel from single food sources. This behavior is not captured by our model, but for sufficiently small colonies such as those analyzed in [10], our description is acceptable. Letting agents pick up food only one at a time simplifies the model and also leads to a more controlled flow of food into the system at large interaction radii.

⁵For simplicity, our model assumes that the refractory period (or in other words, the duration) of food exchanges between ants equals the refractory period after a food intake from the source. In general (and reality), this might not be the case and two different time periods or average durations should be used instead. See Section 9.3 for more on this and other possible extensions of the model.

3. The food concentration

$$\Delta c_{i \rightarrow j}(t) = \min(\sigma c_i(t), c_{\max} - c_j(t)) \quad (4.6)$$

$$= \begin{cases} \sigma c_i(t) & \text{if } c_j(t) + \sigma c_i(t) \leq c_{\max} \\ c_{\max} - c_j(t) & \text{otherwise} \end{cases} \quad (4.7)$$

is transferred from agent i to agent j . In this way, the food receiving agent j takes only as much of the share $\sigma c_i(t)$ from the donating agent i as it can carry. If the receiving agent cannot carry all of the food it is offered, the remainder $\sigma c_i(t) - (c_{\max} - c_j(t))$ stays in the donating agent. In the special case that the randomly selected receiver is already full ($c_j(t) = c_{\max}$), no food is transferred ($\Delta c_{i \rightarrow j}(t) = 0$).

4. Both food exchange partners i and j are immediately set to be refractory for the next $T/\Delta t$ time steps, irrespective of the actual amount $\Delta c_{i \rightarrow j}(t) \geq 0$ transferred, even if no food was transferred because the receiver was already full. In consequence, both agents cannot give, receive, or pick up food again in this iteration (and the next $T/\Delta t$ time steps as well).

This set of rules introduces no bias in the random choice of available food exchange partners and requires no active information exchange between agents. The single agent always offers the percentage σ of its own food to a blindly chosen partner, without knowing if the other one is already full or completely empty.⁶ An agent can only infer that its partner is at the carrying capacity after the food exchange when some of the offered food was returned ($\Delta c_{i \rightarrow j}(t) < \sigma c_i(t)$). It is important to note that consequently both the motion and the food exchange rules between the agents are completely random.

4.2 Simulation parameters

In order to study our simulation model numerically, we derive a complete set of dimensionless control parameters in this section. First, we give an overview of the model's parameters in dimensional terms (Section 4.2.1), and then group them according to dimensional analysis (Section 4.2.2).

⁶The majority of trophallactic food exchanges between real ants have been found to be initialized by the food receiving ant, not by the food donating ant as described in our model ([30, 5] and cf. Section 2.3). However, if we assume no information exchange to be involved in the choice of food exchange partners, there is no difference in who initiates the food exchange.

4.2.1 Dimensional parameters

The agents' motion is controlled by the fixed absolute value of their velocity vectors v (translation speed) and the rotational diffusivity D_r (average rotation speed) (cf. Section 4.1.1). The food dynamics is controlled by the agents' carrying capacity c_{\max} (maximum concentration per agent), their interaction radius R (maximum distance for food exchange or intake), and the refractory period T (effective duration of food exchange or intake) (cf. Sections 4.1.2 and 4.1.3). In addition, the edge length L of the square system controls the geometric size of the simulated system. Finally, Δt controls the time discretization of the equations of motion (Eqs. (4.1) and (4.2)) and the trophallaxis algorithm (cf. Sections 4.1.2 and 4.1.3).

Two of the simulation model's parameters (the food exchange ratio σ , and the number of agents N) are already dimensionless and thus not included in the dimensional analysis. We consider them in Section 4.2.2. All parameters are listed in Table 4.1.

symbol	parameter	dimension
c_{\max}	carrying capacity	food
D_r	rotational diffusivity	1/time
L	system length	length
N	number of agents	-
R	interaction radius	length
σ	food exchange ratio	-
T	refractory period	time
Δt	discretization time step	time
v	ant velocity	length/time

Table 4.1: List of all simulation parameters and their dimensions.

4.2.2 Dimensionless parameters

The parameter space spanned by the dimensional simulation parameters listed in Table 4.1 can be completely described by the dimensionless parameter set defined in Table 4.2, after choosing a scale for nondimensionalization for each of the parameters physical dimensions. We choose the refractory period T as the time scale, the carrying capacity c_{\max} as the food scale, and the system length L as the length scale for nondimensionalization.

This dimensionless parameter set is of course not unique. The rest of this section therefore explains the physical interpretations of the parameters we chose and their relations to various time and length scales of the system.

Dimensional analysis of Table 4.1 yields five different time scales of the simulation

symbol/definition	parameter
$\nu := \frac{T}{\left(\frac{R}{v}\right)} = \frac{vT}{R}$	ant velocity parameter
$\theta := \frac{T}{\left(\frac{1}{D_r}\right)} = TD_r$	ant rotation parameter
$\lambda := \frac{R}{L}$	interaction range parameter
$\tau := \frac{T}{\Delta t}$	refractory period parameter
σ	food exchange ratio
N	number of agents

Table 4.2: List of all dimensionless simulation parameters and their definitions.

model:

1. the trophallactic interaction time scale T ,
2. the discretization time scale Δt ,
3. the rotational motion time scale $1/D_r$,
4. the local translational motion time scale R/v , and
5. the global translational motion time scale L/v .

Each of the dimensionless parameters in Table 4.1 can be constructed by the ratio of two from these five time scales, except for the food exchange ratio σ and the number of agents N , which are defined dimensionless already.

The ant velocity parameter ν compares the trophallactic interaction time scale (1) with the local translational motion time scale (4), or in other words: it relates the duration of a food exchange to the maximum time an agent takes to travel one interaction radius. In terms of length scales this corresponds to the ratio of the maximum distance vT an agent travels during one interaction duration and the trophallactic interaction length scale R . This is a meaningful nondimensionalization of the ant agent velocity, because it uses the local time and length scales relevant to a food exchange. A value of ν close to zero indicates that the ants motion is negligible with regard to how far they can get within one refractory period.⁷ A ν value close to one means the ants move at a speed that allows them to cover a distance comparable to their interaction radius during one interaction. Values of ν larger than one finally represent simulations where the ants move fast enough to actually leave one interaction range during a refractory period.

⁷It is important to keep in mind here that all agents keep moving at the same speed at all times in our simulation model; even during trophallaxis.

The ant rotation parameter θ compares the trophallactic interaction time scale (1) with the rotational motion time scale (3). This gives an information about how fast the simulated ants randomly change their orientation of motion compared to the food exchange duration. Low values ($\theta < 1$) correspond to slow rotations, and high values ($\theta > 1$) to fast rotations.

The interaction range parameter λ compares the local translational motion time scale (4) with the global translational motion time scale (5), which is the ratio of the maximum times an agent takes to move through one interaction radius and to move through the whole system. Maybe more informative, λ can also be interpreted in terms of length scales, as it compares the trophallactic interaction length scale R with the system length scale L . It defines the fraction of the system an ant can interact with. The maximum λ value is $\lambda = \sqrt{2}$, when the interaction disk covers the whole square system from any position.

The refractory period parameter τ compares the trophallactic interaction time scale (1) with the discretization time scale (2). It equates to the number of iteration steps the simulation algorithm performs during one refractory period, and thus does not have a physically meaningful interpretation. In order to ensure that non-refractory ants cannot pass each other's interaction ranges without trying to exchange food, the discrete time step Δt has to fulfill $v\Delta t \ll R$, or in dimensionless terms $\nu \ll \tau$.

The food exchange ratio σ and the number of agents N are not related to the time scales discussed above, but they still control the simulation behavior. As can be seen from Eq. (4.7), the food exchange ratio σ determines the maximum amount of food agents can exchange relative to their own current amount of food. The number of agents N becomes physically meaningful, when put in relation to the system size. For example, N/L^2 gives the agent number density of the system that can be used to modify the dimensionless control parameter λ to become $N\lambda^2$, which then combines the length scale relation discussed above with the number density.

4.3 Simulated scenarios

As Section 4.2 showed, the dynamics of our simulation model is controlled by seven dimensional parameters (c_{\max} , D_r , L , R , T , Δt , v) and two dimensionless parameters (σ , N). The dimensional analysis reduced this to six dimensionless parameters (ν , θ , λ , τ , σ , N), after fixing the time scale T , the length scale L and the food scale c_{\max} . We focus on studying the influence of the three parameters that are most important to the food distribution in ant colonies: the ant velocity parameter ν , the interaction range parameter λ , and the food exchange ratio σ .

The remaining parameters θ , τ , and N are kept constant throughout all presented simulations, besides a few specifically marked cases. Almost all simulation results are calculated as averages over an ensemble of simulation runs. If not stated otherwise, we calculate ensemble average based on 100 independent simulation runs. Increasing the number of simulation runs further does not change the ensemble averaged results.

As described in Section 1.3, the simulation results are presented in two parts: one without explicit motion (Part II), and one with explicit motion (Part III). For all the simulations in Part II, we set the ant velocity parameter equal to zero ($\nu = 0$), and vary only λ and σ . Only for the simulations in Part III, we vary ν , λ and σ .

Although we do not model the movement of the ants explicitly in Part II, it is implicitly taken into account through the interaction radius. As mentioned before, real ant colonies exhibit spatial fidelity zones (cf. Section 1.3 and [11, 12]). Our simulations without explicit motion can therefore still be used to describe real ant colonies with moving ants, if the radii of their spatial fidelity zones matches our interaction radius.

In order to compare our simulations with analytical descriptions, we also simulate a one-dimensional (1D) version of the model presented in Section 4.1, without explicit motion. As we will demonstrate in Section 6.1.1, this 1D scenario behaves qualitatively similar to the two-dimensional (2D) setup to a large degree, which justifies this strong simplification. We proceed with describing the three simulation scenarios (1D without explicit motion, 2D without explicit motion, and 2D with explicit motion) in the rest of this section.

4.3.1 1D without explicit motion

The 1D simulation scenario supplies data to validate our analytic models. It is constructed through limiting the agents' positions to the one-dimensional interval $[0, L]$, so that L now describes the interval length instead of the edge length of the 2D square system. The maximum interaction range parameter in 1D is $\lambda = 1$ (instead of $\lambda = \sqrt{2}$ in 2D), which is achieved when $R = L$. Boundary conditions and equations of motion are not necessary in this scenario, because the agents do not move explicitly ($v = 0$ and D_r is meaningless). The location of the source is at the left system boundary $x_{\text{source}} = 0$ (instead of $\vec{x}_{\text{source}} = (L/2, 0)$ in 2D).

The agents initial positions are drawn from a random uniform distribution over the interval $[0, L]$, under the constraint that all of the agents' interaction ranges overlap in a way that food from the source can at least indirectly reach every agent. This constraint becomes irrelevant for $\lambda = 1$ and leads to an equidistant position distribution for $\lambda \rightarrow 1/N$. Interaction range values of $\lambda < 1/N$ are thus not allowed. Since $v = 0$, the agents keep their initial positions throughout the whole simulation.

Every simulation run in one ensemble uses new randomized positions.

Table 4.3 lists the parameter values that we use throughout all 1D simulations without explicit motion, if not stated otherwise.

parameter	symbol	value
ant velocity parameter	ν	0
ant rotation parameter	θ	-
interaction range parameter	λ	varied
refractory period parameter	τ	1
food exchange ratio	σ	varied
number of agents	N	100

Table 4.3: Nondimensional simulation parameter values for the simulation scenarios without explicit motion (1D and 2D).

4.3.2 2D without explicit motion

The 2D simulation scenario without explicit motion serves as a link between the 1D scenario, for which we derive analytic descriptions in Part II and the full simulation dynamics with explicit motion we investigate in Part III. In Sections 6.1.1 and 6.3 we will show that the 2D scenario without explicit motion is still captured qualitatively by our 1D analytic predictions to a large degree. This gives reason to believe that our analytic models provide groundwork for more detailed descriptions that include explicit motion.

Additionally, as explained for the 1D scenario without explicit motion above, also the 2D scenario without explicit motion can be used to model real ant colonies, if they show spatial fidelity zones.

Boundary conditions and equations of motion are thus also not necessary in this scenario, because the agents do not move explicitly ($v = 0$ and D_r is meaningless).

The position initialization procedure in this scenario is also similar to the 1D scenario without explicit motion: All agents are assigned a uniformly distributed random position inside the $[0, L] \times [0, L]$ simulation box, under the same constraint as in 1D (food from the source can at least indirectly reach every agent). In 2D, this constraint is always fulfilled for $\lambda = \sqrt{2}$ and cannot be met for $\lambda < 1/\sqrt{N}$. Again, for small λ values, the positions will be less random and more grid-like.

We use the same parameter values for this scenario as for the 1D scenario (Table 4.3).

4.3.3 2D with explicit motion

This simulation scenario includes the full dynamics as described in Section 4.1. No constraint is applied to the agents uniform random initial positions this time, because they change anyway in the course of the simulation.

Since $\nu > 0$ in this scenario, the refractory period parameter τ has to be adjusted with ν , so that $\nu \ll \tau$ (cf. Section 4.2.2). We tested that a discretization precision of 10^{-3} (so that $\nu \leq 10^{-3}\tau$ through $\tau := 10^3\nu$) is sufficient to not produce any artefacts.

The ant rotation parameter θ also has to be chosen in this scenario, to control the strength of the rotational noise in the agents motion. A value of $\theta = 0.2$ proved to give reasonable smooth active Brownian motion trajectories and was thus used for all simulations of this scenario.

All the parameter values for the 2D simulations with explicit motion are listed in Table 4.4.

parameter	symbol	value
ant velocity parameter	ν	varied
ant rotation parameter	θ	0.2
interaction range parameter	λ	varied
refractory period parameter	τ	$10^3\nu$
food exchange ratio	σ	varied
number of agents	N	100

Table 4.4: Nondimensional simulation parameter values for the 2D simulation scenarios with explicit motion.

4.4 Observables

As the last piece of introductory material, this section introduces and defines all of the observables that will be used throughout this thesis.

The aim of this work is to investigate how food, localized at the source, spreads through the initially empty system of agents ($c_i(0) = 0, \forall i$), until every agent is at its carrying capacity ($c_i(t) = c_{\max}, \forall i$). Quantifying this nonequilibrium transport process is complex, and care needs to be taken in choosing appropriate observables.

The simplest, but surprisingly informative quantities of interest we will use as observables are global measures that characterize the temporal dynamics of the amount of food inside the whole nest (Section 4.4.1).

These observables only contain information about how much food is carried by the ants, but not where it is located in space and how the food spreads from the

source through the system. In order to quantify this, we also use spatial measures (Section 4.4.2).

Finally, the individual amounts of food carried by the ants can be observed to study how the food is distributed among the ants, independent of their location (Section 4.4.3).

4.4.1 Global measures

In this section, we define the total amount of food inside the nest, the average food concentration of all ants, the variance of the ants' food concentrations, and the time until the colony is half full (half-time) as observable at the macroscopic colony level.

Total food

The total amount of food $F(t)$ in the ant colony at time t is calculated as the simple sum

$$F(t) := \sum_{i=1}^N c_i(t) \quad (4.8)$$

over the N agents' food concentrations $c_i(t)$. We use it in units of the maximum amount of food the colony can carry $f_{\max} = Nc_{\max}$, so that $F(t)/f_{\max} = 1$ when the colony is full. Its time evolution measures the transport of food into the system.

Average food concentration

The average food concentration

$$\langle c(t) \rangle := \frac{1}{N} \sum_{i=1}^N c_i(t) \quad (4.9)$$

at time t is closely related to the total food $F(t)$, because $\langle c(t) \rangle = F(t)/N$.⁸ We use it in units of the carrying capacity of a single ant c_{\max} , so that again $\langle c(t) \rangle / c_{\max} = 1$, when the colony is full. In fact, $F(t)/f_{\max} = \langle c(t) \rangle / c_{\max}$, so that both the normalized total food and the normalized average food concentration measure the food transport into the system with the same numeric values.

⁸Throughout the whole thesis angle brackets $\langle X \rangle$ denote the average $(1/N) \sum_{i=1}^N X_i$ of X_i over all N agents, or ants.

Food concentration variance

The food concentrations variance

$$\langle \Delta c^2 \rangle := \frac{1}{N} \sum_{i=1}^N [c_i(t) - \langle c(t) \rangle]^2 \quad (4.10)$$

$$= \frac{1}{N} \sum_{i=1}^N \left[c_i(t) - \frac{1}{N} \sum_{j=1}^N c_j(t) \right]^2 \quad (4.11)$$

measures how uniform the food is distributed in the whole colony at time t . Analogue to the food concentration average, we use it in units of c_{\max}^2 . A variance of $\langle \Delta c^2 \rangle / c_{\max}^2 = 0$ means that every ant carries the same amount of food at time t , and the larger $\langle \Delta c^2 \rangle / c_{\max}^2 > 0$, the bigger the differences between the ants' individual food concentrations are.

Half-time

Food can only enter and never leave the nest in our simulation model. The total food $F(t)$ thus increases monotonically in time. For that reason, there is a unique time $t_{1/2}$, for that

$$\langle c(t_{1/2}) \rangle = \frac{1}{2} c_{\max} \quad (4.12)$$

for the first time: the time until the colony is half full, which we will call 'half-time'. It measures the global food intake time scale of the colony's saturation dynamics.

4.4.2 Spatial measures

In this section, we define the spatial distribution of food in the nest and the mean squared distance the food has spread from the source as spatial observables.

Spatial food distribution

In our simulation model, food can only exist at discrete positions in space, the ants' positions. Nevertheless, when binned in space and ensemble averaged over multiple simulation runs, the spatial food distribution can be visualized with the ensemble average of the food concentration $\langle c(\vec{x}, t) \rangle$ as a function of space and time.

Mean squared food distance

In order to condense the two-dimensional spatial food distribution function into a simpler one-dimensional function, we define the ‘mean squared food distance’

$$\text{MSD}(t) := \langle d(t)^2 c(t) \rangle \quad (4.13)$$

$$= \frac{1}{N} \sum_{i=1}^N d_i(t)^2 c_i(t) , \quad (4.14)$$

where

$$d_i(t) := |\vec{x}_i(t) - \vec{x}_{\text{source}}| \quad (4.15)$$

is the distance between agent i and the food source at time t . This quantity is a generalization of the mean squared displacement of a Brownian particle in statistical mechanics. In our case, the distance of each agent from the reference point is weighted by the amount of food it is carrying. With this observable, we are able to monitor the spatio-temporal transport of food, as it spreads from the source through the system.

Since $\lim_{t \rightarrow \infty} c_i(t) = c_{\max}$ and the system is finite, we can easily calculate the ensemble average steady state value of $\text{MSD}(t)$ from the system geometry by considering

$$\lim_{\substack{t \rightarrow \infty \\ N \rightarrow \infty}} \text{MSD}(t) = \lim_{\substack{t \rightarrow \infty \\ N \rightarrow \infty}} \frac{1}{N} \sum_{i=1}^N d_i(t)^2 c_i(t) \quad (4.16)$$

$$= c_{\max} \lim_{\substack{t \rightarrow \infty \\ N \rightarrow \infty}} \frac{1}{N} \sum_{i=1}^N d_i(t)^2 \quad (4.17)$$

$$= c_{\max} \frac{1}{A} \int_A (\vec{x} - \vec{x}_{\text{source}})^2 dA. \quad (4.18)$$

Here, A is the total system area. For the 2D simulation scenario $A = L^2$ and $\vec{x}_{\text{source}} = (L/2, 0)$, so that

$$\lim_{\substack{t \rightarrow \infty \\ N \rightarrow \infty}} \text{MSD}_{2\text{D}}(t) = \frac{5}{12} c_{\max} L^2 . \quad (4.19)$$

For the 1D simulation scenarios $A = L$ and $\vec{x}_{\text{source}} = x_{\text{source}} = 0$, so that

$$\lim_{\substack{t \rightarrow \infty \\ N \rightarrow \infty}} \text{MSD}_{1\text{D}}(t) = \frac{1}{3} c_{\text{max}} L^2 \quad (4.20)$$

instead.

We can then define a dimensionless version of $\text{MSD}(t)$ which we designate by $\overline{\text{MSD}}(t)$:

$$\overline{\text{MSD}}(t) := \frac{\text{MSD}(t)}{\lim_{\substack{t \rightarrow \infty \\ N \rightarrow \infty}} \text{MSD}(t)} .$$

Note that $\overline{\text{MSD}}(t) \in [0, 1]$, and when $\overline{\text{MSD}}(t) = 1$ the steady state has been reached (colony is full).

4.4.3 Individual measures

In this section, we define the distribution of food among individual ants as an observable for the microscopic individual ant level.

Distribution of food among individual ants

Similarly to the spatial food distribution, the distribution of food among individual ants can be achieved through binning and ensemble averaging. Only here, we bin the food concentrations instead of the agents' positions. As a function of time, this measures how many ants $P(c(t))$ carry how much food at time t , independent of their position.

In addition, $P(c(t))$ can also be calculated in spatial bins, instead of for the whole colony, to obtain a combined microscopic measure $P(c(t))(x)$ of how the food is distributed in space and among individual ants.

Part II

Trophallaxis without Explicit Motion

5 Mean-field Limit

To understand the limits of trophallactic behavior in our system, we will first consider the simple well mixed case in this chapter that takes place when either the interaction radius is large enough to cover the maximum distance between any two points in the nest, or equivalently when the ants' velocity is high enough to ensure equiprobable encounters between any pair of ants. In this mean-field limit case, every ant has the chance to interact with every other ant and the source at all times.

It is important to note here that the system becomes independent of space and hence dimension in this limit. Any analytic mean-field description of the system therefore applies to both 1D and 2D simulation setups, and even to all setups with or without explicit motion if the interaction radius is chosen to cover the whole system ($R = L$ or $\lambda = 1$ in 1D and $R = \sqrt{2}L$ or $\lambda = \sqrt{2}$ in 2D).

Sections 5.1 and 5.2 will present an analytic description of the mean-field limit and Section 5.3 will compare the predictions of these descriptions with simulation results.

5.1 Mean-field model

In the mean-field limit every ant has the same probability to interact with another ant or the source. These probabilities only depend on the number of ants and the interaction time scale and can therefore be calculated easily. This allows to derive a governing equation for the systems dynamics, which then leads to a simple prediction of the average food concentration.

5.1.1 Governing equation

We can formulate an analytic mean-field model if we approximate the discrete food exchanges as continuous processes. In this approximation, the expected food

concentration $c_i(t)$ of every ant i follows

$$c_i(t + dt) = c_i(t) + \underbrace{\sum_{\substack{j=1 \\ j \neq i}}^N p_{j \rightarrow i} \Delta c_{j \rightarrow i}(t)}_{\text{gain from other ants}} - \underbrace{\sum_{\substack{j=1 \\ j \neq i}}^N p_{i \rightarrow j} \Delta c_{i \rightarrow j}(t)}_{\text{loss to other ants}} + \underbrace{p_{\text{source}}(c_{\text{max}} - c_i(t))}_{\text{gain from source}}, \quad (5.1)$$

where dt is an infinitesimal time interval, during which $p_{j \rightarrow i}$ and $p_{i \rightarrow j}$ are the probabilities of a food exchange from ant j to ant i and from ant i to ant j , and p_{source} is the probability for an ant to pick up food from the source; $\Delta c_{j \rightarrow i}(t)$ and $\Delta c_{i \rightarrow j}(t)$ are the food concentrations exchanged from ant j to ant i and from ant i to ant j (as defined in Eq. (4.7)); c_{max} is the maximum food concentration due to the finite carrying capacity; and N is the number of ants.

The probabilities in Eq. (5.1) are

$$p_{j \rightarrow i} = p_{i \rightarrow j} = \frac{dt}{(N-1)T} \quad (5.2)$$

and

$$p_{\text{source}} = \frac{dt}{NT}, \quad (5.3)$$

where T is the refractory period introduced in Section 4.1, dt/T is the probability of an individual ant not to be refractory, $1/(N-1)$ is the probability of selecting an individual ant for a food exchange; and $1/N$ is the probability of selecting an individual ant to pick up food from the source.

Thus, the mean-field food dynamics is governed by the ordinary differential equation

$$\frac{dc_i(t)}{dt} = \frac{1}{(N-1)T} \sum_{j=1}^N (\Delta c_{j \rightarrow i}(t) - \Delta c_{i \rightarrow j}(t)) + \frac{1}{NT} (c_{\text{max}} - c_i). \quad (5.4)$$

This directly allows us to derive a mean-field prediction of the average food. The food variance, unfortunately, cannot be predicted by the mean-field model with the same ease. We do however present an analytic prediction of the food variance in Section 5.2 for another limit case.

5.1.2 Average food concentration

Equation (5.4) can easily be solved analytically for the average food concentration $\langle c(t) \rangle$ in the mean-field limit:

$$\frac{d\langle c(t) \rangle}{dt} = \frac{1}{N} \sum_{i=1}^N \frac{dc_i(t)}{dt} \quad (5.5)$$

$$= \frac{1}{N(N-1)T} \underbrace{\sum_{i=1}^N \sum_{j=1}^N (\Delta c_{j \rightarrow i}(t) - \Delta c_{i \rightarrow j}(t))}_{=0} + \frac{1}{NT} \left(c_{\max} - \underbrace{\frac{1}{N} \sum_{i=1}^N c_i(t)}_{=\langle c(t) \rangle} \right) \quad (5.6)$$

$$= \frac{1}{NT} (c_{\max} - \langle c(t) \rangle) \quad (5.7)$$

When taking the average, the summations in Eq. (5.6) are symmetric with respect to i and j and cancel. Interestingly, this makes the average food independent of the food exchange ratio σ .

The solution of Eq. (5.7) is

$$\langle c(t) \rangle = c_{\max} \left(1 - e^{-\frac{t}{NT}} \right). \quad (5.8)$$

This agrees with the exponential saturation laws for the food intake observed in experiments and gives a microscopic interpretation to the proposed phenomenological models [10, 19]. A similar equation for the number of fed individuals as a function of time was derived in [66, 65].

5.2 Binary food concentration approximation

Early in the food dissemination process, the majority of the ants have a completely empty crop. For small times, we can initially neglect the food exchange between ants as the food distribution in the nest is mostly dominated by food intake events from the source. The population of ants is then roughly separated into two groups: the ants that have a full crop, whose number n increases linearly with time as $n = t/T$; and the ants who are empty. This binary approximation becomes exact when the food exchange ratio is $\sigma = 1$. In this case, the ants exchange the entirety of their crop contents and the separation of the ant population in two groups, full and empty, is always exact.

We can now derive simple analytic predictions of the average food and the food

variance from this binary approximation.

5.2.1 Average food concentration

The total amount of food in the colony is simply given by the number $n = t/T$ of full ants times the carrying capacity c_{\max} under these assumptions. Consequently, for small times or large σ , the average food concentration increases linearly with time as

$$\langle c(t) \rangle = \frac{c_{\max} t}{NT} . \quad (5.9)$$

5.2.2 Food concentration variance

From Eq. (5.9) follows

$$\langle \Delta c(t)^2 \rangle = \frac{c_{\max}^2 t}{NT} \left(1 - \frac{t}{NT} \right) , \quad (5.10)$$

which gives an analytic prediction of the food concentration variance for small times or large σ .

5.3 Comparison of simulations and analytic predictions

In this section, we compare the derived analytic predictions Eqs. (5.8) to (5.10) first with simulation results of the true mean-field limit setup, where the interaction radius spans the whole system ($\lambda = 1$); and then with simulation results, where the interaction radius does not span the whole system anymore ($\lambda < 1$). The case of $\lambda < 1$ introduces a dependency on the ants' positions to the system, that does not exist for $\lambda = 1$ and is thus not accounted for in the mean-field model. This allows us to evaluate the predictions' extent of validity. We use the 1D simulation setup without explicit motion for this section (Section 4.3).

5.3.1 Results with system wide interaction range

Figure 5.1 directly compares the analytic mean-field prediction for the average food concentration of Eq. (5.8) (red dashed line) and the binary food concentration approximations for the average and the variance Eqs. (5.9) and (5.10) (orange dot-dashed line) with the ensemble averaged simulation data for different food exchange ratios σ .

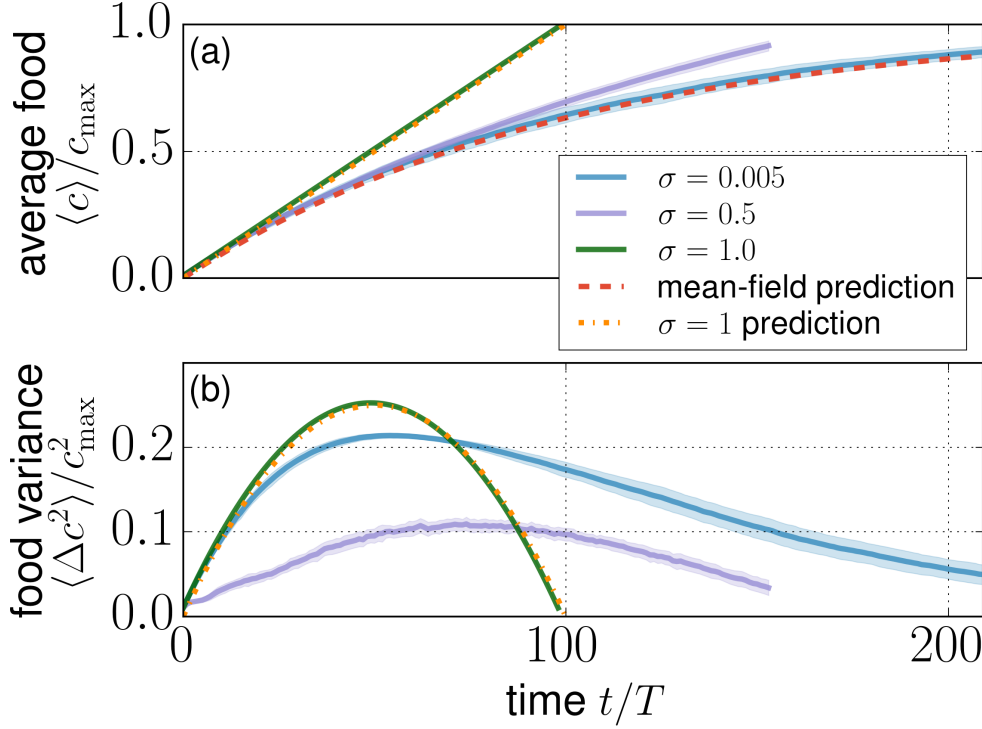


Figure 5.1: (a) Average food concentration $\langle c \rangle$ (measured in units of c_{\max}) and (b) food variance $\langle \Delta c^2 \rangle$ (measured in units of c_{\max}^2) versus time (in units of T) when $\lambda = 1$. Blue solid line $\sigma = 0.005$, purple solid line: $\sigma = 0.5$, green solid line: $\sigma = 1$, red dashed line: mean-field prediction (Eq. (5.8)), orange dash-dotted line: $\sigma = 1$ prediction (Eq. (5.9) for (a) and Eq. (5.10) for (b)). Even for σ as high as 0.5, the mean-field model offers a very good approximation of the food intake dynamics. The width of the shaded area around each line indicates the standard deviation.

For small values of σ , Eq. (5.8) gives an excellent prediction of the average food. As σ increases the prediction becomes progressively worse. Especially when the ants attempt to give each other more than half of the food they carry ($\sigma \gtrsim 0.5$), Eq. (5.8) does not provide a valid approximation for the whole dynamics anymore. In fact, the mean-field model is valid for a certain initial time interval that decreases with increasing food exchange ratio σ . For a low value ($\sigma = 0.005$), agreement is achieved throughout the whole simulation.

In our simulations ants do not attempt to pick up food from the source when their crop is full. This is in disagreement with the setup of the mean-field model as the probability for an ant to pick up food from the source is calculated with the total number of ants, and not with the number of empty ants (cf. Eq. (5.3)). Modifying the feeding rules to allow ants to attempt to pick up food from the source even when full only minimally affects the simulation results in the mean-field

limit and the agreement with the mean-field model is still very good.

As explained in Section 5.2, Fig. 5.1 also shows that the binary food concentration approximations provide an exact prediction in the $\sigma = 1$ case.

5.3.2 Results with intermediate interaction ranges

In Fig. 5.2 we explore to what extent the mean-field model finding Eq. (5.8) holds when $R < L$ (or $\lambda < 1$), i.e. leaving the mean-field limit with an interaction radius smaller than the system size. In particular, we consider the linear function

$$f(t) = \gamma t = \ln \left(1 - \frac{\langle c(t) \rangle}{c_{\max}} \right) \quad (5.11)$$

in the exponent of the exponentially saturating average food concentration for different λ values, $\sigma = 0.5$ (Fig. 5.2(a)) and $\sigma = 0.005$ (Fig. 5.2(b)). The slope γ of $f(t)$ and therefore the slopes in Fig. 5.2 correspond to an inverse time scale that we will call ‘(global) food intake rate’. For the mean-field model (Eq. (5.8)), the expected food intake rate is simply

$$\gamma_{\lambda=1} = \frac{1}{NT} \quad (5.12)$$

(red dashed line in Fig. 5.2).

For small σ , we observe that the system switches from a fast food intake rate that agrees very well with the mean-field model in the initial stages of the process to a slower food intake rate that depends on the interaction radius. The time when the transition occurs decreases with the interaction radius. There is a simple interpretation for this behavior. Initially, all the ants near the nest entrance that have access to the source are empty, and the trophallactic dynamics is dominated by the ants at the entrance picking up food. The mean-field theory holds until the moment when the ants within reach of the source are approximately at capacity. After this transition, the behavior stops being well explained by mean-field theory because the food is now diffusing out of the nest entrance vicinity via ant to ant trophallactic interactions. The transition between the two regimes is abrupt for small σ , and becomes less pronounced for large σ , due to higher fluctuations of the food concentration in space and time.

Past the transition time, the average food can be approximated by

$$\langle c(t) \rangle = c_{\max} - (c_{\max} - \langle c(t^*) \rangle) e^{-\gamma(t-t^*)}, \quad (5.13)$$

where t^* is the transition time and γ is the new food intake rate. The time t^* of

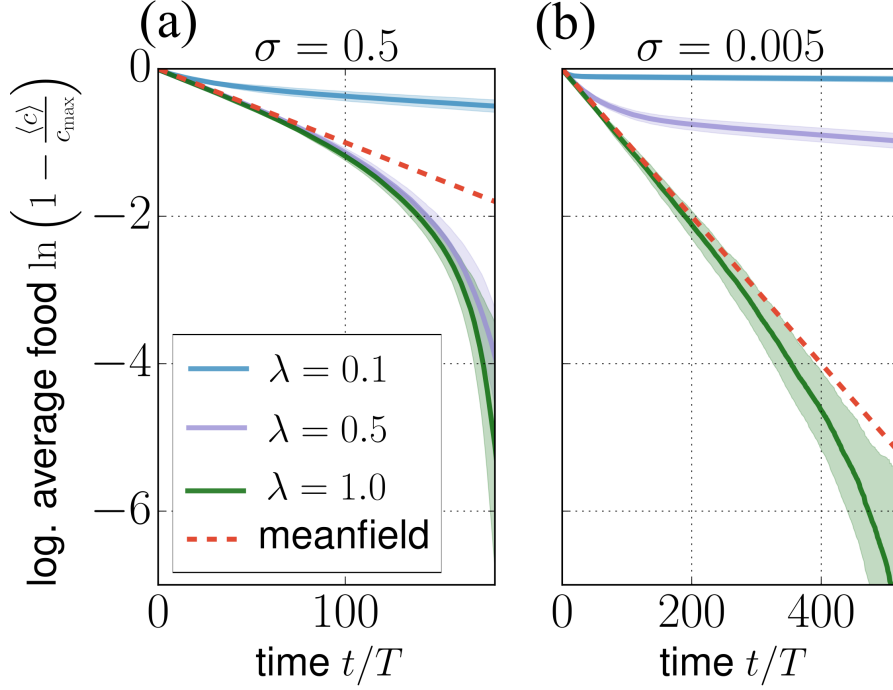


Figure 5.2: Exponential saturation exponent $\ln\left(1 - \frac{\langle c(t) \rangle}{c_{\max}}\right)$ of the average food concentration $\langle c(t) \rangle$ as a function of time (in units of T) (cf. Eq. (5.11)). Blue solid line $\lambda = 0.1$, purple solid line: $\lambda = 0.5$, green solid line: $\lambda = 1$, red dashed line: mean-field prediction (Eq. (5.8)). At the beginning of the dynamics, the average food is described well by the mean-field model (red dashed line). Later, different dynamics occur, depending on the parameter values. (a) For a large σ ($\sigma = 0.5$), the amount of food is well described by the mean-field model for values of λ between 1 and 0.5. (b) For a small σ ($\sigma = 0.005$), the mean-field model is valid for a reasonable length of time only for $\lambda \rightarrow 1.0$. The system switches from a fast food intake rate that agrees very well with the mean-field model in the initial stages of the process to a slower dynamics that depends on the interaction radius. The time when the transition occurs decreases with the interaction radius. The width of the shaded area around each line indicates the standard deviation.

the transition increases with λ , whereas γ decreases with λ .

Chapter 6 will be devoted to deriving an approximate value for γ . We will construct a continuum model to approximate how the food diffuses away from the nest entrance vicinity to the rest of the nest and use this to study the saturation behavior of food in the colony.

6 Diffusive Limit

In Chapter 5, we discussed a mean-field model that allowed spatially independent, all-to-all interactions. In this chapter, we explore the opposite regime of small interaction radii. As already mentioned, this can be interpreted as ants that occupy spatial fidelity zones. The ants' explicit velocity is still zero ($v = 0$, cf. Section 4.1.1), but their effective spatial fidelity zone is a circular region of radius R centered around their (preferred) location \vec{x}_i , for each ant i . In this limit, the behavior of the system becomes strongly spatially dependent and the mean-field model fails. The goal of this chapter is to derive a set of equations that describe the food dissemination process in this case and to compare it with the simulation results.

Given the nature of the trophallactic process with small interaction ranges (compared to the system size), it is tempting to describe the food flow as a simple diffusion process with a fixed diffusion coefficient and a source term. This is deceptive, as the finite crop capacities, the finite system size, and agents picking up food to capacity at the source render this problem more complex. All of these complications are essential to describe trophallaxis, but make the problem of finding an exact solution to the appropriate dynamical equations analytically intractable. In order to gain some intuition about the behavior of the system, we will first derive a full diffusion equation in Section 6.1. In Section 6.2, we will then adopt a series of simplifying assumptions that allow us to analytically solve the derived equation, and arrive at a global food intake rate. Finally, Section 6.3 will demonstrate that this analytically predicted time scale qualitatively agrees with the global system behavior of the full trophallactic dynamics, obtained by simulations.

6.1 Diffusion approximation derivation

In order to keep the analytic description of trophallaxis in the diffusive limit simple, we will first show in Section 6.1.1 that it is reasonable to work in 1D. Section 6.1.2 then introduces the continuum notation necessary to easily derive space dependent equations, and Section 6.1.3 finally gives the derivation of the full diffusion equation.

6.1.1 Comparison of 1D and 2D spatial simulation results

While the mean-field model was spatially independent and its predictions should hold for any number of dimensions, any spatially dependent model will in principle depend on the dimensionality of the system. Since this thesis primarily seeks to understand qualitative behaviors, the analytic trophallaxis models in this work are written down and solved in 1D for simplicity.

In Fig. 6.1, we present a time series of the spatial food distribution in a 2D square nest for various food exchange ratios σ and interaction range parameters λ . In Fig. 6.2 we show a time series of the food distribution in space (solid red line) and among the ants (blue background), again for various σ and λ values, but for a 1D system.

Figures 6.1 and 6.2 indicate several qualitative similarities between the 2D and the 1D system. First, for small σ and λ (row (a)), the food initially quickly saturates the area at the vicinity of the nest entrance (the area within interaction range of the source), and then disperses to the whole nest via an initially narrow and subsequently broadening moving front. Second, for small σ but larger λ (row (b)), the area within interaction range of the source takes longer to saturate before the food diffuses away. Third, for large σ and small λ (row (c)) there is no clear separation between the time the area close to the nest entrance fills at capacity and the time the diffusion of food out of that area becomes important. However, like in the previous cases, there is still a gradient of food density from the source at the nest entrance to the opposite border of the nest. Finally, for large σ and λ (row (d)), the gradient disappears, and the nest acquires food roughly uniformly.

This qualitative similarity between 2D and 1D in the simulation gives reason to assume that analytic predictions valid in 1D also hold for 2D.

6.1.2 Continuum variables

In order to write down space dependent models that are analytically solvable, we will replace the discrete, agent-based variables with a description that is continuous in space and food exchange.

In the agent-based simulation model, the maximal absolute amount of food

$$f_{\max} := Nc_{\max} \tag{6.1}$$

in the system is determined by the number of ants N , and by how much food one ant can carry: the food concentration capacity c_{\max} (food per ant). Therefore, it is a natural choice, to describe the amount of food an ant i at position x and time t is carrying with $c(x_i, t)$, the food per ant concentration.

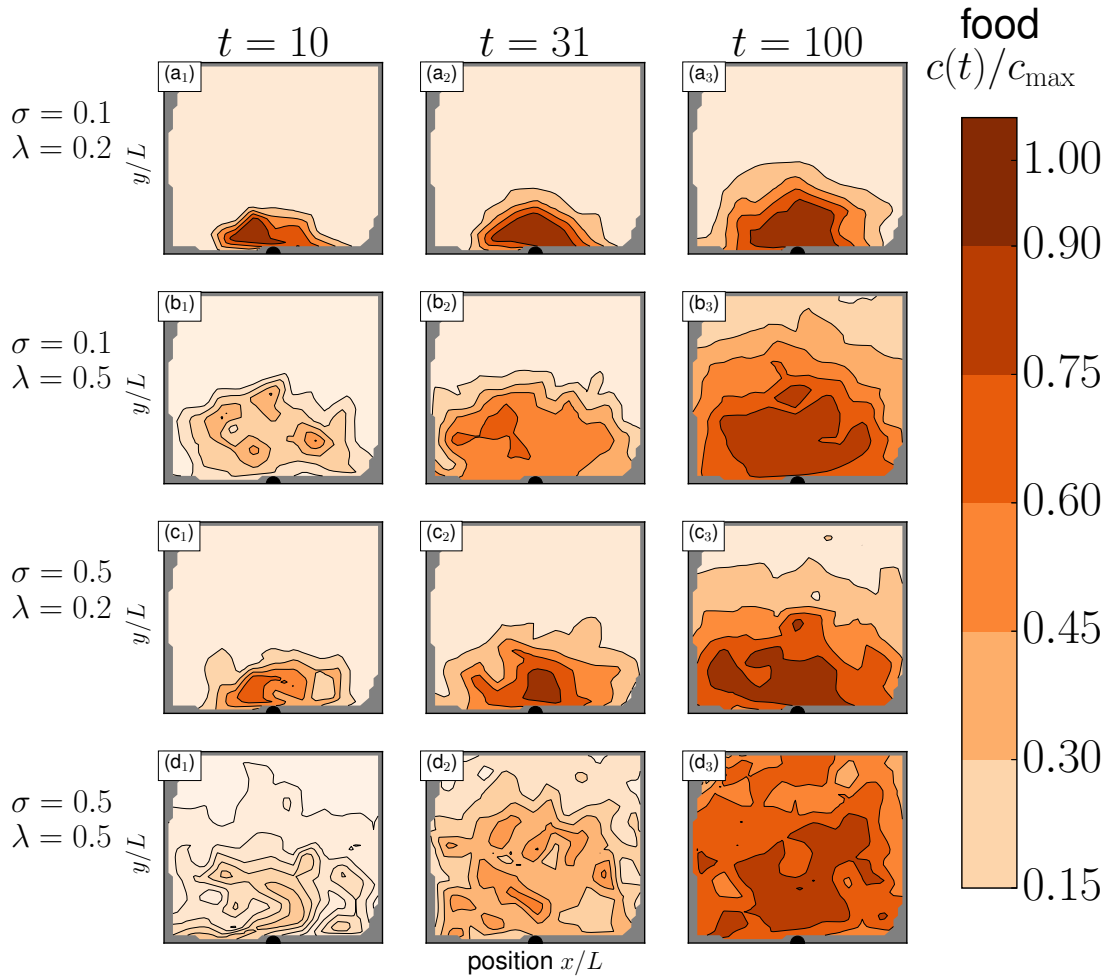


Figure 6.1: Time series of 2D spatial food distribution pattern for various parameter values σ and λ . The food source of the nest is at the center of the bottom nest border ($x = L/2, y = 0$), and indicated with a black semicircle. The distribution is the result of an ensemble average over 10 independent realizations of the simulation for the same (random) ant positions. The time indices t are given in units of the refractory period T . One hundred ants are initially distributed at random in the nest, with a uniform probability distribution. Since the uniform probability typically produces a very inhomogeneous distribution of ants in the nest, a repulsive potential is applied to ensure that the ants occupy the nest more homogeneously before their position is fixed. For small values of σ and λ , the dynamics is approximately diffusive with food being distributed locally amongst close agents. For larger values, food becomes delocalized and spreads among many agents that are far from each other.

6 Diffusive Limit

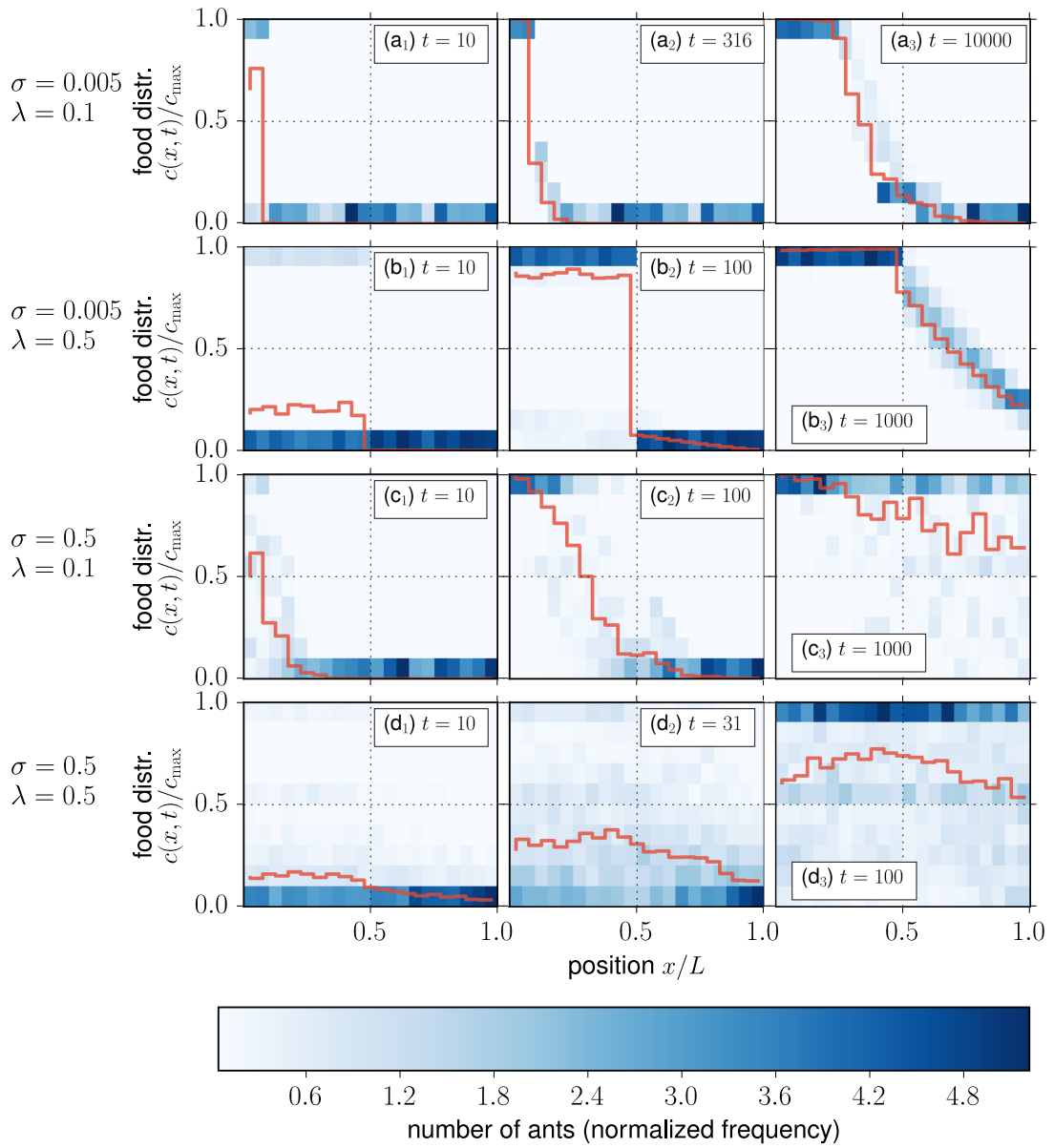


Figure 6.2: Time series of 1D food distribution in space and among ants for various parameter values σ and λ . Red line: spatially binned average food concentration, blue background: histogram of the food distribution among ants binned in food and space. The time indices t are given in units of the refractory period T . The distribution is the result of an ensemble average over 100 independent realizations of the simulation for the same (uniform random) ant positions. The 1D behavior dependence on σ and λ qualitatively follows that of the 2D system, displayed in Fig. 6.1.

The diffusion approximation of this section is on the contrary technically derived in the limit of $N \rightarrow \infty$, where measuring food in per agent concentrations becomes meaningless. Instead, it is more informative to use a spatial food density $\rho(x, t)$, describing the average amount of food per volume at position x and time t . In the 1D case, this volume is simply the system length L . The maximal amount of food in the system is then calculated through integrating over the maximal (final) food densities $\rho_{\max} := \lim_{t \rightarrow \infty} \rho(x, t)$:

$$f_{\max} = \int_L dx \lim_{t \rightarrow \infty} \rho(x, t) = \int_L dx \rho_{\max} = L \rho_{\max} . \quad (6.2)$$

This value should equal the maximal amount of food in the simulations. Thus, combining Eq. (6.1) and Eq. (6.2) yields

$$f_{\max} = N c_{\max} = L \rho_{\max} . \quad (6.3)$$

Analogue, the relationship between the continuum and discrete food variables at a given position x and time t is given through multiplying with the ant number density N/L :

$$\rho(x, t) = c(x, t) \frac{N}{L} . \quad (6.4)$$

6.1.3 Governing equation

Using the continuum variables of Section 6.1.2, we can now derive the analytic diffusion approximation for small interaction ranges λ . For simplicity, we initially assume that the ants (or rather points in space) only interact with their nearest neighbors, i.e. we consider the limit of $\lambda \rightarrow 0$.

The balance equation describing the food exchange between any neighboring points not within range of the source at positions x , $x + \Delta x$, and $x - \Delta x$ in the time interval Δt is

$$\frac{\rho(x, t + \Delta t) - \rho(x, t)}{\Delta t} = \frac{1}{\Delta t} \left(\Delta \rho_{x+\Delta x \rightarrow x}(t) - \Delta \rho_{x \rightarrow x+\Delta x}(t) - \Delta \rho_{x \rightarrow x-\Delta x}(t) + \Delta \rho_{x-\Delta x \rightarrow x}(t) \right) , \quad (6.5)$$

where

$$\begin{aligned} \Delta\rho_{x'\rightarrow x}(t) &:= \begin{cases} \sigma\rho(x', t) & \text{if } \rho(x, t) + \sigma\rho(x', t) \leq \rho_{\max} \\ \rho_{\max} - \rho(x, t) & \text{otherwise} \end{cases} \quad (6.6) \\ &= \Theta(\rho_{\max} - \sigma\rho(x', t) - \rho(x, t)) \sigma\rho(x', t) \\ &\quad + \Theta(\sigma\rho(x', t) + \rho(x, t) - \rho_{\max}) \Theta(\rho_{\max} - \rho(x, t)) (\rho_{\max} - \rho(x, t)) \end{aligned} \quad (6.7)$$

gives the density of food transferred from position x' to position x , as a function of the respective local food densities and is nothing but a continuous version of the food exchange rule Eq. (4.7) in the simulation model (Section 4.1). $\Theta(x)$ is the Heaviside step function. Taking the limit of $\Delta t \rightarrow 0$ gives

$$\begin{aligned} \frac{\partial\rho(x, t)}{\partial t} &= \frac{1}{\Delta t} (\Delta\rho_{x+\Delta x\rightarrow x}(t) - \Delta\rho_{x\rightarrow x+\Delta x}(t) \\ &\quad - \Delta\rho_{x\rightarrow x-\Delta x}(t) + \Delta\rho_{x-\Delta x\rightarrow x}(t)) . \end{aligned} \quad (6.8)$$

By replacing $\rho(x, t)$ in Eq. (6.8) with

$$\rho(x \pm \Delta x, t) = \rho(x, t) \pm \Delta x \frac{\partial\rho(x, t)}{\partial x} + \frac{1}{2} \Delta x^2 \frac{\partial^2\rho(x, t)}{\partial x^2} , \quad (6.9)$$

its Taylor expansion in Δx up to the order $O(\Delta x^2)$, the balance equation (Eq. (6.8)) becomes a diffusion-like spatio-temporal partial differential equation for $\rho(x, t)$. Since the Heaviside functions are not smooth, we regularize them using the identity

$$\Theta(x) = \lim_{k \rightarrow \infty} \Theta_k(x) = \lim_{k \rightarrow \infty} \left(\frac{1}{2} + \frac{1}{\pi} \arctan(kx) \right) . \quad (6.10)$$

By first replacing all $\Theta(x)$ with $\Theta_k(x)$, then expanding $\rho(x, t)$ in Eq. (6.8) with Eq. (6.9), and finally taking the limit $k \rightarrow \infty$, we derive

$$\frac{\partial\rho(x, t)}{\partial t} = D(\rho(x, t)) \frac{\partial^2\rho(x, t)}{\partial x^2} , \quad (6.11)$$

where

$$D := \begin{cases} \sigma \frac{\Delta x^2}{\Delta t} & \text{if } \frac{\rho(x, t)}{\rho_{\max}} (1 + \sigma) < 1 \\ \frac{\Delta x^2}{\Delta t} & \text{if } \frac{\rho(x, t)}{\rho_{\max}} (1 + \sigma) > 1 \end{cases} . \quad (6.12)$$

is a food density dependent diffusion constant.

If the ants are evenly spaced and each ant interacts only with its nearest neighbors, then $\Delta x^2 \approx (L/N)^2$ and $\Delta t = T$. If the ants have more trophallactic partners than their nearest neighbors, Δx^2 would be replaced by $\overline{r^2}$, the ensemble averaged squared distance between an ant and all its possible interaction partners. This is an important geometric property of the system, because it captures the length scale that is important to the diffusion of food between ants with finite interaction radii.

Assuming ants at uniformly distributed random positions on the one-dimensional interval $x \in [0, L]$, this average squared distance can be calculated analytically in the continuous limit. The resulting expression is a function of the interaction radius R , or $\lambda = R/L$ in nondimensional terms.¹ Its derivation is given in Appendix B. The final result is

$$\frac{\overline{r^2}}{L^2} = \begin{cases} -\frac{1}{9}\lambda^3 + \frac{1}{3}\lambda^2 & \text{if } \lambda \in [0, \frac{1}{2}] \\ -\frac{5}{9}\lambda^3 + \lambda^2 - \frac{1}{3}\lambda + \frac{1}{18} & \text{if } \lambda \in [\frac{1}{2}, 1] \end{cases}. \quad (6.13)$$

Equation (6.11) is a diffusion equation with a density dependent diffusion constant (Eq. (6.12)). Using $\Delta x^2 = \overline{r^2}$ and $\Delta t = T$, the effective diffusion constant becomes

$$D = \begin{cases} \frac{\sigma \overline{r^2}}{T} & \text{if } \frac{\rho(x,t)}{\rho_{\max}}(1 + \sigma) < 1 \\ \frac{\overline{r^2}}{T} & \text{if } \frac{\rho(x,t)}{\rho_{\max}}(1 + \sigma) > 1 \end{cases}. \quad (6.14)$$

This means that for densities smaller than the threshold $\rho_{\max}/(1 + \sigma)$, the effective diffusion constant is smaller than for densities larger than that threshold. As a consequence of the finite crop capacity, food thus diffuses effectively faster very close to the nest entrance and not slower, as one might naively expect, because the food densities are higher close to the entrance.

When assuming that the crop capacity is not exactly the same for every ant, such that $\rho_{\max,i} = \rho_{\max} + \xi_i$ with ξ_i drawn from a Gaussian distribution with width τ , the discontinuous step in Eq. (6.11) is smoothed out into a sigmoidal of width τ after averaging over Eq. (6.8). Equation (6.11) then becomes

$$\frac{\partial \rho(x, t)}{\partial t} = \langle D(\rho(x, t)) \rangle \frac{\partial^2 \rho(x, t)}{\partial^2 x}, \quad (6.15)$$

¹In 1D, the interaction radius R simply defines the maximum distance to the left or to the right of an ant's position, at which it can exchange food with other ants.

with the averaged diffusivity

$$\langle D(\rho(x, t)) \rangle = \frac{1}{2} \left(\sigma + 1 + (\sigma - 1) \operatorname{erf} \left(\frac{\rho_{\max} - \rho(x, t)(1 + \sigma)}{\sqrt{2}\tau} \right) \right) \frac{\Delta x^2}{\Delta t}, \quad (6.16)$$

where $\operatorname{erf}(x)$ is the standard error function. As $\tau \rightarrow 0$, Eq. (6.11) is recovered.

6.2 Diffusion approximation solutions

In the previous section, we showed an estimate of the effective diffusion constant in the nest, and saw that the diffusion constant depends on the food concentration in the nest (cf. Eq. (6.14)). Solving the derived diffusion equation (Eq. (6.11)) analytically is not straightforward.

We therefore assume that in the initial stages of the trophallactic process the majority of the ants far from the source are not full, (in particular that $\rho(x, t) < \rho_{\max}/(1 + \sigma)$), so that the diffusion constant is

$$D = \frac{\sigma \overline{r^2}}{T}. \quad (6.17)$$

In reality, the diffusion constant should switch to its high food density value near the source (see Eq. (6.11)), but for simplicity, we will just consider D to be constant in space and time in the following derivations of this section.

In addition, it is a priori unclear how to handle the food source. At first sight, the food supply of the nest f_{\max} could be treated as an initial condition of the diffusion equation, e.g. a delta distribution located at the nest entrance ($\rho(x = 0, t = 0) = \delta(x)f_{\max}$). However, this would turn the nest entrance into yet another food carrying point in space, indistinguishable from the ants. But that is not the case, since the nest entrance cannot receive food and does not have a carrying capacity. The food located at the nest entrance is not really part of the system, which is why it should rather be treated either as a boundary condition or as a source term of the diffusion equation. We explore these two possibilities in this section.

In Section 6.2.1, we model the food source as a boundary condition, fixing the amount of food at the nest entrance. And in Section 6.2.2, we model the source as an explicit source term, continuously disbursing food into the nest. We derive a predictions for the global food intake rate that defines a fundamental time scale in both cases and show that they are in agreement.

6.2.1 Food source as a boundary condition

At the source, ants should be at carrying capacity. This means that the source can be implemented as a boundary condition. Namely, if the source is at $x = 0$, we fix $\rho(0, t) = \rho_{\max}$. We therefore have to solve the standard diffusion equation without a source term in a 1D finite system. The appropriate boundary and initial conditions are

$$\rho(x, 0) = 0 \text{ for } x \in (0, L] \quad (6.18)$$

(initially, there is no food in the system), and

$$\rho(0, t) = \rho_{\max}, \quad \left. \frac{\partial \rho(x, t)}{\partial x} \right|_{x=L} = 0 \quad (6.19)$$

(at $x = 0$ the source fixes the food density to its maximum, and at $x = L$ a reflective wall allows no flux across the system boundary).

The solution can be found using standard methods (see Appendix C.1) and expressed as a series:

$$\frac{\rho(x, t)}{\rho_{\max}} = 1 - \frac{4}{\pi} \sum_{n=1}^{\infty} \frac{\sin\left(\frac{(2n-1)\pi x}{2L}\right)}{2n-1} e^{-\left(\frac{(2n-1)\pi}{2L}\right)^2 Dt}. \quad (6.20)$$

Keeping only the dominant first term ($n = 1$), the solution reads:

$$\rho(x, t) \approx \rho_{\max} \left[1 - \frac{4}{\pi} \sin\left(\frac{\pi x}{2L}\right) e^{-\left(\frac{\pi}{2L}\right)^2 Dt} \right]. \quad (6.21)$$

In Fig. 6.3, we compare Eq. (6.20) (solid lines) and Eq. (6.21) (dashed lines) for times $t = 0.001L^2/D$, $t = 0.1L^2/D$ and $t = 0.5L^2/D$. We see that for large enough times, Eq. (6.21) is an excellent approximation of Eq. (6.20).

Note also that the overall shape of the spatial food distribution and its time dependence qualitatively match the small λ simulations displayed in Fig. 6.2. However, this continuum approach cannot capture the very interesting dynamics of the food distribution among individual ants (cf. histograms in Fig. 6.2). For example, we see that in several regimes the spatially binned average food concentration is not a good indicator of the actual food concentration of individual ants at that location (eg. Fig. 6.2(a1)). Although $\langle c(t=10) \rangle_{x=0.1} \approx 0.75$, there are no individual ants in the bin $x \in [0.05, 0.1]$ with $c_i(t=10) = 0.75$. Instead, the food is distributed bimodally among the ants at that location, with approximately 75% of the ants

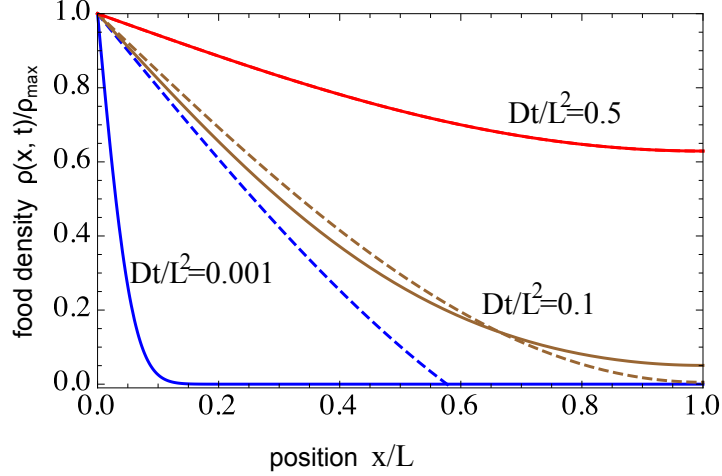


Figure 6.3: Analytic predictions of the spatial food distribution for times $t = 0.001L^2/D$ (blue line, bottom), $t = 0.1L^2/D$ (brown line, middle), and $t = 0.5L^2/D$ (red line, top). Solid lines show the full solution (Eq. (6.20)) and dashed lines the first order approximation (Eq. (6.21)). The dashed line for $t = 0.5L^2/D$ overlaps with the solid line and is not visible.

at capacity and 25% empty. The mean of this bimodal distribution is hence not informative, but the continuum approach cannot predict these variations around the mean.

From Eq. (6.20), we can calculate $\langle c(t) \rangle$ by integration, keeping only the slowest decaying term. The approximate average food density in the system is then found to be

$$\langle \rho(t) \rangle \approx \rho_{\max} \left(1 - \frac{8}{\pi^2} e^{-\left(\frac{\pi}{2L}\right)^2 Dt} \right), \quad (6.22)$$

and the mean squared food distance

$$\overline{\text{MSD}}(t) \approx 1 - \frac{96(\pi - 2)}{\pi^4} e^{-\left(\frac{\pi}{2L}\right)^2 Dt}. \quad (6.23)$$

Associating the resulting exponential decay constant $\left(\frac{\pi}{2L}\right)^2 D$ with the food intake rate γ of Eq. (5.13) yields

$$\gamma = \left(\frac{\pi}{2L} \right)^2 D. \quad (6.24)$$

Substituting the initial assumption of a constant diffusivity $D = \sigma \overline{r^2}/T$ (cf. Eq. (6.17)), we obtain an analytic prediction for the global food intake rate that

will prove to be remarkably universal and thus marks an important achievement of this thesis:

$$\gamma \sim \frac{\sigma \overline{r^2}}{TL^2} . \quad (6.25)$$

For equidistant agents with nearest neighbor interactions, using $\overline{r^2} = (L/N)^2$, this reduces to

$$\gamma \sim \frac{\sigma}{TN^2} . \quad (6.26)$$

6.2.2 Food source as a source term

In this section, we consider the alternative case of modeling the food source as an explicit source term of the diffusion equation. We use this approach to estimate an upper bound on the food intake rate γ .

For computational ease, we approximate the 1D system to be bounded on only one side ($x \geq 0$), with the source being located at that boundary ($x = 0^+$). The diffusion equation that governs the dynamics of the system then reads

$$\frac{\partial \rho(x, t)}{\partial t} = D \frac{\partial^2 \rho(x, t)}{\partial x^2} + q(x, t), \quad (6.27)$$

where $\rho(x, t)$ is the food density, D the diffusivity, and $q(x, t)$ the source term.

We assume food to be taken up at the single point $x = 0$ at an exponential rate with unknown exponent γ , similarly to what is observed in experiments [10]. Also, we again focus on the initial stages of the trophallactic process, assuming a constant $D = \sigma \overline{r^2}/T$ as in Eq. (6.17). As we showed in Chapter 5, the average food concentration inside the nest follows an exponential saturation dynamics (cf. Eq. (5.8) and Figs. 5.1 and 5.2). The amount of food remaining at the nest entrance thus decays approximately exponentially in time. If the total amount of food available initially is f_{\max} (as introduced in Section 6.1.2, cf. Eq. (6.2)), then the total amount of food still available at the source at time t is $f_{\max} e^{-\gamma t}$ and the source term reads

$$\begin{aligned} q(x, t) &= -\frac{\partial}{\partial t} f_{\max} e^{-\gamma t} 2\delta(x) \\ &= 2\gamma f_{\max} e^{-\gamma t} \delta(x) . \end{aligned} \quad (6.28)$$

where $\delta(x)$ the Dirac delta distribution, as the nest entrance is located at $x = 0^+$.

6 Diffusive Limit

For normalization purposes we include a factor of 2 in Eq. (6.28), because

$$\int_0^\infty \delta(x) dx = \frac{1}{2}. \quad (6.29)$$

Equation (6.27) can be nondimensionalized by choosing the time scale s_t , length scale s_x and food density scale s_ρ to be

$$s_t = \frac{1}{\gamma}, \quad s_x = \sqrt{\frac{D}{\gamma}} \quad \text{and} \quad s_\rho = 2f_{\max}/s_x. \quad (6.30)$$

Denoting a nondimensional variable as $\tilde{X} := \frac{X}{s_x}$, Eq. (6.27) becomes

$$\frac{\partial \tilde{\rho}(\tilde{x}, \tilde{t})}{\partial \tilde{t}} = \frac{\partial^2 \tilde{\rho}(\tilde{x}, \tilde{t})}{\partial \tilde{x}^2} + e^{-\tilde{t}} \delta(\tilde{x}). \quad (6.31)$$

With a reflective boundary condition

$$\left. \frac{\partial \rho(\tilde{x}, \tilde{t})}{\partial \tilde{x}} \right|_{\tilde{x}=0} = 0 \quad (6.32)$$

at the only system boundary $\tilde{x} = 0$, and no initial food

$$\rho(\tilde{x}, 0) = 0 \quad \text{for} \quad \tilde{x} \geq 0, \quad (6.33)$$

the general solution of the semi-infinite system $\tilde{x} \in [0, \infty)$ in nondimensional terms is

$$\tilde{\rho}(\tilde{x}, \tilde{t}) = \int_0^\infty d\tilde{x}' \int_0^{\tilde{t}} d\tilde{t}' \tilde{K}(\tilde{x}, \tilde{x}', \tilde{t} - \tilde{t}') e^{-\tilde{t}'} \delta(\tilde{x}'), \quad (6.34)$$

where

$$\tilde{K}(\tilde{x}, \tilde{x}', \tilde{t}) := \frac{1}{\sqrt{4\pi\tilde{t}}} e^{-\frac{(\tilde{x}-\tilde{x}')^2}{4\tilde{t}}} \quad (6.35)$$

is the heat kernel of Eq. (6.31). Equation (6.34) integrates to the final nondimensional solution

$$\tilde{\rho}(\tilde{x}, \tilde{t}) = e^{-\tilde{t}} \left[-\frac{1}{2} \operatorname{Im} \left(e^{i\tilde{x}} \operatorname{erfc} \left(\frac{\tilde{x}}{2\sqrt{\tilde{t}}} + i\sqrt{\tilde{t}} \right) \right) \right], \quad (6.36)$$

where

$$\operatorname{erfc}(z) := 1 - \operatorname{erf}(z) \quad (6.37)$$

is the complementary error function, and $\operatorname{Im}(z)$ denotes the imaginary part of z . The full derivation is given in Appendix C.2.

Some simpler analytic approximations can be derived from Eq. (6.36) by considering the limits of the complementary error function. For large times and far from the source,

$$\rho(\tilde{x}, \tilde{t}) \approx \frac{1}{2} \sqrt{\frac{\tilde{t}}{\pi}} \frac{1}{\left(\frac{\tilde{x}^2}{4\tilde{t}} + \tilde{t}\right)} e^{-\frac{\tilde{x}^2}{4\tilde{t}}} \quad (6.38)$$

approximates Eq. (6.36) well, whereas for short times and close to the source

$$\rho(\tilde{x}, \tilde{t}) \approx 2\sqrt{\frac{\tilde{t}}{\pi}} e^{-\frac{\tilde{x}^2}{4\tilde{t}}} - |\tilde{x}| e^{-\tilde{t}} \quad (6.39)$$

is a good approximation.

We now explore the relationship between the food intake rate γ and the food diffusivity D under consideration of the finite food density capacity. The higher γ is, the faster the nest absorbs food from the source. However, a very large γ would lead to a very large food density $\rho(x, t)$ in the vicinity of the nest entrance, which contradicts the finite carrying capacity. This interplay gives an upper limit for γ that is consistent with the finite food density capacity ρ_{\max} . In the remainder of this section, we derive this upper limit.

Going back to dimensional notation, Eq. (6.36) evaluated near the source ($x \rightarrow 0$) reads

$$\rho(0, t) = -f_{\max} \sqrt{\frac{\gamma}{D}} e^{-\gamma t} \operatorname{Im} \left(\operatorname{erfc} (i\sqrt{\gamma t}) \right) . \quad (6.40)$$

Since $\gamma t \geq 0$,

$$\operatorname{Im} \left(\operatorname{erfc} (i\sqrt{\gamma t}) \right) = -\frac{2}{\sqrt{\pi}} \int_0^{\sqrt{\gamma t}} e^{-z^2} dz , \quad (6.41)$$

and Eq. (6.40) becomes

$$\rho(0, t) = \frac{2f_{\max}}{\sqrt{\pi}} \sqrt{\frac{\gamma}{D}} e^{-\gamma t} \int_0^{\sqrt{\gamma t}} e^{-z^2} dz . \quad (6.42)$$

The finite crop capacity is reached at a time t_f , such that

$$\rho(0, t_f) = \rho_{\max}. \quad (6.43)$$

The time t_f when this equality is fulfilled depends on γ and σ . A large γ or a small σ will lead to fast food saturation near the source and vice versa.

In fact, for every time t , the food density near the source has to be less than or equal to ρ_{\max} , so that

$$\rho(0, t) \leq \rho_{\max} \quad (6.44)$$

$$\Leftrightarrow \tilde{\rho}(0, \tilde{t}) \leq \frac{\rho_{\max}}{s_\rho} = \frac{\rho_{\max}}{2f_{\max}} \sqrt{\frac{D}{\gamma}} = \frac{1}{2L} \sqrt{\frac{D}{\gamma}} \quad (6.45)$$

$$\Leftrightarrow \gamma \leq \frac{D}{(2L\tilde{\rho}(0, \tilde{t}))^2}, \quad (6.46)$$

where the tildes denote dimensionless quantities again, s_ρ is taken from Eq. (6.30), and the relation $f_{\max} = L\rho_{\max}$ (cf. Eq. (6.2)) was used.

By numerically evaluating Eq. (6.42), we find that the dimensionless food density at the origin $\tilde{\rho}(0, \tilde{t})$ initially increases, reaches the maximum value of $\tilde{\rho}(0, \tilde{t}) \approx 0.31$ and then decreases as the finite amount of food at the source diffuses to infinity. Due to Eq. (6.46), every value of $\tilde{\rho}(0, \tilde{t})$ results in a different upper limit for γ . Hence, if γ is constant throughout the process, the upper bound for γ is given through the minimum value of $1/(\tilde{\rho}(0, \tilde{t}))^2$ in time, because D and L are constant as well:

$$\gamma \leq \frac{D}{(2L\tilde{\rho}(0, \tilde{t}))^2} \lesssim 10.4 \frac{D}{(2L)^2} \forall \tilde{t}. \quad (6.47)$$

This is consistent with the food intake rate derived for the finite system with the food source modeled as a boundary condition (Eq. (6.24)), because $\pi^2 \approx 9.87 < 10.4$.

The D/L^2 dependency of γ is not surprising, as it could have been easily predicted by considering the dimensionless groups that can be constructed with the equation parameters γ , D and L . However, note that L is not an explicit length scale of the semi-infinite system presented in this section, but enters Eq. (6.46) only through the equation relating the total amount of food f_{\max} and the food density capacity ρ_{\max} (Eq. (6.2)). If Eq. (6.2) is not used, Eq. (6.46) can be re-expressed as

$$\gamma \lesssim 10.4 \frac{D\rho_{\max}^2}{(2f_{\max})^2}. \quad (6.48)$$

Thus, we have shown how the diffusion coefficient and the implicit system length scale provide an upper bound for the global food intake rate.

6.3 Comparison of simulations and analytic predictions

The analytic prediction of the global food intake rate γ in the diffusive limit (Eq. (6.25)) gives a characteristic time scale $1/\gamma$ of the system that can be used to rescale the simulation results in a systematic way.

In this section, we show that this rescaling leads to an at least partial collapse on a master curve of the simulation data for various parameters. The collapse is not only observed for the 1D system, but for the 2D simulations as well, and consistently shows in the average food concentration (Section 6.3.1), the mean squared food distance (Section 6.3.2), and the food concentration variance (Section 6.3.3). Finally, Section 6.3.4 shows how the simulated food intake time scale relates to the analytic prediction of γ in the diffusive limit derived in this chapter and the γ prediction in the mean-field limit (Eq. (5.12) in Section 5.3).

6.3.1 Average food concentration

In Fig. 6.4 we plot the simulated average food concentration $\langle c(t) \rangle$ for a range of parameters in a 1D (panels (a) and (b)) and a 2D system (panels (c) and (d)). In panel (a) and (c) we plot $\langle c(t) \rangle$ as a function of t/T (time nondimensionalized with the refractory period), whereas in panel (b) and (d), we rescale the time to the nondimensional rescaled time γt using

$$\gamma \sim \frac{\overline{\sigma r^2}}{TL^2} \quad (6.49)$$

from Eq. (6.25).

We find a relatively good collapse of the data after an initial period where the dynamics is dominated by direct source food intakes from agents in range of the source. This indicates that despite the oversimplifications of the continuous analytic diffusion approximation, the time scale

$$\frac{1}{\gamma} = \frac{TL^2}{\overline{\sigma r^2}} \quad (6.50)$$

captures the dynamics of the discrete agent-based simulation model.

Note that the 2D rescaled data curves collapse in terms of the food exchange ratio σ , but separate in terms of the interaction range parameter λ . This indicates

6 Diffusive Limit

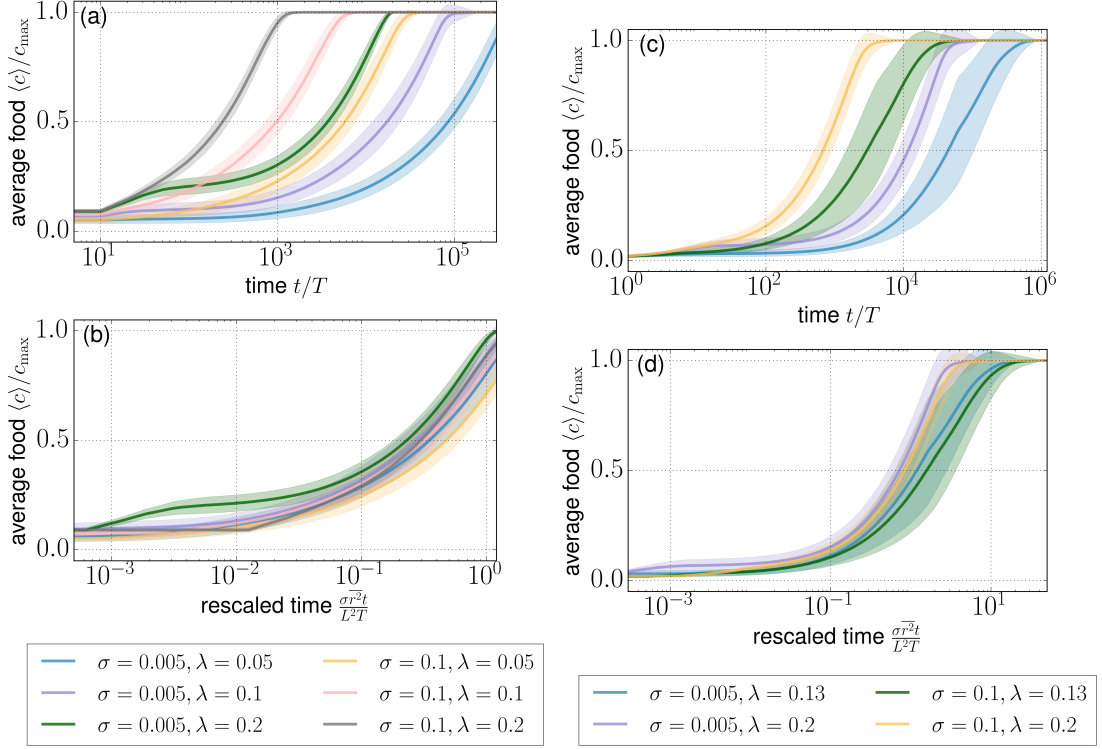


Figure 6.4: Normalized average food concentration $\langle c \rangle / c_{\max}$ in a 1D (left column) and a 2D system (right column): (a)/(c) as a function of time t/T and (b)/(d) as a function of rescaled time γt , for various food exchange ratios σ and interaction range parameters λ . After rescaling the time with Eq. (6.25), the curves collapse to a good degree. The width of the shaded area around each line indicates the standard deviation.

a good predictive power of the linear σ dependency of the 1D scaling Eq. (6.25) even in 2D systems, but less predictive power of the λ dependent \bar{r}^2/L^2 part. Since the latter was derived from the 1D geometry, a loss of predictive power going from 1D to 2D is to be expected and could possibly be improved through including the more complicated geometric constraints of the 2D system.

6.3.2 Mean squared food distance

Analogue to Fig. 6.4, we plot the normalized mean squared food distance $\overline{\text{MSD}}(t)$ in Fig. 6.5 for a range of parameters in a 1D (panels (a) and (b)) and a 2D (panels (c) and (d)) system. Again, in panel (a) and (c) we plot the observable as a function of t/T (time nondimensionalized with the refractory period), whereas in panel (b) and (d), we rescale the time to the nondimensional rescaled time γt using Eq. (6.25). The same collapse as described in Section 6.3.1 can be observed.

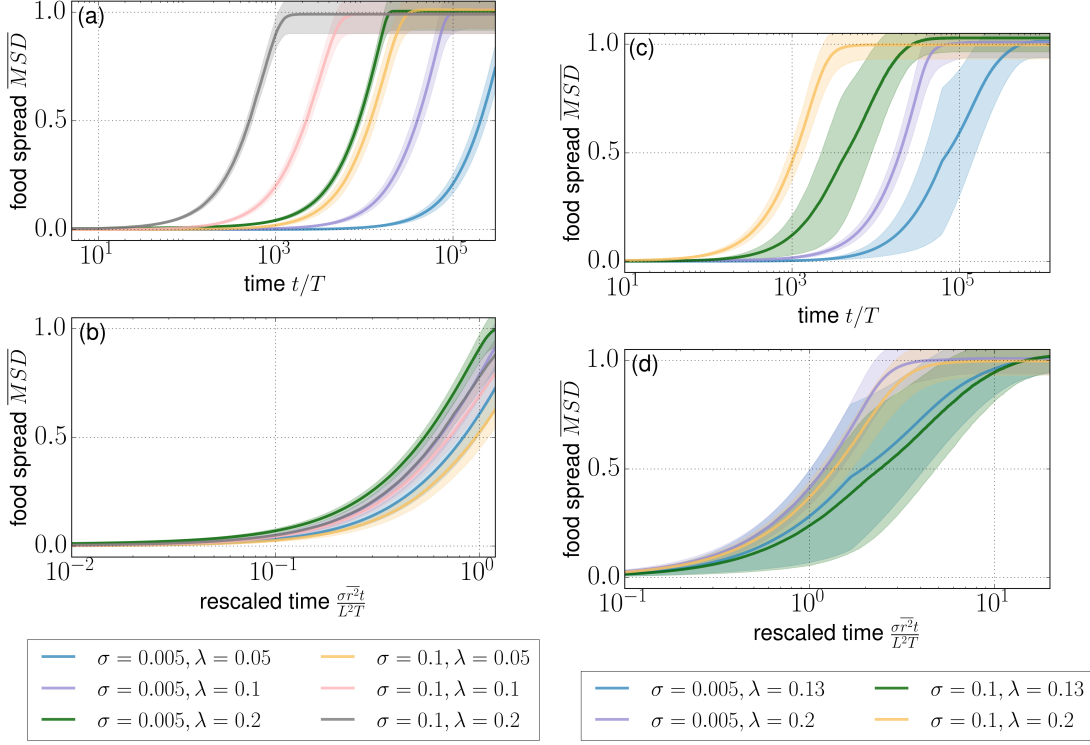


Figure 6.5: Normalized mean squared food distance \overline{MSD} in a 1D (left column) and a 2D system (right column): (a)/(c) as a function of time t/T and (b)/(d) as a function of rescaled time γt , for various food exchange ratios σ and interaction range parameters λ . After rescaling the time with Eq. (6.25), the curves collapse on the same master curve. The width of the shaded area around each line indicates the standard deviation.

6.3.3 Food concentration variance

Analogue to Figs. 6.4 and 6.5, we plot the simulated food concentration variance $\langle c(t)^2 \rangle$ in Fig. 6.6 for a range of parameters in a 1D (panels (a) and (b)) and a 2D (panels (c) and (d)) system. Again, in panel (a) and (c) we plot the observable as a function of t/T (time nondimensionalized with the refractory period), whereas in panel (b) and (d), we rescale the time to the nondimensional rescaled time γt using Eq. (6.25).

In contrast to the average food, we only find a good collapse of the data at the later stages of the dynamics, starting just before $\langle c(t)^2 \rangle$ reaches its maximum. We therefore shortly discuss the simulated variance dynamics in the rest of this section.

The food variance $\langle \Delta c(t)^2 \rangle$ is a proxy of how well the available food is distributed among the ants in the colony, independent of their spatial position. After an initial increase, the variance plateaus for some time, until it reaches a maximum approximately at a time $\gamma t \approx 0.2$ (for 1D) or $\gamma t \approx 1$ (for 2D). This roughly matches

6 Diffusive Limit

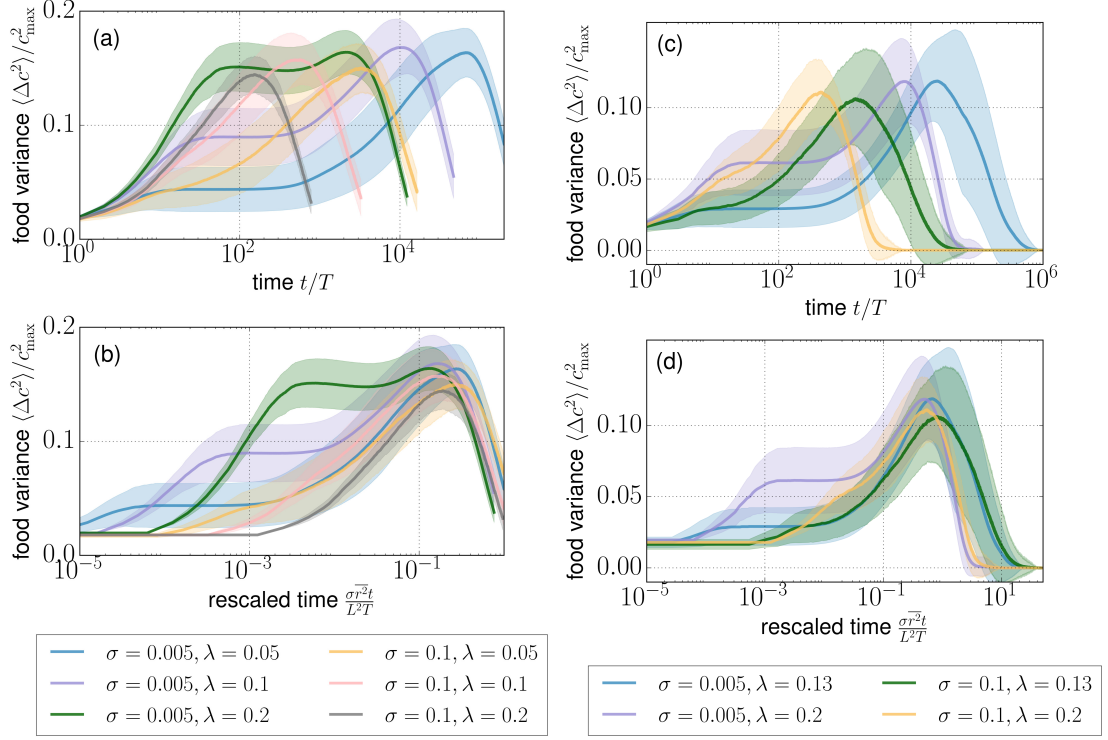


Figure 6.6: Normalized food variance $\langle \Delta c(t)^2 \rangle / c_{\max}^2$ in a 1D (left column) and a 2D system (right column): (a)/(c) as a function of time t/T and (b)/(d) as a function of rescaled time γt , for various food exchange ratios σ and interaction range parameters λ . After rescaling the time with Eq. (6.25), the curves collapse on the same master curve at the later stages of the dynamics. The variable shapes and plateau sizes of the initial stages of the dynamics reflect the complicated spatial food distributions presented in Figs. 6.1 and 6.2. The width of the shaded area around each line indicates the standard deviation.

$\gamma t_{1/2}$, the rescaled time when the colony is half full. After that time, the variance is monotonically decreasing, as the food is distributed better, due to the emerging saturation of the colony.

At the beginning of the food dissemination process, the behavior of the variance showcased in Fig. 6.6 reflects the food intake dynamics when there is no saturation near the source. During the initial sharp increase of the small σ curves, the ants inside the interaction radius of the source, initially all empty, quickly take up food at a rate similar to the mean-field model prediction $\gamma_{\lambda=1} = 1/(NT)$ (cf. Eq. (5.12)). As σ is small, the rate at which the food diffuses away from that zone is slower than the fast intake of food at the entrance. Consequently, $\langle \Delta c(t)^2 \rangle$ increases quickly, and a growing proportion of the ants near the entrance reaches saturation. The food intake rate of the area near the source then becomes approximately equal

to the rate at which the food diffuses out of that zone, and the slope of $\langle \Delta c(t)^2 \rangle$ decreases. Eventually, when that area is close to saturation, it acts as an effective boundary condition $\rho(R, t) = \rho_{\max}$, and the food diffuses to the rest of the nest as a propagating front (as can be seen in Fig. 6.2 (a₁)-(a₃)). This clear separation of the two time scales happens only for small σ . For large σ , the plateau disappears.

Since for relatively small σ the front between the ants that are at capacity (to the left of the propagating front of Fig. 6.2) is relatively sharp, we can approximate the normalized variance as $\langle \Delta c(t)^2 \rangle / c_{\max}^2 \approx n/N - (n/N)^2$, where n is the number of ants at capacity (similarly to the approach of Section 5.2). This is maximized when $n = N/2$, i.e. when the colony is half full, in agreement with the simulation results of Figs. 6.4 and 6.6.

6.3.4 Global food intake time scale

The time $t_{1/2}$ it takes the colony to acquire half of the available food provides a reasonable time scale of the global food intake. We therefore plot this half-time in Fig. 6.7 for a range of parameters in a 1D (panels (a) and (b)) and a 2D (panels (c) and (d)) simulation system. Similarly to the previous sections, but now on the y-axis, we plot the observable nondimensionalized with the refractory period in panel (a) and (c), and rescaled with Eq. (6.25) in panel (b) and (d).

In panel (a) and (c), we see that the half-time decreases with increasing food exchange ratio σ and interaction range parameter λ . Latter is a proxy of how well mixed the colony is (or alternatively how broad the spatial fidelity zones of the ants are), so less spatial separation leads to a faster global food intake. Additionally, we see that the half-time $t_{1/2}$ dependence on σ declines with increasing λ , as food exchanges between ants become less important than feeding from the source. For large interaction ranges, the half-time tends to $t_{1/2}/T = \ln(2)/(\gamma_{\lambda=1}T) \approx 70$, as can be deduced from (5.8).

In panel (b) and (d), we can observe a collapse of the simulation data for small interaction ranges. The half-time is approximately $\gamma t_{1/2} \approx 0.2$ for 1D and $\gamma t_{1/2} \approx 1$ for 2D.

The two analytically predicted food intake rates $\gamma = (\overline{\sigma r^2})/(TL^2)$ (Eq. (6.25)) and $\gamma_{\lambda=1} = 1/(NT)$ have therefore proven to capture the global food intake time scale in the respective limits of small (diffusive) and large (mean-field) interaction ranges, independent of σ .

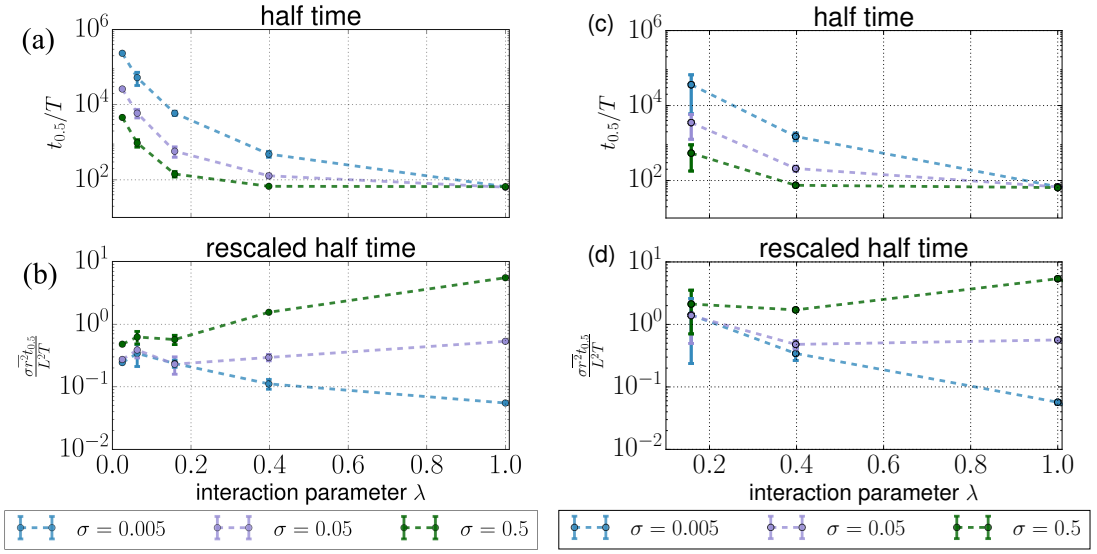


Figure 6.7: (a)/(c) Nondimensional time $t_{1/2}/T$ and (b)/(d) rescaled nondimensional time $\gamma t_{1/2}$ until the average food in the colony reaches $0.5c_{\max}$ as a function of the interaction range parameter λ for different food exchange ratios σ in a 1D (left column) and a 2D system (right column). The half-time decreases with increasing λ and σ . The σ and λ dependence of $t_{1/2}$ is at least roughly predicted by the scaling of Eq. (6.25) for a large parameter range. For high λ , the σ dependence gradually disappears, and Eq. (6.25) fails to explain the behavior. In that limit, the relevant time scale is predicted by Eq. (5.12).

7 Master Equation Description

This last chapter of Part II contains yet another analytic approach to describe trophallaxis dynamics: a probabilistic master equation description. The strength this approach will show is a time resolved prediction of the observables, even for parameter sets beyond the scope of the mean-field and diffusive limit cases. This is particularly useful for intermediate interaction ranges that are too small for a mean-field approximation and too large for a diffusion approximation. The downside of the master equation description is its analytic complexity that only allows numeric solutions of the full dynamics description, even without explicit motion.

All the equations presented in this chapter make use of the continuum variables introduced in Section 6.1.2 and approximate the system to a one-dimensional interval of length L , similar to the diffusion approximation (cf. Section 6.1). The agent-based food concentrations at discrete positions in space used in the simulation model are therefore replaced by spatial food densities, to enable a description that is continuous in food, space and time. We start with the derivation of a basic differential equation that describes the time evolution of the food density as a function of space and time in the absence of carrying capacities and food sources in Section 7.1. In Section 7.2, we then proceed with extending the basic equation to also include capacity limits on the food density and a source term that correctly describes the flow of food into the colony. Numerical solutions of this complete analytic description are then compared to our simulation results in Section 7.3.

7.1 Basic equation without carrying capacity and source term

In this section, we present the first step towards a master equation description of our agent-based trophallaxis simulation. It is a first step, because the food carrying capacities are not included, and the food flow into the nest is not yet modeled as a source term. A simple food inflow could be incorporated as a boundary condition of this basic master equation, although we do not show this here. The purpose of the equation derived in this section is to lay ground for the full equation that we

develop in Section 7.2. Due to its simplifications, the basic equation of this section is however still solvable analytically, in contrast to the full equation. We give a formal solution, after introducing the basic master equation description.

7.1.1 Governing equation

In the continuum limit, the spatial food density dynamics $\rho(x, t)$ can be approximated by the following phenomenological partial integro-differential equation (without taking carrying capacities into account):

$$\frac{\partial \rho(x, t)}{\partial t} = - \underbrace{\frac{\sigma}{T} \rho(x, t)}_{\text{food outflow}} + \underbrace{\frac{\sigma}{T} \int_0^L dx' K_{x' \rightarrow x} \rho(x', t)}_{\text{food inflow}}, \quad (7.1)$$

where $\sigma \rho(x, t)$ is the expected food density fraction flowing away from the position x per time interval T ; L is the length of the 1D system; and $K_{x' \rightarrow x}$ is a kernel function, describing the food density fraction measured in units of $\sigma \rho(x', t)/T$ flowing from the position x' to the position x per interaction range and time interval T . The unit of $K_{x' \rightarrow x}$ is inverse length. Equation (7.1) is derived by taking the limits $T \rightarrow 0$ and $\sigma \rightarrow 0$, while keeping $\sigma \rho(x, t)/T$ fixed.

Although we omit a formal derivation, Eq. (7.1) can be interpreted as a master equation when normalized with the maximum food density. The spatial positions $x \in [0, L]$ then represent a continuum of system states and the normalized food densities $\rho(x, t)/\rho_{\max}$ become probabilities describing the occupation of these states. The transition rates between the states are then defined by the kernel $K_{x' \rightarrow x}$. Whenever we name our equations for the food density time evolution ‘master equation’, we implicitly refer to this interpretation.

In contrast to the mean-field model, we can now define the spatial kernel function $K_{x' \rightarrow x}$ to limit the interaction range of the food exchanges (or food density flows, in continuous terms). We will therefore refer to it as the ‘interaction kernel’.

In order to derive $K_{x' \rightarrow x}$, we start of by imagining the system to be the infinite real line. The interaction kernel would then be

$$K_{x' \rightarrow x}^{[-\infty, \infty]} = \begin{cases} \frac{1}{2R} & \text{if } |x - x'| < R \\ 0 & \text{otherwise} \end{cases} \quad (7.2)$$

$$= \frac{\Theta(x - x' + R)\Theta(x' + R - x)}{2R}, \quad (7.3)$$

where R is the interaction range and $\Theta(x)$ is the Heaviside step function. Similarly, if the system would be a half-infinite line with a boundary at $x = 0$, the kernel

would be

$$K_{x' \rightarrow x}^{[0, \infty]} = \begin{cases} \frac{1}{x'+R} & \text{if } 0 < x' < R \text{ and } |x - x'| < R \\ \frac{1}{2R} & \text{if } R < x' \text{ and } |x - x'| < R \\ 0 & \text{otherwise} \end{cases} \quad (7.4)$$

$$= \underbrace{\Theta(R - x')\Theta(x')\frac{\Theta(x)\Theta(x' + R - x)}{x' + R}}_{\text{within left boundary range}} + \underbrace{\Theta(x' - R)K_{x' \rightarrow x}^{[-\infty, \infty]}}_{\text{out of boundary range}}. \quad (7.5)$$

The left boundary term comes from the fact that ants close to the boundary have fewer other ants to choose from, when they want to transfer food. For the real model system, a two-sided bounded interval of length L is needed. That adds another term for the right boundary, analogue to the left boundary term in Eq. (7.5):

$$K_{x' \rightarrow x} = \begin{cases} \frac{1}{x'+R} & \text{if } 0 < x' < R \text{ and } |x - x'| < R \\ \frac{1}{2R} & \text{if } R < x' < (L - R) \text{ and } |x - x'| < R \\ \frac{1}{L+R-x'} & \text{if } (L - R) < x' < L \text{ and } |x - x'| < R \\ 0 & \text{otherwise} \end{cases} \quad (7.6)$$

$$= \underbrace{\Theta(R - x')\Theta(x')\frac{\Theta(x)\Theta(x' + R - x)}{x' + R}}_{\text{within left boundary range}} \quad (7.7)$$

$$+ \underbrace{\Theta(x' - R)\Theta(L - R - x')K_{x' \rightarrow x}^{[-\infty, \infty]}}_{\text{out of boundary range}} \quad (7.8)$$

$$+ \underbrace{\Theta(x' - L + R)\Theta(L - x')\frac{\Theta(x - x' + R)\Theta(L - x)}{L + R - x'}}_{\text{within right boundary range}} \quad (7.9)$$

$$= \frac{\Theta(R - x')\Theta(x')\Theta(x)\Theta(x' + R - x)}{x' + R} \quad (7.10)$$

$$+ \frac{\Theta(x' - R)\Theta(L - R - x')\Theta(x - x' + R)\Theta(x' + R - x)}{2R} \quad (7.11)$$

$$+ \frac{\Theta(x' - L + R)\Theta(L - x')\Theta(x - x' + R)\Theta(L - x)}{L + R - x'}. \quad (7.12)$$

This Kernel is only valid for $R \leq L/2$. In the following, only $K_{x' \rightarrow x}$ will be used.

It effectively splits the food inflow integral of Eq. (7.1) into three consecutive integrals over the intervals $[0, R]$, $[R, (L - R)]$, and $[(L - R), L]$, weighted with the

respective interaction ranges $x' + R$, $2R$ and $L + R - x'$.

7.1.2 Formal analytic solution

The presented basic master equation (Eq. (7.1)) is a partial integro-differential equation. In order to solve the equation, it can be simplified by transforming it into a system of coupled ordinary differential equations. This is achieved through discretizing it in space, so that

$$\rho(x, t) \rightarrow \rho(x_i, t) =: \rho_i(t) \quad \text{and} \quad (7.13)$$

$$K_{x' \rightarrow x} \rightarrow K_{x_j \rightarrow x_i} =: K_{ij} , \quad (7.14)$$

with $x_i = i\Delta x \forall i \in [0, n - 1]$, where Δx is chosen, such that $L = n\Delta x$. Equation (7.1) then becomes

$$\frac{d\rho_i(t)}{dt} = -\frac{\sigma}{T}\rho_i(t) + \frac{\sigma}{T} \sum_{j=0}^{n-1} K_{ij}\rho_j(t)\Delta x \quad (7.15)$$

$$= \frac{\sigma}{T} \sum_{j=0}^{n-1} \underbrace{[-\delta_{ij} + K_{ij}\Delta x]}_{=: m_{ij}} \rho_j(t) , \quad (7.16)$$

which can be rewritten in vector notation, abbreviating the operator matrix of elements m_{ij} with $M := (m_{ij})_{i=0, \dots, n-1; j=0, \dots, n-1}$:

$$\frac{d\vec{\rho}(t)}{dt} = \frac{\sigma}{T} M \vec{\rho}(t) . \quad (7.17)$$

This system of coupled ordinary differential equations is linear and can be solved by an exponential ansatz. The solution reads

$$\vec{\rho}(t) = \exp\left(\frac{\sigma}{T} M\right) \vec{\rho}(0) . \quad (7.18)$$

7.2 Full equation with carrying capacity and source term

The basic master equation description presented in Section 7.1 does not include finite carrying capacities and has no expression for the food source. In this section, we present an enhanced version of Eq. (7.1) that provides a full description of the system modeled in our simulations. We derive this full master equation in two steps: first, adding the carrying capacity; and second, adding the source term.

7.2.1 Carrying capacity

The finite carrying capacity of the ants can be described through limiting the local food density $\rho(x, t) \leq \rho_{\max}$ in the continuum description of the master equation. We achieve this through replacing the expected food density fraction $\sigma\rho(x, t)$ that is transferred during trophallaxis with a second integration kernel

$$\Delta\rho_{x' \rightarrow x}(t) := \begin{cases} \sigma\rho(x', t) & \text{if } \rho(x, t) + \sigma\rho(x', t) \leq \rho_{\max} \\ \rho_{\max} - \rho(x, t) & \text{otherwise} \end{cases} \quad (7.19)$$

$$= \Theta(\rho_{\max} - \sigma\rho(x', t) - \rho(x, t)) \sigma\rho(x', t) \quad (7.20)$$

$$+ \Theta(\sigma\rho(x', t) + \rho(x, t) - \rho_{\max}) \Theta(\rho_{\max} - \rho(x, t)) (\rho_{\max} - \rho(x, t)) , \quad (7.21)$$

that will be called 'food exchange kernel'. It gives the density of food transferred from position x' to position x , as a function of the respective local food densities and is nothing but the continuous version of the food exchange rule Eq. (4.7) in the simulation model (Section 4.1) that has already been used for the diffusion approximation in Section 6.1 (Eq. (6.6)). Note that, in contrast to the interaction kernel, $\Delta\rho_{x' \rightarrow x}(t)$ is not only space but also time dependent, because the local food density $\rho(x, t)$ changes over time. Its unit is amount of food per length.

Consequently, integrating x' over both kernels (the interaction kernel $K_{x' \rightarrow x}$ and the food exchange kernel $\Delta\rho_{x' \rightarrow x}(t)$) averages the food density exchanges at a given time t over the interaction range from a given point x in space. Depending on the order of arguments,

$$\int_0^L dx' K_{x' \rightarrow x} \Delta\rho_{x' \rightarrow x}(t) \quad (7.22)$$

gives the average food density change due to food received at position x and time t , and

$$\int_0^L dx' K_{x \rightarrow x'} \Delta\rho_{x \rightarrow x'}(t) \quad (7.23)$$

gives the average food density change due to food given away from position x at time t .

Combining the two integrals, the basic master equation (Eq. (7.1)) can be

rewritten to include the food capacity as:

$$\frac{\partial \rho(x, t)}{\partial t} = \underbrace{\frac{1}{T} \int_0^L dx' K_{x' \rightarrow x} \Delta \rho_{x' \rightarrow x}(t)}_{\text{food inflow}} - \underbrace{\frac{1}{T} \int_0^L dx' K_{x \rightarrow x'} \Delta \rho_{x \rightarrow x'}(t)}_{\text{food outflow}} \quad (7.24)$$

$$= \frac{1}{T} \int_0^L dx' [K_{x' \rightarrow x} \Delta \rho_{x' \rightarrow x}(t) - K_{x \rightarrow x'} \Delta \rho_{x \rightarrow x'}(t)] . \quad (7.25)$$

7.2.2 Source term

The finite range food source in the simulation model (cf. Section 4.1.2) cannot be incorporated into the master equation as a simple boundary condition. Therefore, the following source term describes the rate of change of the food density within range R of the source at $x_{\text{source}} = 0$ (that is $|x - x_{\text{source}}| \leq R \Leftrightarrow x \leq R$) only due to picking up food from the entrance:

$$p(\rho(x, t), x) \frac{1}{T} (\rho_{\max} - \rho(x, t)) , \quad (7.26)$$

where $p(\rho(x, t), x)$ is the probability of receiving food from the source at position x and time t , as a function of the local food density $\rho(x, t)$; and $(\rho_{\max} - \rho(x, t))/T$ is the amount of food per time and length, picked up from the source.

The probability $p(\rho(x, t), x)$ reflects the way food is brought into the system by the source in the simulation model: Every time interval T only one of the ants that are within range of the source, and neither full nor refractory, is selected to receive ($c_{\max} - c(x_i, t)$). The spatially limited scope of the source can once again be described with Heaviside step functions, as

$$\Theta(R - x)\Theta(x) , \quad (7.27)$$

and the space continuous version of the selection rate of ants below carrying capacity can effectively be described with the term

$$\frac{1}{N \frac{R}{L}} \frac{(\rho_{\max} - \rho(x, t))}{\rho_{\max}} , \quad (7.28)$$

where N is the total number of ants and L the 1D system length. It is composed of the probability $1/(NR/L)$ to select one of the NR/L ants on average within range of the source; and the correction term $(\rho_{\max} - \rho(x, t))/\rho_{\max}$, which continuously approximates the probability of selecting an ant below carrying capacity at position x and time t to be proportional to the free local capacity $(\rho_{\max} - \rho(x, t))$.

Combining Eqs. (7.27) and (7.28), the probability $p(\rho(x, t), x)$ of receiving food from the source at position x and time t (cf. Eq. (7.26)) reads

$$p(\rho(x, t), x) := \frac{\Theta(R - x)\Theta(x)(\rho_{\max} - \rho(x, t))}{N \frac{R}{L} \rho_{\max}} \quad (7.29)$$

and the source term (Eq. (7.26)) becomes

$$\frac{\Theta(R - x)\Theta(x)(\rho_{\max} - \rho(x, t))^2}{N \frac{R}{L} \rho_{\max} T}. \quad (7.30)$$

Note that since both $p(\rho(x, t), x)$ and the amount of food $(\rho_{\max} - \rho(x, t))/T$ picked up from the source per time and length are linear in $\rho(x, t)$, the source term is nonlinear in $\rho(x, t)$.

7.2.3 Governing equation

Having derived the food exchange kernel to model the effect of the carrying capacity (Eq. (7.25)) and the source term correctly describing the simulated dynamics (Eq. (7.30)), we can now combine everything to arrive at a full master equation description:

$$\frac{\partial \rho(x, t)}{\partial t} = \frac{1}{T} \int_0^L dx' [K_{x' \rightarrow x} \Delta \rho_{x' \rightarrow x}(t) - K_{x \rightarrow x'} \Delta \rho_{x \rightarrow x'}(t)] \quad (7.31)$$

$$+ \frac{\Theta(R - x)\Theta(x)(\rho_{\max} - \rho(x, t))^2}{N \frac{R}{L} \rho_{\max} T}, \quad (7.32)$$

with the interaction kernel

$$K_{x' \rightarrow x} := \frac{\Theta(R - x')\Theta(x')\Theta(x)\Theta(x' + R - x)}{x' + R} \quad (7.33)$$

$$+ \frac{\Theta(x' - R)\Theta(L - R - x')\Theta(x - x' + R)\Theta(x' + R - x)}{2R} \quad (7.34)$$

$$+ \frac{\Theta(x' - L + R)\Theta(L - x')\Theta(x - x' + R)\Theta(L - x)}{L + R - x'} \quad (7.35)$$

and the food exchange kernel

$$\Delta\rho_{x'\rightarrow x}(t) := \Theta(\rho_{\max} - \sigma\rho(x', t) - \rho(x, t))\sigma\rho(x', t) \quad (7.36)$$

$$+ \Theta(\sigma\rho(x', t) + \rho(x, t) - \rho_{\max})\Theta(\rho_{\max} - \rho(x, t))(\rho_{\max} - \rho(x, t)) . \quad (7.37)$$

Unfortunately, Eq. (7.31) cannot be solved analytically. It can however be solved numerically after discretizing it in time and space.

7.3 Comparison of simulations and analytic predictions

Neither the mean-field model (Chapter 5), nor the diffusion approximation (Chapter 6) provided analytical predictions that were able to give a time resolved description of the simulation dynamics for intermediate interaction ranges. This section shows that a numerical solution of the presented master equation can do this at least to some extent.

7.3.1 Total food

Figure 7.1 compares the total amount of food inside the system from the numerical solution of the full master equation (Eq. (7.31)) with that from the simulation result in a 1D setup with a food exchange ratio of $\sigma = 0.05$ and an interaction range parameter of $\lambda = 0.2$. Apart from slight deviations at early times, the agreement is very good. It is important to note here that the chosen parameters are well outside the mean-field limit and the mean-field model could hence not predict this data. Figure 7.1 can therefore serve as an example of the predictive power of Eq. (7.31) for any interaction radius up to half the system length ($\lambda \leq 0.5$).

7.3.2 Mean squared food distance

The dimensionless mean squared food distance $\overline{\text{MSD}}(t)$ measures the spatial spreading of food from the source through the system. It is shown in Fig. 7.2, again comparing the numerical solution of the full master equation (Eq. (7.31)) with the simulation result in a 1D setup with a food exchange ratio of $\sigma = 0.05$ and an interaction range parameter of $\lambda = 0.2$. The agreement is not as good as for the total food (Fig. 7.1), but at least qualitative agreement is achieved. The remaining deviations between simulation and the master equation prediction cannot be related to the source term, because the total amount of food in the system (and hence the flow into the system) is predicted well by the master equation (cf. Fig. 7.1). Instead,

the mismatch has to stem from the approximations in the kernels Eqs. (7.33) and (7.36).

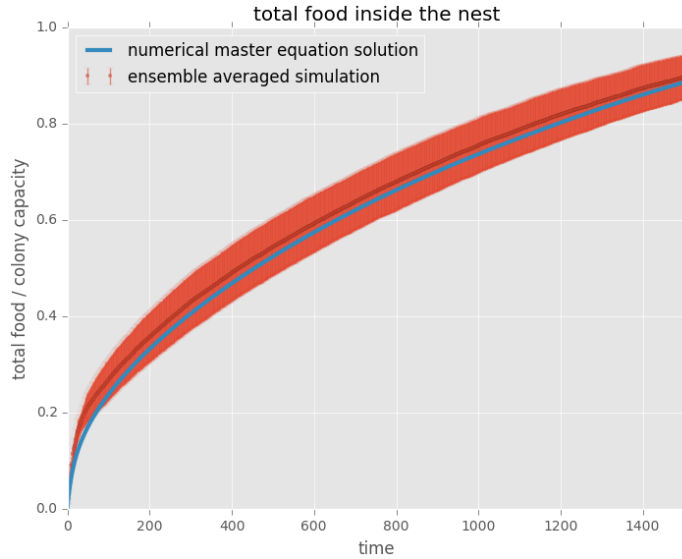


Figure 7.1: Total amount of food $F(t)$ (measured in units of f_{\max}) versus time (in units of T) for $\sigma = 0.05$ and $\lambda = 0.2$ (cf. Section 6.1.2). Blue line: numerical solution of Eq. (7.31), red errorbars: mean and standard deviation of 10 simulations.

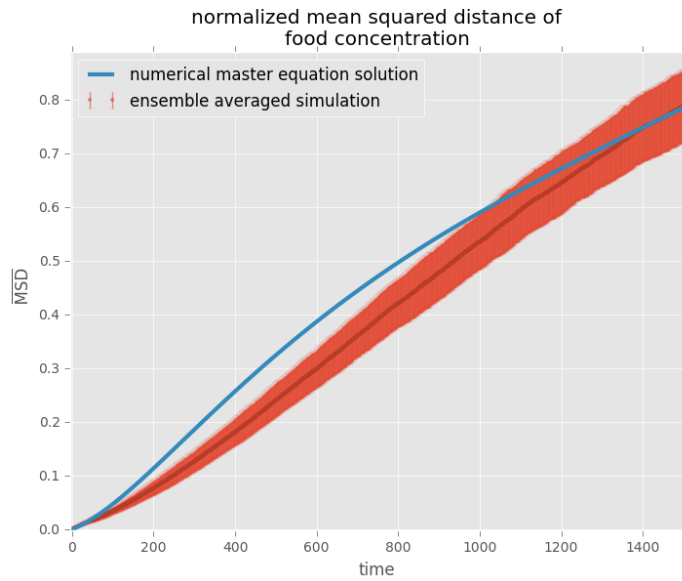


Figure 7.2: Mean squared food distance $\overline{\text{MSD}}(t)$ versus time (in units of T) for $\sigma = 0.05$ and $\lambda = 0.2$. Blue line: numerical solution of Eq. (7.31), red errorbars: mean and standard deviation of 10 simulations.

Part III

Trophallaxis with Explicit Motion

8 Discrete Space Simulation Results

Before we present our main simulation results of trophallaxis with explicit motion, we show some preliminary insights in this chapter, that are obtained from a simplified simulation model.

As a simple primary stage of our full trophallaxis simulation model (cf. Chapter 4), this simplified version uses a discrete finite 2D grid to represent the agents' positions in the tradition of cellular automata. The agents' motion is further simplified to a random walk on this finite 2D grid. At every iteration step, every agent moves to one of the adjacent two to four grid sites with equal probability. Arbitrarily many agents can occupy the same grid site. Trophallactic interactions are only allowed for ants that meet on the same grid site last T steps, in which the food exchanging agents stay at their shared grid site. The same holds for food intakes from the source, which is just one of the grid sites at the middle of one grid boundary. Everything else remains as described in Chapter 4. Apart from the benefit of being simple, the main advantage of the discrete space simulation model is its reduced computational cost, that allows to obtain proof of concept results fast.

Using this toy model, we give a proof of concept comparison between the model and experimental data (Section 8.1), and demonstrate a simple effect of the food exchange ratio σ on the distribution of food among individual ants (Section 8.2).

8.1 Comparison of simulations and experimental work

In this section, we present a qualitative sanity check of our trophallaxis simulation model foundations. We compare our discrete space simulation results with experimental data from [84], using the following three simple observables:

- spatial diffusivity of ants, measured from the mean squared displacements of wall collision free paths
- average interaction rate, measured as the mean number of food exchanges in the whole colony per time interval
- average interaction duration, measured as the mean over all food exchanges

In order to scale the dimensionless simulation results to match the experimental setup, we chose the distance between two grid points to equal $\Delta x = 0.7$ cm (the average length of one ant [84]), the time between two iteration steps to equal $\Delta t = 0.4$ sec, and the number of refractory iteration steps during a food exchange to equal $T/\Delta t = 100$. In combination with choosing $N = 100$ ants and $(L/\Delta x)^2 = 121$ grid sites, we achieved at least an order of magnitude agreement between simulation and experiment across all three observables (Table 8.1).

observable	experiment	simulation
spatial diffusivity of ants [cm ² /sec]	0.25 ± 0.10	0.21 ± 0.04
average interaction rate [1/min]	3 ± 2	10 ± 10
average interaction duration [sec]	35 ± 25	40

Table 8.1: Comparison of discrete simulation and experiments.

This shows, that the basic microscopic spatio-temporal dynamics of our trophallaxis model approach qualitatively agrees with real ant colonies, even under these gross simplifications. The food dynamics however were not compared here (see Section 5.1 for more on this).

8.2 Distribution of food among individual ants

In the results presented so far, we mainly focused on global and spatial food distribution observables. In this section, we instead look at the distribution $P(c(t))$ of food among individual ants.

When the simulated ant colony is presented with only $f_{\max}/2$ food at the source (half of the usual $f_{\max} = Nc_{\max}$ amount of food, enough to fill everyone of the N ants up to the carrying capacity c_{\max}), the question arises how our simple trophallaxis model distributes this limited food among the ants. Figure 8.1 shows, that the answer to this question depend on the microscopic amounts of food exchanged, the food exchange ratio σ .

We find, that when the ants try to exchange larger amounts of food ($\sigma = 0.9$ as compared to $\sigma = 0.1$), the food is distributed less equally among the ants. This can be explained through the finite crop capacities. When σ is large, ants are more likely to be either almost full or almost empty, because once they gathered food for the first time, they always either just received an amount of food close to c_{\max} or just gave away an amount of food close to c_{\max} . For small σ values however, ants can accumulate food over a series of food receptions or progress towards intermediate food concentrations through a series of food donations.

As this result only depends on the food exchange rules, identical to our space

8.2 Distribution of food among individual ants

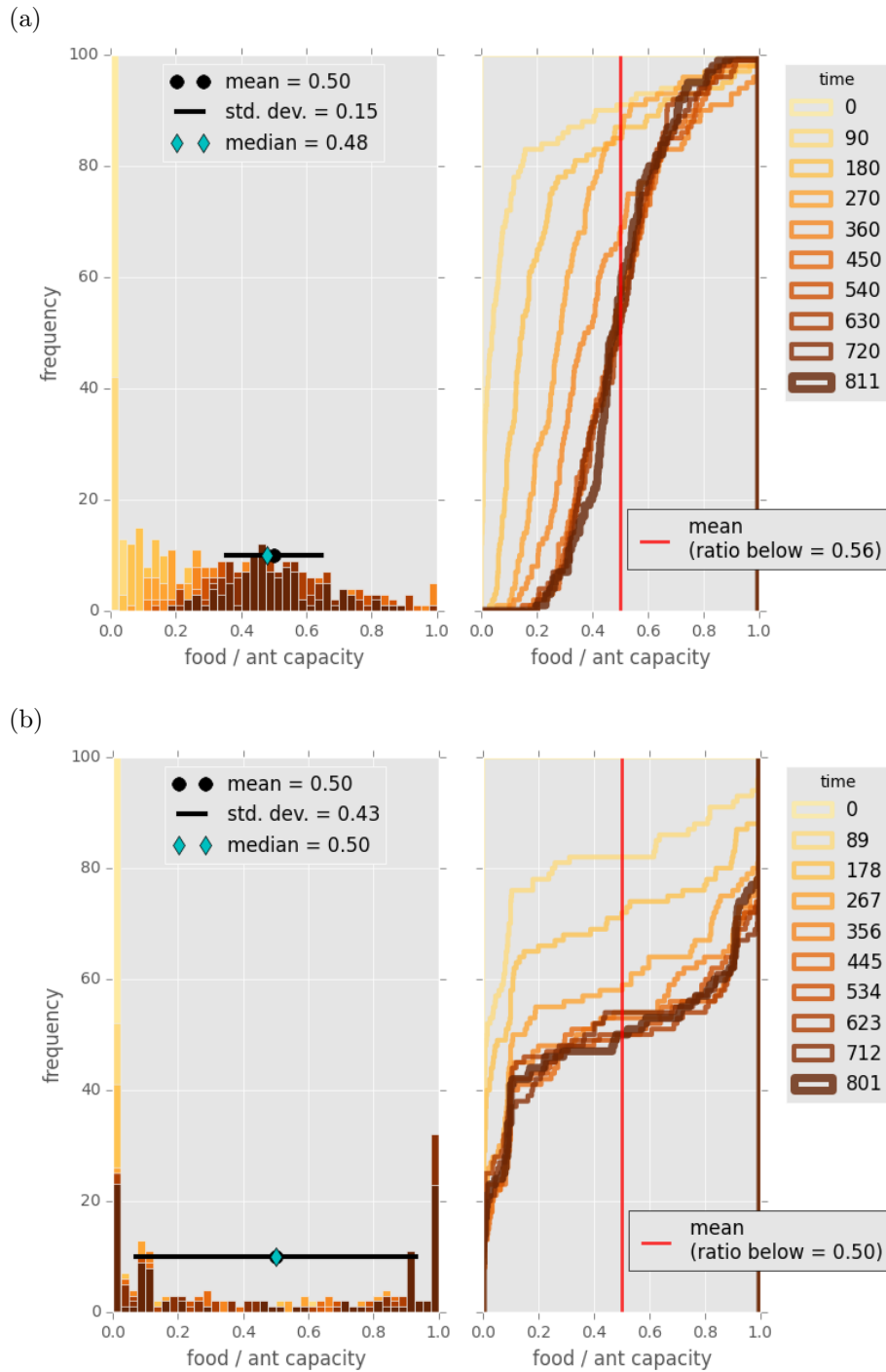


Figure 8.1: Distribution of food among individual ants for (a) a food exchange ratio $\sigma = 0.1$ and (b) a food exchange ratio $\sigma = 0.9$. The left panels show the regular histogram of how many ants carry how much food and the right panels show the corresponding cumulative histograms. Mean, standard deviation, and median are given for the final distribution (brown color). The time evolutions are color coded and time indices given in dimensionless iteration step counts.

8 Discrete Space Simulation Results

continuous simulation model (cf. Section 4.1.3), it can be expected to hold for the continuous model as well. In fact, Fig. D.7 (obtained with the continuous space simulation) shows similar distribution shapes at intermediate times.

9 Continuous Space Simulation Results

This chapter constitutes the core of Part III and contains the main findings of our full trophallaxis simulations with explicit, space continuous ant motion.

We aim to qualitatively answer some question on how fundamental properties of an ant colony influence their self-organized food distribution in this chapter. This influence is mainly monitored by the global food intake time scale, measured with the already introduced half-time (cf. Section 4.4). The fundamental properties we consider specifically are the ants' velocity, their trophallaxis interaction radius, the amounts of food exchanged, the duration of food exchanges, and the nest size. As we will show, these properties influence the global dynamics through an interplay that is at least in parts surprisingly complex.

We group our results in two sections, describing the interplay between the dimensionless simulation parameter groups introduced in Section 4.2. Section 9.1 contains the interplay between the ant velocity parameter and the interaction range parameter and Section 9.2 the interplay between the ant velocity parameter and the food exchange ratio.

Afterwards, we present an extended version of the simulation model introduced in Section 4.1 and compare it to the original version (Section 9.3). The aim of these extensions is to provide a less artificial model, including various random heterogeneities, like agents with different carrying capacities and randomized amounts of exchanged food.

9.1 Ant velocity and interaction range interplay

A question of interest is whether slow ants with large interaction ranges exhibit the same food distribution dynamics as fast ants with small interaction ranges. In this section, we try to answer questions of this kind that arise from the interplay of the ants' velocity, their interaction radius, the duration of food exchanges, and the system size.

We first show the existence of a smooth transition from diffusive to mean-field dynamics going either from slow to fast ant motion or from local to system-wide interaction ranges (Section 9.1.1). We then proceed with presenting qualitative empirical scaling relations for some regimes of this transition (Sections 9.1.2 and 9.1.3).

Finally, Section 9.1.4 shows a peculiarity in the dynamics' dependency on the ant velocity parameter that arises only for very small velocities.

9.1.1 Transition between diffusive and mean-field dynamics

In Chapters 5 and 6, we have already explored the influence of the interaction range parameter on the global food intake time scale for ants without explicit motion (cf. Sections 5.3.2 and 6.3.4 in particular). In this section, we investigate what the explicit motion of ants adds to this.

Figures 9.1 and 9.2 show that the global food intake time scale (again measured with the half-time) not only decreases with the interaction range parameter λ (cf. Fig. 6.7), but also with the ant velocity parameter ν .¹

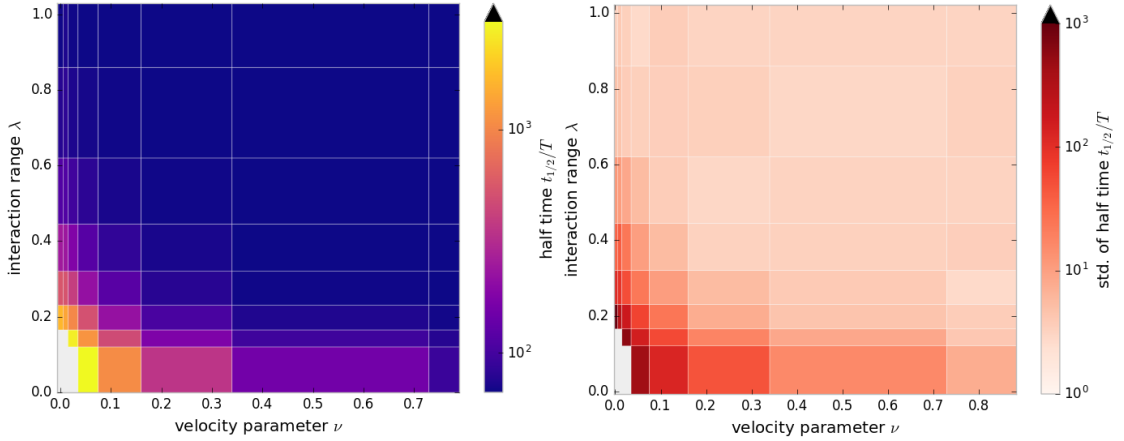


Figure 9.1: Mean (left panel) and standard deviation (right panel) of the half-time $t_{1/2}/T$ (time until the colony is half full) as a function of the ant velocity parameter ν and the interaction range parameter λ , in units of the refractory period T . The food exchange ratio is fixed to $\sigma = 0.05$. Mean and standard deviation are calculated as an ensemble average over 100 independent simulation runs. The gray areas in the bottom left corner of both panels represent parameter values, for which no data was simulated. A closeup of this figure can be found in the appendix (Fig. D.1). See Fig. 9.2 for a line scan version of this figure.

There is in fact a smooth transition along both nondimensional parameter axes going from the slow, diffusive limit where both $\lambda \rightarrow 0$ and $\nu \rightarrow 0$ to the fast, mean-field limit where either $\lambda \rightarrow 1$ or $\nu \rightarrow 1$. Note that $\lambda = R/L \rightarrow 0$ is achieved through a small interaction radius R compared to the system size L , and $\lambda = R/L \rightarrow 1$ is fulfilled when the interaction radius reaches the system size

¹The data shown in Figs. 9.1 and 9.2 was obtained for a relatively small food exchange ratio of $\sigma = 0.05$. This choice allows for broad range of relevant λ and ν values, as larger σ values further decrease the half-time (cf. Fig. 6.7). The influence of σ on the half-time will be studied in detail in Section 9.2.

9.1 Ant velocity and interaction range interplay

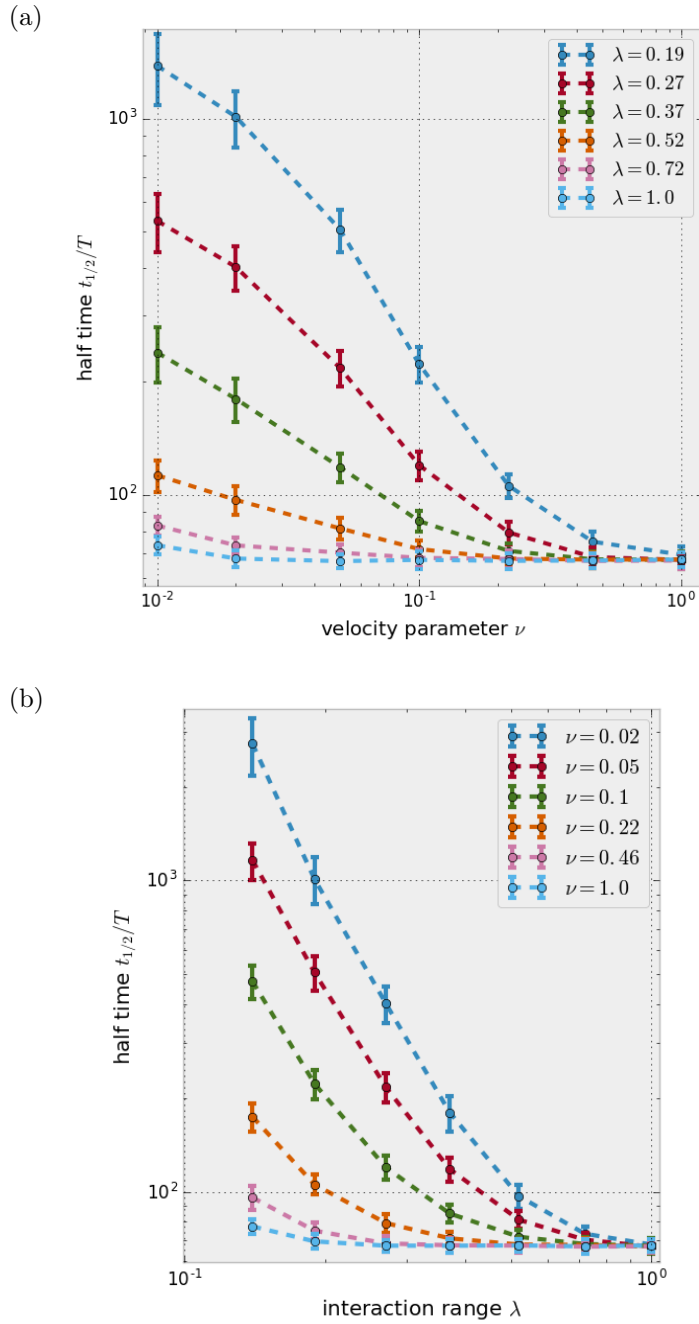


Figure 9.2: Half-time $t_{1/2}$ in units of the refractory period T (a) as a function of the ant velocity parameter ν , varying the interaction range parameter λ ; and (b) as a function of the interaction range parameter λ , varying the ant velocity parameter ν . The food exchange ratio is fixed to $\sigma = 0.05$ in both panels. See Fig. 9.1 for a heat map version of this figure.

($R \approx L$). Likewise, $\nu = (vT)/R \rightarrow 0$ is achieved through a small distance vT traveled with velocity v during the refractory period T compared to the interaction radius R .

If an ant colony were to distribute the food from a source as fast as possible, the optimal intake time scale would be reached at $t_{1/2}/T = \ln(2)/(\gamma_{\lambda=1}T) \approx 70$ in our simulation, as predicted by the mean-field model (cf. Chapter 5 and Eq. (5.8)). This fastest time scale arises from the limited food flow rate into the nest, due to ants picking up food from the source one at a time. Once the colony distributes the food fast enough within the nest to match this inflow rate, it cannot improve further. Figure 9.1 shows that this optimal global time scale can similarly be reached through the ants moving faster or finding their food exchange partners at longer distances, which answers the question posed above. It also shows that even very small increments of ν away from the diffusive limit allow for reaching fast food intake dynamics when increasing λ much faster, and vice versa.

We proceed with exploring the presented transition between diffusive and mean-field dynamics quantitatively through giving empirical scaling laws of how the half-time decreases with ν (Section 9.1.2) and λ (Section 9.1.3).

9.1.2 Ant velocity scaling relation

Figure 9.2 showed the half-time $t_{1/2}$ decays with the ant velocity parameter ν . In fact, the linear regimes in the double logarithmic plot indicate that $t_{1/2}$ follows a power law scaling of the form

$$\frac{t_{1/2}}{T} \sim \nu^a \quad (9.1)$$

for a large regime of ν values. The scaling exponent a can in principle depend on the food exchange ratio σ and the interaction range parameter λ . Figure 9.3 shows linear regressions of $\ln(t_{1/2}/T)$ as a function of $\ln \nu$ for a range of σ values and a fixed demonstrative value $\lambda = 0.13$ of the interaction range parameter. We chose $\lambda = 0.13$ as an example to allow for a wide range of ν values before reaching the mean-field limit. At the same time, $\lambda = 0.13$ is large enough to prevent single ants from getting isolated easily at very small (or even zero) velocities for the standard number of $N = 100$ ants.² Similar qualitative scalings can be derived for other λ values, not shown here.

Except for $\sigma = 1$, all fits gave similar values for the scaling exponent of Eq. (9.1).

²This potential isolation is related to a percolation phenomenon that will be discussed more in Section 9.1.4.

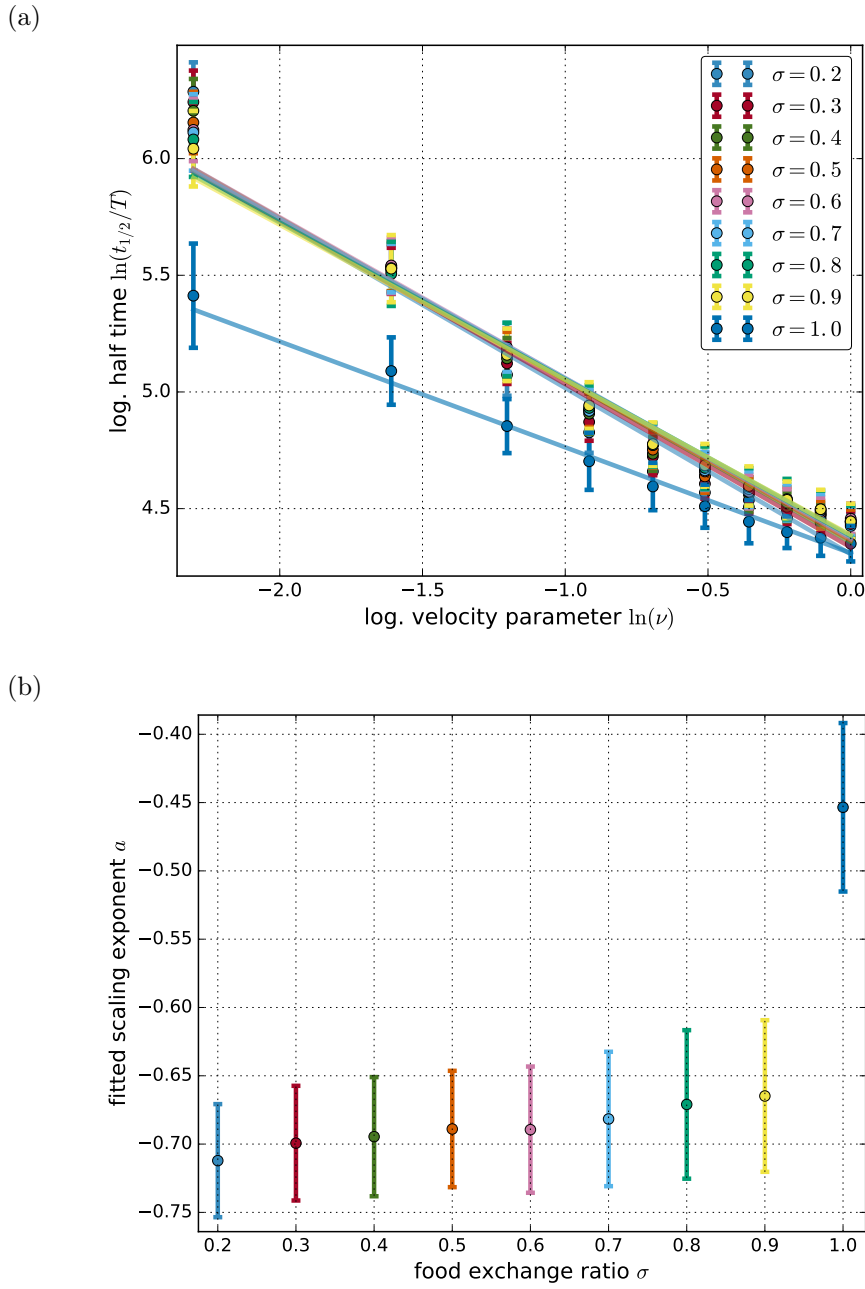


Figure 9.3: (a) Logarithmic half-time $\ln(t_{1/2}/T)$ in units of the refractory period T as a function of the logarithmic ant velocity parameter $\ln(\nu)$, varying the food exchange ratio σ . Lines represent linear regressions $\ln(t_{1/2}/T) = a \ln(\nu) + b$ for each σ value. Their slopes a are given in panel (b). (b) Fitted scaling exponents a as a function of the food exchange ratio σ . The interaction range parameter is fixed to $\lambda = 0.13$.

An average over all $\sigma < 1$ fits gives the scaling

$$\frac{t_{1/2}}{T} \sim \nu^{-0.69 \pm 0.02} \quad (9.2)$$

in the selected regime $\sigma \in [0.2, 0.9]$ and $\lambda = 0.13$.

When the food exchange ratio is maximal ($\sigma = 1$), the simulation model effectively describes a behavior that differs from the regular behavior when $\sigma < 1$. The reason behind this is that all food exchanges are modeled to always take the same time T , irrespective of the amount of food exchanged (cf. Section 4.1.3). Therefore, if $\sigma < 1$, a large portion of the colony can be refractory although only small amounts of food are transferred. If $\sigma = 1$, the ant agents always exchange all of their crop content and are thus always either completely full or empty (cf. Section 5.2). As a consequence, food can be distributed faster, because all refractory agents contribute with transferring large amounts. This explains, why Eq. (9.2) does not hold for $\sigma = 1$. Instead, Fig. 9.3 suggests

$$\frac{t_{1/2}}{T} \sim \nu^{-0.45 \pm 0.07} \quad (9.3)$$

for $\sigma = 1$ and $\lambda = 0.13$.

9.1.3 Interaction range scaling relation

The same approach for obtaining an empirical scaling relation of the transition between diffusive and mean-field dynamics we used for the ant velocity parameter in the previous section can be applied to the interaction range parameter. Figures 9.2 and 9.4 show similar, although shorter, linear regimes in the double logarithmic plot of the half-time $t_{1/2}/T$ as a function of the interaction range parameter λ . Since the functional dependency of $t_{1/2}$ depends on the ant velocity parameter ν this time, we chose an exemplary value of $\nu = 0.1$ here. This value is again small enough to allow for a range of λ values before reaching the mean-field limit, and is also large enough to show no strong dependency of the food exchange ratio σ (as will be explored further in Section 9.2). Also here, similar scaling relations can be obtained for other ν values.

For $\lambda \in [0.05, 0.25]$ and $\nu = 0.1$,

$$\frac{t_{1/2}}{T} \sim \lambda^{-2.41 \pm 0.03} \quad (9.4)$$

gives the average scaling for all σ values (including $\sigma = 1$). As Fig. 9.4 shows, there is a trend to smaller λ scaling exponents with increasing σ . Here, we are however

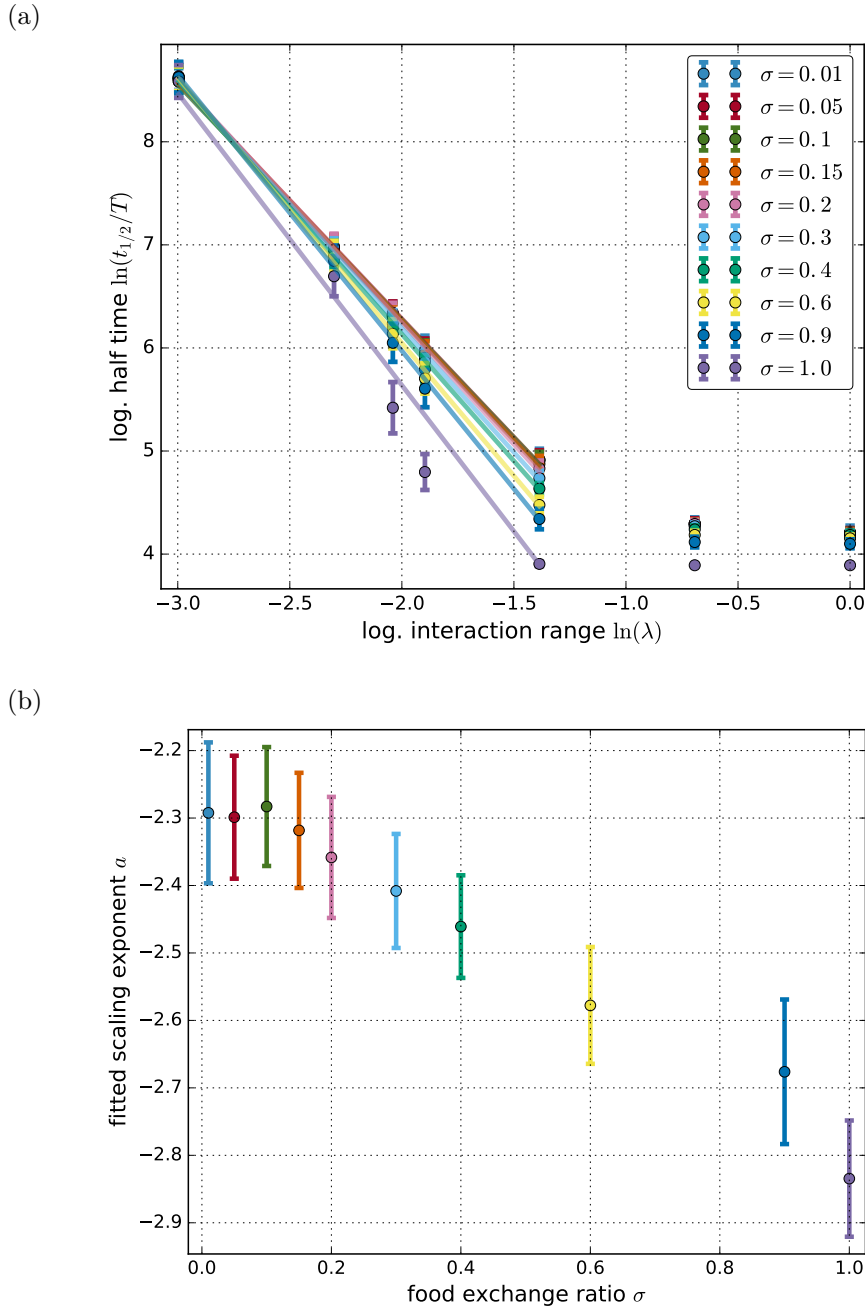


Figure 9.4: (a) Logarithmic half-time $\ln(t_{1/2}/T)$ in units of the refractory period T as a function of the logarithmic interaction range parameter $\ln(\lambda)$, varying the food exchange ratio σ . Lines represent linear regressions $\ln(t_{1/2}/T) = a \ln(\lambda) + b$ for each σ value in the linear regime $\lambda \in [0.05, 0.25]$. Their slopes a are given in panel (b). (b) Fitted scaling exponents a as a function of the food exchange ratio σ . The ant velocity parameter is fixed to $\nu = 0.1$.

only concerned with qualitative relations and refer to Fig. 9.4 for a more detailed view. For interaction ranges $\lambda > 0.25$, the global food intake is already limited by the maximum intake rate of the mean-field limit and the half-time does thus not decrease further (cf. Section 9.1.1).

9.1.4 Slow motion limit case

At very low velocities and small interaction ranges, the global food intake time scale $t_{1/2}$ showed a rapid growth both in its ensemble mean and standard deviation (Fig. 9.1). In addition, the scaling relations Eqs. (9.2) and (9.4) extrapolate to

$$\lim_{\nu \rightarrow 0} \frac{t_{1/2}}{T} \rightarrow \infty \quad (9.5)$$

for finite λ . This contradicts the finite half-time observed in Fig. 6.7. We therefore take a brief look at the dynamics of the system for $\nu < 0.1$ in this section.

Figure 9.5 shows the half-time in this slow motion limit for a system of $N = 500$ ants with an interaction range parameter $\lambda = 0.13$. Clearly, $t_{1/2}$ does not diverge for $\nu \rightarrow 0$. It does however show a maximum at a finite ant velocity parameter value $0 < \nu^* < 0.1$ for both small and large food exchange ratios, and not as intuitively expected at $\nu = 0$.

Figure D.3 in the appendix shows that the standard system of $N = 100$ ants qualitatively behaves similar, only the systematic fluctuations are too high to observe a statistically significant maximum. The reason behind this is that due the way the food source is modeled by our simulation model, decreasing the number of ants effectively increases the food flow rate into the system compared to the distribution rate within the nest (cf. Section 4.1). This is simply, because only one ant feeds of the source per refractory period, whereas every food carrying ant can potentially feed another ant in this time.³

A maximum of $t_{1/2}$ at $\nu^* > 0$ inevitably also leaves a region where moving ants take up food slower than stationary ants ($t_{1/2}(\nu) > t_{1/2}(\nu = 0.0)$). A possible explanation for this counter-intuitive effect can be found in percolation effects. All the simulations presented in Figs. 9.5 and D.3 were simulated with $\lambda = 0.13$, the interaction range value that merely ensures that food can percolate from the source to every ant for $N = 100$ almost all the time, even when they are not moving. Only the simulations with stationary ants ($\nu = 0$) are initialized in a way that guarantees connectedness for the ants' random initial positions. For $\nu > 0$, the random initial positions are not checked for this percolation condition, because

³Note that this is also reflected in the two analytic predictions for the food intake rates $\gamma_{\lambda=1} = 1/(NT)$ (Eq. (5.12)) and $\gamma = (\sigma\bar{r}^2)/(TL^2)$ (Eq. (6.25)). The source dominated $\gamma_{\lambda=1}$ scales with the number of ants N , whereas γ derived in the not source dominated diffusive limit does not.

9.2 Ant velocity and food exchange ratio interplay

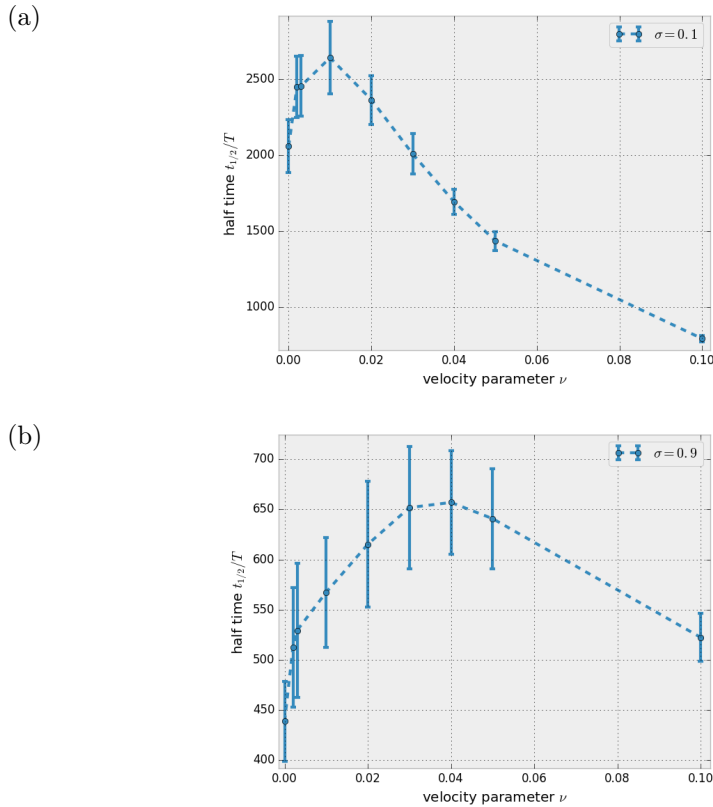


Figure 9.5: Half-time $t_{1/2}$ in units of the refractory period T as a function of the ant velocity parameter ν with a food exchange ratio of (a) $\sigma = 0.1$ and (b) $\sigma = 0.9$. The interaction range parameter is fixed to $\lambda = 0.13$ and the number of ants changed to $N = 500$.

their positions changes in the course of the simulation. As a consequence, there can be random initial position setups with isolated clusters of ants, i.e. ants without a connection to the source through other ants. For high velocities ($\nu \gtrsim 0.1$), the ants are moving - and thus mixing - fast enough to effectively ensure food percolation from the source to every ant. For low velocities ($\nu \lesssim 0.1$) however, an initially unconnected position setup could take a significantly long time to connect every ant with the source or another food carrying ant. Subgroups of ants not connected to other ants and unable to receive food for a long time can arise and thus explain the delay in the half-time.

9.2 Ant velocity and food exchange ratio interplay

In this section, we first show how the transition between diffusive and mean-field dynamics caused by changing the ant velocity parameter influences the dependency

of the global food intake times scale on the food exchange ratio (Section 9.2.1). In particular, we find a strong dependency on the food exchange ratio in the diffusive limit that gradually disappears, when going from slow to fast ant motion. We then proceed with presenting a qualitative scaling relation for the food exchange ratio dependency in the diffusive limit (Section 9.2.2). Finally, Section 9.2.3 shows a small parameter regime with an inverted dependency on the food exchange ratio.

9.2.1 Transition between diffusive and mean-field dynamics

In the diffusive limit, that is small interaction range parameter λ and low ant velocity parameter ν , the global food intake time scale depends on the food exchange ratio σ . Section 6.3 showed that for static ants ($\nu = 0$) with small λ , the half-time $t_{1/2}$ decreases with σ . This is intuitively clear, because exchanging more food per refractory period allows the colony to distribute the food faster. In fact, for small λ , exchanging more food is the only way to decrease $t_{1/2}$, if the ants are not moving.

When the ants are moving, this changes. Food now also spreads better, the faster the ants move (cf. Section 9.1). In fact, Fig. 9.6 shows there is a smooth transition from σ dependent diffusive dynamics to σ independent mean-field dynamics, going from $\nu = 0$ to $\nu = 1$, again for $\lambda = 0.13$ (cf. Section 9.1.2).

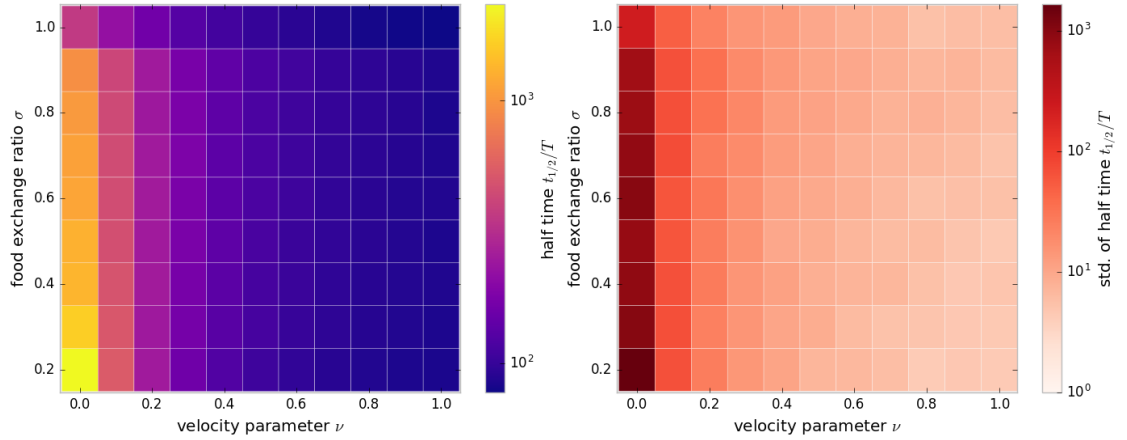
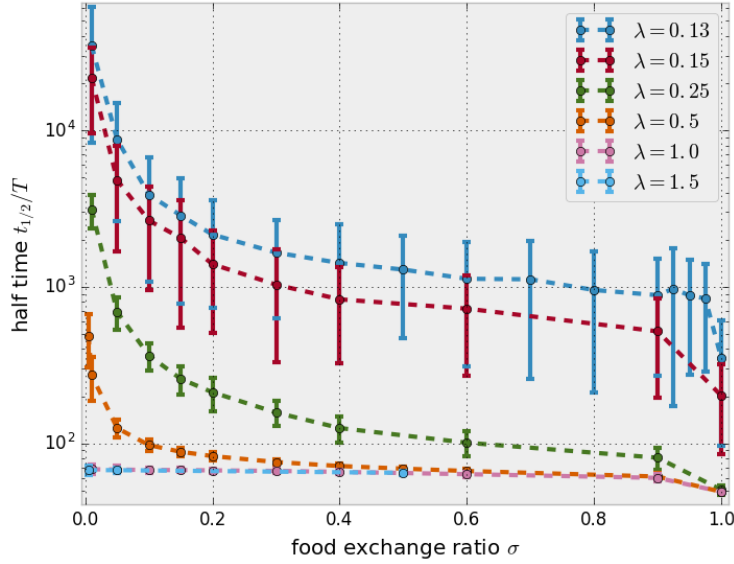


Figure 9.6: Mean (left panel) and standard deviation (right panel) of the half-time $t_{1/2}/T$ (time until the colony is half full) as a function of the ant velocity parameter ν and the food exchange ratio σ , in units of the refractory period T . The interaction range parameter is fixed to $\lambda = 0.13$. Mean and standard deviation are calculated as an ensemble average over 100 independent simulation runs.

That indicates that the increasing spatial mixing of ants renders the exchange of large food amounts unnecessary, when the ants are moving. Figures 9.7 and 9.8

show exemplary line scans of Fig. 9.6 for $\nu = 0; 0.1; 0.3; \text{ and } 1$, not only for $\lambda = 0.13$, but for larger interaction ranges as well.

(a)



(b)

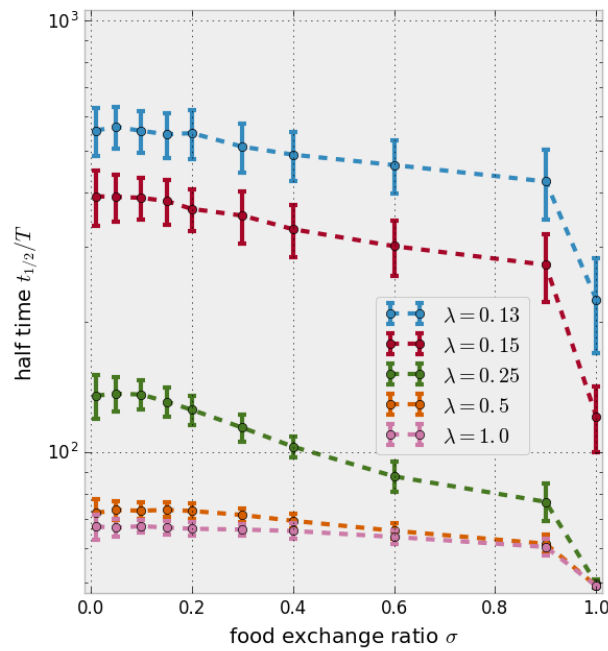


Figure 9.7: Half-time $t_{1/2}$ in units of the refractory period T as a function of the food exchange ratio σ , varying the interaction range parameter λ , with an ant velocity parameter of (a) $\nu = 0$ (no motion) and (b) $\nu = 0.1$ (slow motion).

9 Continuous Space Simulation Results

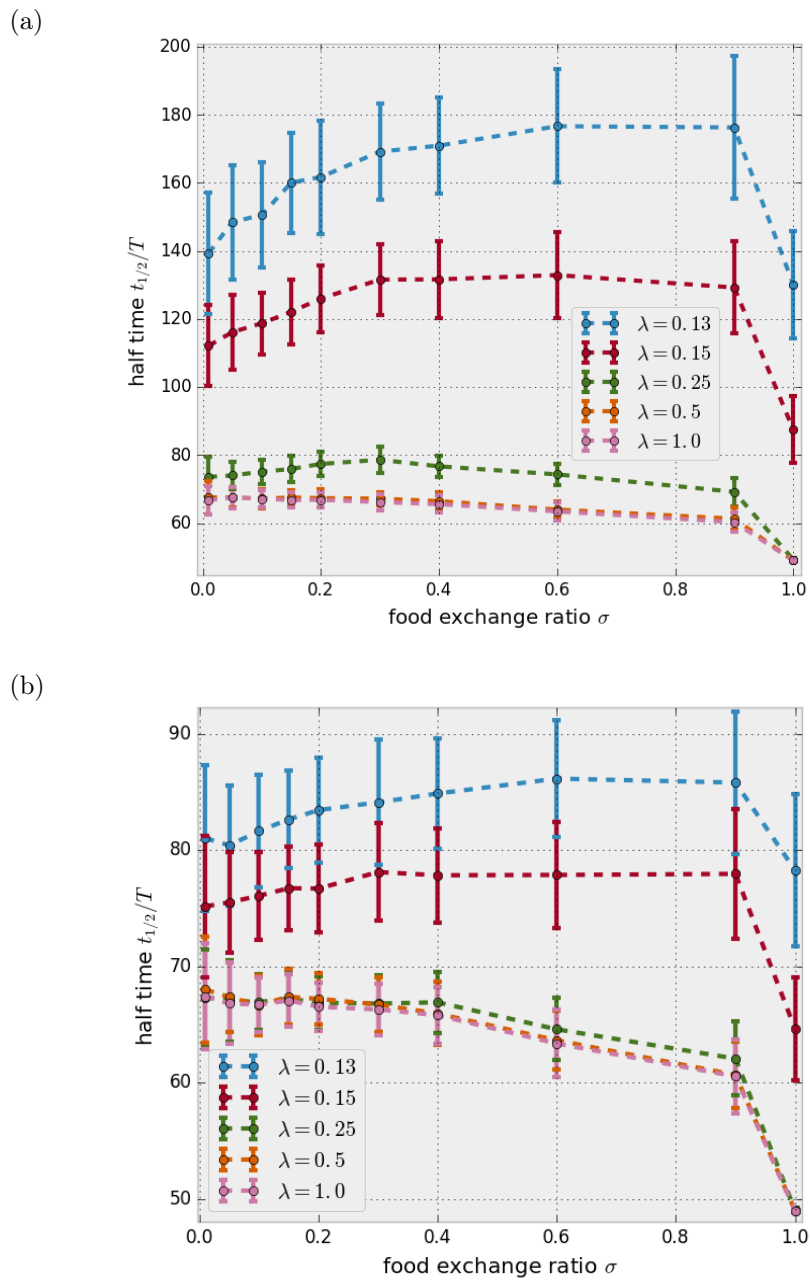


Figure 9.8: Half-time $t_{1/2}$ in units of the refractory period T as a function of the food exchange ratio σ , varying the interaction range parameter λ , with an ant velocity parameter of (a) $\nu = 0.3$ (medium fast motion) and (b) $\nu = 0.1$ (fast motion).

When the ants are not moving ($\nu = 0$), we can observe smaller $t_{1/2}$ values and thus faster food uptake with increasing σ for almost the whole range of meaningful λ values. Only for very large λ values, close to the mean-field limit, no σ dependency can be observed anymore, because the food saturation dynamics of the colony is dominated by the fast uptake of food from the source. Note that $t_{1/2}$ decreases up to two orders of magnitude from small to large σ .

This decay of $t_{1/2}$ with σ vanishes slowly, when the ants start moving. For $\nu = 0.1$ there is still some dependency on σ for intermediate interaction ranges. For faster ants ($\nu \gtrsim 0.3$), $t_{1/2}$ does not depend on σ anymore. In fact, there is even a weak tendency towards longer half-times with increasing σ , at least for small λ values. We will examine this regime further in Section 9.2.3.

Concluding the insights of this section, Fig. 9.9 presents a combined plot of Figs. 9.6 to 9.8.

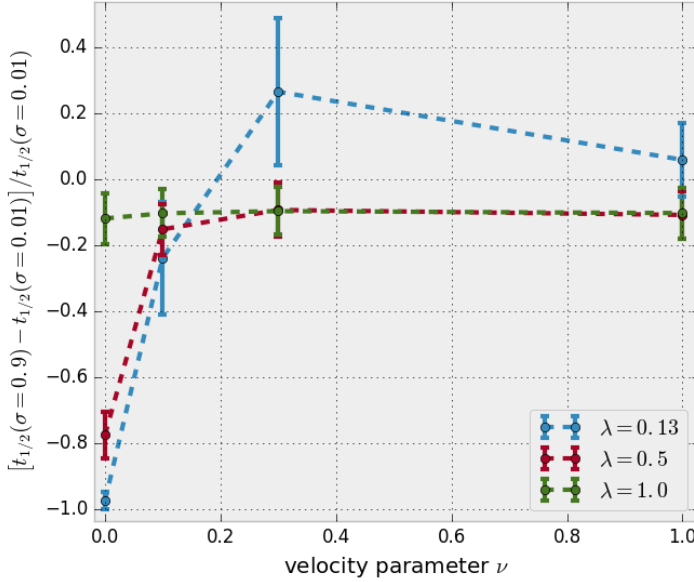


Figure 9.9: Relative half-time change $\Delta t_{1/2}(\sigma_1, \sigma_2)/t_{1/2}(\sigma_1)$ between low ($\sigma_1 = 0.01$) and high ($\sigma_2 = 0.9$) food exchange ratio σ as a function of the ant velocity parameter ν , varying the interaction range parameter λ .

It shows

$$\frac{\Delta t_{1/2}(\sigma_1, \sigma_2)}{t_{1/2}(\sigma_1)} = \frac{t_{1/2}(\sigma_2) - t_{1/2}(\sigma_1)}{t_{1/2}(\sigma_1)}, \quad (9.6)$$

the relative change of the half-time between two food exchange ratios σ_1 and σ_2 ,

varying both ν and λ . Using $\sigma_1 = 0.01$ and $\sigma_2 = 0.9$, this allows for a concise overview of the discussed interplay between the ant velocity parameter and the food exchange ratio. A negative value of $\Delta t_{1/2}(\sigma_1, \sigma_2)/t_{1/2}(\sigma_1)$ (as can be observed for static and slow ants) indicates a decrease of $t_{1/2}$ with σ , whereas a positive value (as observed for $\nu = 0.3$ with small λ) indicates an increase of $t_{1/2}$ with σ . A value close to zero (as observed for fast ants) finally proves no significant σ dependency.

9.2.2 Food exchange ratio scaling relation

Similarly to Sections 9.1.2 and 9.1.3, we can also empirically obtain a power law scaling of the half-time $t_{1/2}$ with the food exchange ratio σ in a small parameter region.

Since Section 9.2.1 showed that $t_{1/2}$ depends strongest on σ for static ants, we chose to extract the scaling for $\nu = 0$, but once again, similar relations can be obtained for other small nonzero ν values.

Figure 9.10 shows food exchange ratio power law dependencies for $\lambda \in [0.13, 0.25]$ and $\sigma \in [0.01, 0.95]$.⁴ The average over the linear regressions in this regime yields

$$\frac{t_{1/2}}{T} \sim \sigma^{-0.8 \pm 0.05} . \quad (9.7)$$

It is to be expected that this forms an upper limit for the scalings with $\nu > 0$, since $t_{1/2}$ only decreases less with σ for $\nu > 0$, compared to $\nu = 0$ (see Fig. 9.9).

For interaction ranges $\lambda > 0.25$, consistent with the observations of Section 9.1.3, the global food intake and hence the half-time is already limited by the maximum intake rate of the mean-field limit (cf. Section 9.1.1). The diffusive regime, for which Eq. (9.7) holds, is then also limited to small food exchange ratios σ (cf. Fig. 9.10).

9.2.3 Inverted food exchange ratio dependency regime

Figures 9.8 and 9.9 indicated a small parameter regime for which the intuitive dependency of the half-time $t_{1/2}$ on the food exchange ratio σ is inverted. In this regime, exchanging more food leads to a slowdown of the global food intake. This section examines this effect.

Figure 9.11 and Fig. D.3 in the appendix show the relevant parameter range of ant velocity parameter values $\nu \approx 0.3 - 0.7$ out of the whole range shown in Fig. 9.6, but with a higher half-time resolution.

⁴Note that values of $\lambda < 0.13$ are not meaningful for $\nu = 0$, because some ants could be isolated and thus not able to receive food (cf. Section 9.1.4). Also $\sigma \in [0.01, 0.95]$ sufficiently covers the whole range of σ values except for the special case $\sigma = 1$ (cf. Section 9.1.2).

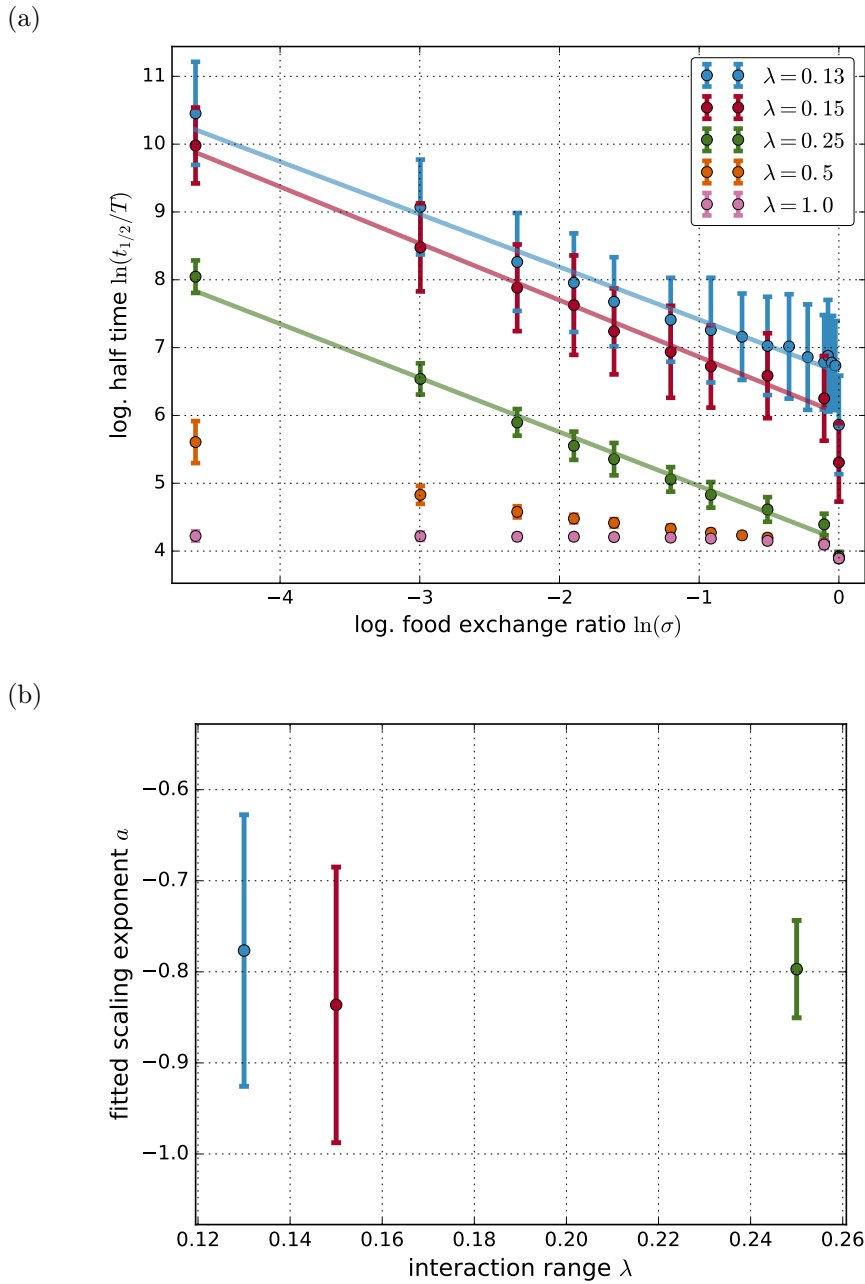


Figure 9.10: (a) Logarithmic half-time $\ln(t_{1/2}/T)$ in units of the refractory period T as a function of the logarithmic food exchange ratio $\ln(\sigma)$, varying the interaction range parameter λ . Lines represent linear regressions $\ln(t_{1/2}/T) = a \ln(\sigma) + b$ for $\lambda \leq 0.25$ in the linear regime $\sigma \lesssim 1$. Their slopes a are given in panel (b). (b) Fitted scaling exponents a as a function of the interaction range parameter λ . The ant velocity parameter is fixed to $\nu = 0$.

9 Continuous Space Simulation Results

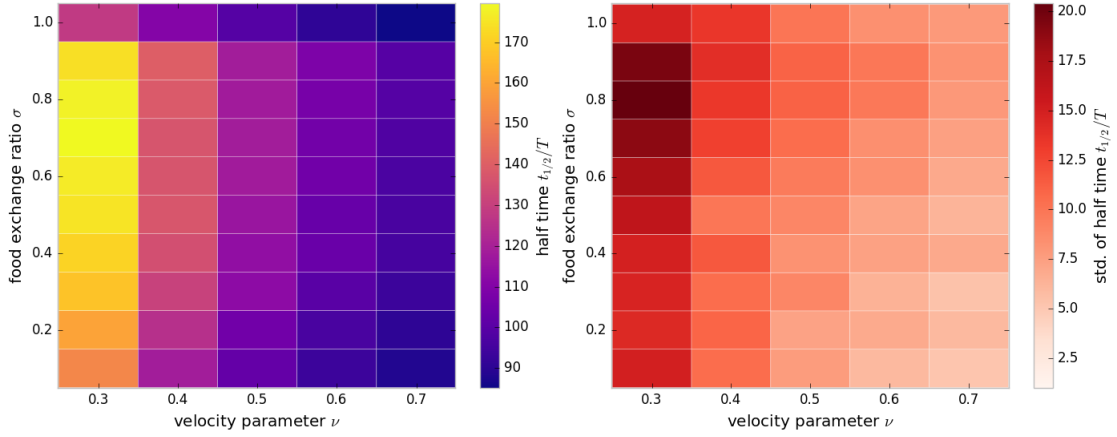


Figure 9.11: Mean (left panel) and standard deviation (right panel) of half-time $t_{1/2}$ as a function of the ant velocity parameter ν and the food exchange ratio σ , in units of the refractory period T . The interaction range parameter is fixed to $\lambda = 0.13$. Mean and standard deviation are calculated as an ensemble average over 100 independent simulation runs. This is a closeup of Fig. 9.6. See Fig. D.3 for a line scan version of this figure.

Not only the half-time, but the whole time evolution of food in the colony and its spatial spreading slows down with σ in this parameter regime (see Figs. D.4 and D.6 in the appendix).

Unfortunately, there does not seem to be an easy explanation for this inversion, as we will illustrate through an example. The inversion effect cannot simply be explained through irregularities in the distribution of food among the ants, as this does not show qualitatively different behavior between in and outside the inverted σ dependency regime (see Fig. D.7 in the appendix).

It is important to also take the standard deviation of $t_{1/2}$ and not only its mean into consideration. Especially Fig. D.3 shows that the random noise in the system barely make the inversion effect statistically significant. This is mainly because of the large random fluctuations in the simulated food dissemination dynamics. These random fluctuations result from two independent random processes: the first being the rotational diffusion in the active Brownian motion of the simulated ant agents; and the second being the randomness in the food transfer, e.g. agents or the source choosing random food exchange partners. In order to estimate how much of the fluctuation seen in the half-time is produced by each of these two sources of randomness, it is useful to run alternated simulations, where one source of randomness is switched off and only the other one is active. This can be achieved by implementing two independently seeded pseudo-random number generators, of which one is used with a new seed for every simulation run of the ensemble

for one source of randomness; and the other one is used with the same seed for every simulation run of the ensemble for the other source of randomness. Fig. D.5 shows the food concentration mean and variance for the alternated simulation ensemble, where the randomness of the rotational diffusion and thus the motion of the simulated ants is exactly the same (random) motion for every one of the 100 runs in the ensemble average. Comparing the result with the regular simulations, where motion and food exchange are seeded new every run (Fig. D.4) clearly shows that there is an insignificantly small influence of the motion randomness on the variance in the ensemble averaged half-time. Ergo, the large variance is mainly caused by the random food exchange partner choices.

9.3 Heterogeneous case study

This last section of Chapter 9 first presents an extended version of our agent-based trophallaxis simulation model (Section 9.3.1) and then compares its results to the original version (Section 9.3.2). The simulation extensions provide a more heterogeneous, and hence more detailed model of trophallaxis. It aims to mimic real ant colonies better than the simpler original model. Within the scope of this case study, interestingly, we do not find qualitatively different behavior, compared to the original model.

9.3.1 Simulation model extensions

A series of simplifying assumptions might make the agent-based simulation model we proposed in this work look too unrealistic, to adequately describe the food distribution of real ant colonies. We therefore introduce the following extensions for the standard model (Section 4.1) in this section, to achieve a more detailed description:

- individual carrying capacities $c_{\max,i}$
- randomly distributed food exchange ratios $P(\sigma)$
- separate refractory periods for ant-ant (T_{ants}) and ant-source (T_{source}) interactions
- randomly distributed refractory periods $P(T_{\text{ants}})$ and $P(T_{\text{source}})$

In the following we describe these extensions in more detail.

Individual carrying capacities

Real ants do not all have exactly the same crop sizes within one colony and can therefore all carry different amounts of food. Even if two ants of the same colony have the same crop size, they might not be able or want to carry the same amounts of food for other unknown reasons. This heterogeneity could influence the food distribution dynamics.

We incorporate them in our simulation model through initially assigning all ant agents individual random carrying capacities $c_{\max,i}$, drawn from the uniform distribution $u([\bar{c}_{\max} - \delta_{c_{\max}}, \bar{c}_{\max} + \delta_{c_{\max}}])$, where $\delta_{c_{\max}} < \bar{c}_{\max}$ parameterizes the range of possible $c_{\max,i}$ values, so that

$$\langle c_{\max,i} \rangle = \frac{1}{N} \sum_{i=1}^N c_{\max,i} = \bar{c}_{\max} \quad (9.8)$$

is the expected mean. The agents then keep their individual capacity throughout the whole simulation run, but are assigned a new $c_{\max,i}$ for every run in an ensemble.

Random food exchange ratios

Little is known about how real ants determine the amounts of food exchanged during trophallaxis. In our simulations so far, we modeled the ratio between offered and not offered food to always be the same fixed value σ . It is reasonable to assume that the food exchange ratio for real ants performing trophallaxis is subject to natural fluctuations however.

We therefore extend our model through drawing σ randomly from a beta distribution for every food exchange between ants. The beta distribution

$$P(\sigma) := \frac{\sigma^{\alpha-1}(1-\sigma)^{\beta-1}}{B(\alpha, \beta)} \quad (9.9)$$

is characterized through two shape parameters α and β , where

$$B(\alpha, \beta) := \int_0^1 x^{\alpha-1}(1-x)^{\beta-1} dx \quad (9.10)$$

is the beta function. For $\alpha, \beta > 1$, it distributes σ unimodal in the interval $[0, 1]$ with mean

$$\langle \sigma \rangle = \frac{\alpha}{\alpha + \beta} \quad (9.11)$$

and standard deviation

$$\langle \Delta \sigma^2 \rangle = \frac{1}{\alpha + \beta} \sqrt{\frac{\alpha \beta}{\alpha + \beta + 1}} , \quad (9.12)$$

and serves as a suitable random distribution for the food exchange ratio.

Separate and random refractory periods

As mentioned already in Section 4.1.3, real ants do not necessarily take the same time for exchanging food with nestmates as for bringing new food into the nest (even if they just receive new food from foraging ants that bring it into the nest). On top of that, all food exchanges may vary in duration.

To cope with this, we can first separate the two refractory periods T_{ants} and T_{source} , and second, also randomize them. We again use a uniform distribution, similar to the random carrying capacities, but this time draw new random refractory periods for every food exchange or intake at the source. The distributions can be characterized as

$$P(T_{\text{ants}}) := u([\bar{T}_{\text{ants}} - \delta_{T_{\text{ants}}}, \bar{T}_{\text{ants}} + \delta_{T_{\text{ants}}}] , \quad (9.13)$$

where $\delta_{T_{\text{ants}}} < \bar{T}_{\text{ants}}$ parameterizes the range of possible values, with \bar{T}_{ants} as the mean; and

$$P(T_{\text{source}}) := u([\bar{T}_{\text{source}} - \delta_{T_{\text{source}}}, \bar{T}_{\text{source}} + \delta_{T_{\text{source}}}] , \quad (9.14)$$

where $\delta_{T_{\text{source}}} < \bar{T}_{\text{source}}$ parameterizes the range of possible values, with \bar{T}_{source} as the mean.

9.3.2 Comparison of heterogeneous and standard simulations

Despite all the new heterogeneities, the extended simulation model qualitatively shows the same behavior as the standard model. Figure 9.12 gives an exemplary view of the food concentration average and variance evolution. In the appendix (Fig. D.8), we also show the spatial food spreading.

Apart from marginally larger fluctuations of the food concentration variance and the mean squared food distance, no qualitative difference to Figs. D.4 and D.6 can be observed. We therefore conclude that our simple simulation model suffices to describe slightly more complex, and especially more heterogeneous systems. This gives reasons to believe that it can successfully serve as a starting point to model real ant colonies.

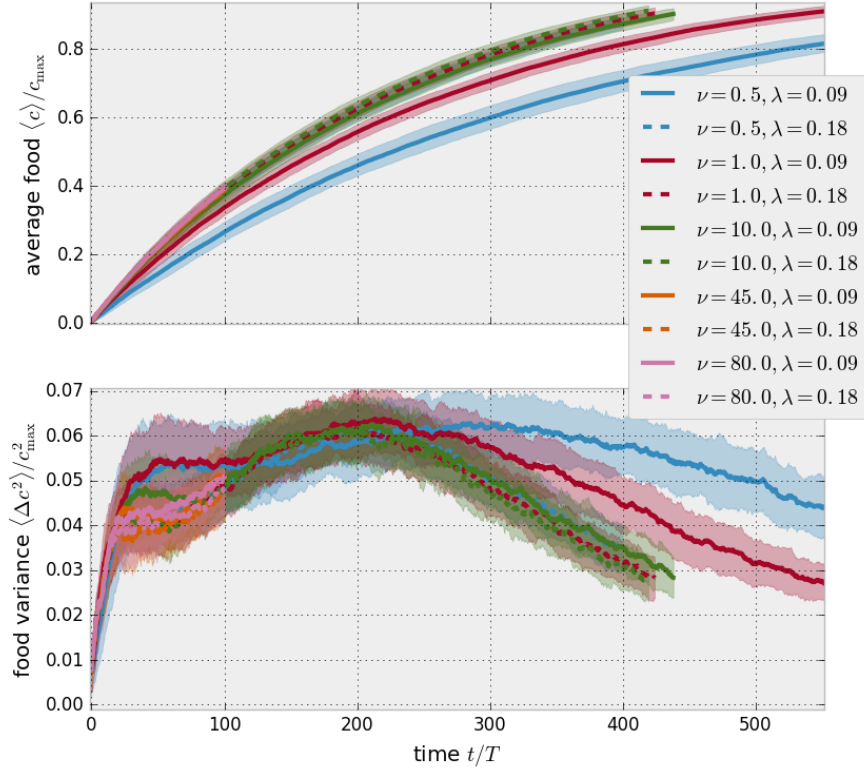


Figure 9.12: Mean $\langle c(t) \rangle$ and variance $\langle \Delta c(t)^2 \rangle$ of the food concentration (in units of the average carrying capacity \bar{c}_{\max}) as a function of time (measured in units of the average ant refractory period \bar{T}_{ants}) for various ant velocity parameters ν and interaction range parameter λ values. The food exchange ratio is beta distributed with mean $\langle \sigma \rangle \approx 0.14$ and standard deviation $\langle \Delta \sigma^2 \rangle \approx 0.1$. The source refractory period is uniformly distributed with $\bar{T}_{\text{source}} = 2\bar{T}_{\text{ants}}$, $\delta_{T_{\text{source}}} = 1.4$, and $\delta_{T_{\text{source}}} = 0.7$. The carrying capacities are initialized using a uniform distribution with $\bar{c}_{\max} = f_{\max}/N$ and $\delta_{c_{\max}} = 0.2$.

Part IV

Epilogue

10 Summary and Discussion

In this chapter, we summarize the main findings of our four approaches to understand the self-organized food distribution in ant colonies: the novel simulation model and its results (Section 10.1), the microscopic mean-field model (Section 10.2), the diffusion equation approach (Section 10.3), and the master equation description (Section 10.4). The findings' implications are discussed in the respective sections.

10.1 Simulation model

As the literature review in Section 3.4 has shown, a fundamental simulation model of trophallaxis, the mouth-to-mouth distribution of food in ant colonies, was missing so far. We presented a simple agent-based model to fill this gap (Chapter 4). For the first time, we developed a biophysical trophallaxis model that captures all the essential features (cf. Sections 1.3 and 3.3).

The agents (ants) in our model have finite carrying capacities and can move in a finite nest. Their interaction is confined to a finite zone (the spatial fidelity zone) which, depending on the parameter selection, can extend to the whole nest. The agents pick an interaction partner at random to whom they donate a fixed percentage of their crop content, limited by the recipient's crop capacity. Agents that can reach the entrance of the nest are picked at random to fill their crop to capacity with food from the source which represents returning foragers bringing food to the nest. Our model describes the trophallactic food distribution process in the simplest possible terms, assuming stochastic effects over central control, intentional individual behavior or strategy wherever possible.

We confirmed that the trophallaxis dynamics produced from our model qualitatively agrees with previous experimental and theoretical work (Sections 5.3 and 8.1). The colony saturates with food exponentially, so that the global food intake rate is the characteristic time scale of the food distribution via trophallaxis (Sections 5.3.2 and 6.3.4). In Sections 5.3, 6.1.1 and 6.3, and especially in Chapter 9, we showed how the speed of this global food intake depends on the individual ant behavior in our model.

In particular, as intuitively expected, we found that the colony saturates faster when the ants are either moving faster, exchanging food faster, or exchange food

with other ants in larger interaction regions (Sections 5.3, 6.3 and 9.1).

An upper limit of food dissemination speed is given by the flow of food into the nest which only depends on the number of ants and the average duration of food intakes at the nest entrance (Sections 5.3.1, 6.3.4, 9.1.1 and 9.2.1). This maximum dissemination speed is reached in the well-mixed limit, where the probability of any two ants to engage in trophallaxis is always the same. Our simulations showed that this well-mixed colony can either be described explicitly through a fast ant motion or implicitly through large interaction areas (Section 9.1.1). This builds an insightful connection to the experimental finding of Sendova-Franks *et al.* that an increased spatial mixing can cause an increased speed of food distribution in real ant colonies after experiencing a period of starvation [66] (cf. Section 3.4.3). Furthermore, we gave examples of how our model provides empirical scaling laws to describe the transition towards the well-mixed limit (Sections 9.1.2 and 9.1.3).

Possibly less intuitively expected, we found that the global food intake of the colony only depends on the individual food amounts transferred if the ants move slowly and interact locally (Sections 6.3.4 and 9.2). If the ants are moving faster or interact in larger spatial fidelity zones, the exchanged crop content percentages play a progressively smaller role in determining the characteristic time scale, due to an increased mixing of individuals. This represents an important relationship between individual behavior (i.e. motion and interaction) and the global food distribution dynamics.

Finally, we presented both simplifications (Section 4.3) and extensions (Section 9.3) of the basic simulation model that qualitatively show the same global dynamics (Sections 6.1.1 and 9.3.2). Since the numerical results found in 1D and without explicit motion can satisfactorily be predicted by analytic models (Part II), this robustness of the global dynamics upon employing a more detailed simulation model (e.g. by adding heterogeneity) gives our analytic models also predictive power over real ant colonies or related trophallaxis systems (cf. Section 3.2).

10.2 Mean-field model

In order to understand the food distribution behavior for a well-mixed colony (i.e. quickly moving ants or large interaction ranges), we derived an analytic mean-field model of trophallaxis (Chapter 5). Similarly to our simulation model, it is the first description of the physical mechanisms behind self-organized food distribution in ant colonies that includes all the essential features, at least in the well-mixed limit (cf. Section 3.3).

The mean-field analytic predictions for the global food dynamics qualitatively agree with previous experimental and theoretical work [10, 19]). Moreover, they

provide a so far missing microscopic explanation for the experimentally observed and macroscopically predicted exponential food saturation (cf. Section 3.4.1).

We also showed that our mean-field model is quantitatively consistent with our simulation results in the appropriate regime (Section 5.3). With Eq. (5.12), we derived the characteristic time scale for the food intake of the colony in the well-mixed limit.

It is important to note here that this well-mixed limit described by the mean-field model is not solely academic. As pointed out before, there is experimental evidence that real ant colonies can become well-mixed at least to some extent, for example depending on the colony hunger level [66].

Another important link between our mean-field model and past and future research is its binary limit that describes ants as simply either full or empty (Section 5.2). It connects our work to epidemic models and information spreading research (Sections 3.4.3 and 3.4.4).

10.3 Diffusion model

The majority of this thesis' analytic work was dedicated to a diffusion model, intended to complement the mean-field model (Chapter 6). It describes the food distribution process of an ant colony that is not well-mixed, i.e. ants only interact within a given region (their spatial fidelity zone, or interaction range) around their preferred fixed position (Section 4.3). Our approach to derive a macroscopic food diffusion equation from a microscopic balance equation describing trophallaxis dynamics in ants is novel. A formally similar approach has been used in the context of self-organizing robot swarms [59] (cf. Section 3.2).

We found a diffusion equation with a diffusion constant that depends non-linearly on the local food density (and therefore depends on space and time) (Section 6.1.3). This equation led to a remarkably universal prediction of the characteristic time scale of the colony's food intake in the diffusive (not well-mixed) limit (Eq. (6.25), Section 6.2.1). According to this prediction, the global food intake rate increases as the percentage of food exchanged or the spatial fidelity zones become larger. This acceleration of food intake is also reflected in the time scales of the spatial food spreading in the nest and the distribution of food among individual ants. Our simulation results were consistent with the analytically predicted time scales in a surprisingly large parameter range (spatial fidelity zones covering up to around 40 percent of the system and food exchanges of up to around 10 percent of the individual carrying capacity) (Section 6.3).

More generally, we showed that, due to the ants' finite crop size, this time scale is an upper limit of how fast a colony with spatial fidelity zones can absorb food

(Section 6.2.2). This leads us to conclude that in the case of spatial fidelity zones, a drastically different individual behavior would be needed to significantly accelerate food uptake, e.g. by having dedicated foragers that enter the nest and freely deliver food to all locations, instead of staying close to the entrance and relying on diffusion for food dissemination.

Once more, we thus discovered connections between the individual ant behavior and the collective food dynamics of the colony that were unknown so far.

10.4 Master equation model

Both our mean-field and our diffusion model cannot describe the food distribution for ant colonies with spatial fidelity zones of intermediate size. If the ranges over which ants can reach each other are too small for a mean-field approximation and too large for a diffusion approximation, both models fail (cf. Section 6.3.4). To cover this analytically challenging intermediate range, we proposed an integro-differential equation for the time evolution of the spatial food density (Chapter 7).

Similarly to the approach in [61], it led to a master equation probabilistically describing the food distribution through trophallaxis. The main result of this model is a successful numerical prediction of the time resolved, simulated food distribution dynamics, even for spatial fidelity zones beyond the scope of the mean-field and diffusive limit cases (Section 7.3). The downside of this master equation model is its analytic complexity that only allows numerical solutions. In return, it provides predictions in the interesting range between the mean-field and the diffusive limit that we could not achieve otherwise.

11 Outlook

This thesis lays the theoretical foundations for a quantitative description of trophallaxis in eusocial insects in terms of simple quantities of individual behavior. But what is there to build upon this groundwork?

In this chapter, we point out some ideas about further research directions, including experimental (Section 11.1), computational (Section 11.2), and analytical work (Section 11.3).

11.1 Experiments

All of the free parameters that we consider (number of ants, system size, extent of spatial fidelity zones, ant velocity, proportion of food exchanged, and interaction duration time) are measurable experimentally. The most important next step in order to further our understanding of the self-organization in ant colonies is therefore a direct comparison of high resolution experiments as in [10] with our simulation model and its analytic predictions. Our reductionist simulation model is designed to only contain the essential features of trophallaxis, purely based on non-biased random behavior. It can therefore serve as a null model for statistical hypothesis testing of experimental data. This will hopefully allow to disentangle to what level the observed collective food dynamics emerge from random individual ant behavior or from intentional, strategic behavior.

We found that the amount of food ants exchange during a trophallactic interaction can influence the global distribution of food in space and time. This influence disappears with an increased spatial mixing of ants in the nest. It would therefore be interesting to ascertain the parameter regime of our models in which real ant colonies operate. Is their spatial mixing high enough to overcome the dependency on the food exchange ratios? In general, further measurements of the distribution of exchanged food amounts and food exchange durations would allow for more precise theoretical descriptions.

As observed in [66], ant colonies also adjust their behavior to changes of external conditions, like food availability. Determining how different adaptive responses correspond to different regimes of our models could lead to new insights. Particularly important in that context seems to be the extent of the spatial fidelity zones, or

more precisely, the underlying distribution of distances over which ants exchange food. Is food primarily displaced due to single ants carrying it around the nest or due to being passed on from one ant to the next in a bucket brigade manner? This question is tightly connected to the context of active versus passive transport and experimental evidence in the matter could lead to new connections with existing work in theoretical biophysics.

It would also be interesting to further investigate how ants choose their food exchange partners. Do they base their decision on external stimuli like visual impressions or chemical signals from the trophallaxis partner? If so, over what range? Linking this information to the interaction radius of the simulation agents in our model could once more yield new insights.

Finally, our work showed the importance of the rate at which food enters the nest as an upper bound for the food dissemination speed. We thus propose to also shift the focus of experimental work towards how food enters the nest. Care needs to be exercised in the design of trophallaxis experiments, to ensure a proper control and understanding of the flow of food into the nest.

11.2 Simulation

Similarly to the proposed experimental work, future computational work can build non-random extensions of our simulation model and compare them to the random null model. We saw that adding heterogeneity to our model did not change its qualitative behavior, but adding new hypotheses of food exchange rules (e.g. based on a local information exchange) or biased motion patterns (e.g. to produce more realistic spatial structures like clustering around brood or queens) might.

For example, one could test whether food spreads faster than in our random model, if it is preferably transferred from ants with more food to ants with less food. Once enough experimental data for the distribution of exchanged food amounts has been gathered, especially the dependence on the donating and receiving ants' crop content, the simulation model can be extended to include a randomized food exchange ratio based on the empirical distributions, similarly to the approach we used in Section 9.3.1.

Experiments have observed a spatial aggregation of food inside the nest ([67, 19]). This effect was not reproduced by our simulations. Further modeling work should therefore be performed to address the spatial organization of food inside the nest as it is distributed within the colony. That also includes finding appropriate modeling of the way food enters the nest. As proposed in Section 11.1 for experimental work, we also need computational studies of how differences in the flow of food into the nest effect the food distribution dynamics.

More generally, changing the simulations' boundary conditions to include not only a different food source, but also food sinks would allow to investigate tasks other than the simple saturation of the colony with food. For example, introducing special agents that can consume food (on a time scale comparable to the food distribution), one could model an ant colony with brood. Linking this to the chain of demand simulation work ([27], also cf. Section 3.4.2) could discover novel effects. For instance, if the rates at which food is introduced into the system and taken out again match, steady state flows of food from the source(s) to the sink(s) are to be expected.

An important quantity of interest when studying the food distribution in ant colonies that has not been extensively explored in this thesis, is the distribution of food among individual ants. It becomes particularly interesting when the total amount of food available to the colony is less than enough to fill up the capacity of every ant. The question then is, how uniformly the colony manages to distribute the food among its members. Future work could focus on this inter-individual food distribution and, for example, study how its shape at a given time (e.g. the time when the colony is half full) depends on the model parameters (like ant velocities, amounts of food exchanged, and the extent of interaction ranges).

Another direction that has not been touched at all in this work is the application of network analysis on the trophallaxis simulation data (cf. Section 3.4.3). As this approach led to significant findings when applied to experimental data, valuable insights are to be expected when it is applied to data from our simulation model. After all, analyzing simulations instead of real ant experiments adds flexibility and makes the procedures to gather sufficient amounts of data faster.

The last investigation we propose to follow our work is a computational analysis of the effect of the colony size. Experiments have shown that the colony size of real social insect colonies can influence the food flow and interaction patterns [71, 85]. Again, simulations can ascertain this much easier, assuming the relevant degrees of freedom have been captured.

11.3 Theory

A missing piece in our analytic work is the proper integration of the ants' explicit velocity into the global food intake rate predictions. We successfully predicted the characteristic time scales for variable spatial fidelity zones, implicitly modeling different underlying motion patterns. That also allows us to effectively predict the food dissemination speed for different ant velocities, but a direct prediction would be preferable.

The global food intake time scale predicted by our diffusion model was derived

11 Outlook

under several simplifying assumptions. A significant assumption was to use a 1D instead of a 2D description. Although our 1D prediction also held in 2D to a good degree, a full derivation in 2D could be more accurate. This should especially hold for the calculation of the mean squared interaction distance (cf. Appendix B).

Another useful analytic achievement would be the prediction of the distribution among ants, and its time evolution. At least in some limits, like the well-mixed mean-field case or only nearest neighbor interactions, this should be accomplishable.

12 Concluding Remarks

The main goal of this thesis was to understand the collective properties of the food distribution in ant colonies with the simplest possible computational and analytical models. To this end, we constructed a series of biophysically motivated simulation models and analytical descriptions of trophallaxis that include all its essential features. Our models are the first complete theoretical description of the physical mechanisms behind the self-organized food distribution in ant colonies. Despite our reductionist approach, the models exhibit a number of interesting properties that reproduce some of the behaviors seen in real ant colonies.

We are confident that our models can serve as benchmarks for the behavior of real ant colonies or more biologically detailed models. As statistical null models, they can be used to assess to what extent an observed behavior is due to non-random strategies or due to the collective properties of a stochastic system.

At the beginning, we asked how individual behavior influences the macroscopic, global food distribution dynamics of the colony; and whether the collective colony behavior is predictable from its microscopic properties. The main results we obtained by the study of our novel models contribute to answering these questions. We found and analytically predicted the characteristic time scales of trophallaxis for both well-mixed colonies and colonies with small spatial fidelity zones. We even successfully covered the range between these two limits with semi-analytic predictions.

These newly discovered relationships between individual behavior and global food distribution dynamics provide microscopic explanations of experimental observations and phenomenological theories that were unknown so far.

Appendix

A Active Brownian Motion

The simulation model presented in Section 4.1 describes the ants as active Brownian particles moving in two dimensions. In this chapter, we present and discretize the equations of motion for these 2D active Brownian particles, obtaining Eqs. (4.1) and (4.2).

All particles move at the same constant speed $v_i(t) = v$. Only their direction of motion, represented by a unit orientation vector $\hat{e}_i(t)$, changes with time. It follows rotationally diffusive behavior. Thus, the continuous equations of motion read

$$\frac{d\vec{x}_i(t)}{dt} = v\hat{e}_i(t) \tag{A.1}$$

$$\frac{d\hat{e}_i(t)}{dt} = \vec{\tau}_i(t) \times \hat{e}_i(t) , \tag{A.2}$$

where $\vec{x}_i(t)$ is the position of particle i at time t and

$$\vec{\tau}_i(t) = \hat{e}_i(t) \times \vec{\xi}(t) \tag{A.3}$$

is a torque acting on it, generated from a Gaussian distributed white-noise random force $\vec{\xi}(t)$ within the simulation box plane $[0, L]^2 \subset \mathbb{R}^2$. This noise vector is characterized through its mean

$$\langle \vec{\xi}(t) \rangle = \vec{0} \tag{A.4}$$

and its delta correlated covariance

$$\langle \vec{\xi}(t)\vec{\xi}(t') \rangle = 2D_r\delta(t - t') \tag{A.5}$$

in time, where D_r is the rotational diffusivity and $\delta(t - t')$ the Dirac delta function.

Figure A.1 illustrates how this random force $\vec{\xi}(t)$ and the corresponding torque $\vec{\tau}_i(t)$ act on the particle's orientation $\hat{e}_i(t)$. Note that although $\vec{x}_i(t)$, $\hat{e}_i(t)$ and $\vec{\xi}(t)$ are vectors in \mathbb{R}^3 , they are effectively two dimensional, laying inside the simulation box plane, with zero components orthogonal to this plane. The torque $\vec{\tau}_i(t)$ instead is effectively one dimensional, being always orthogonal to the simulation box plane.

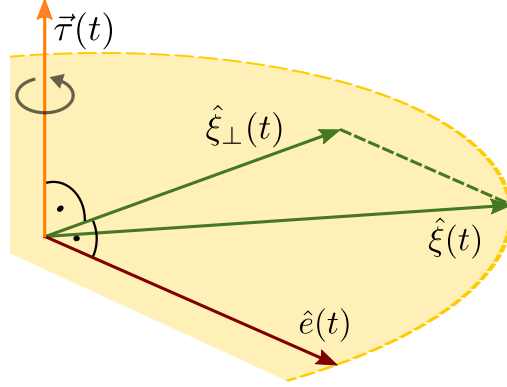


Figure A.1: 3D sketch of an exemplary arrangement of an orientation vector $\hat{e}(t)$, a torque $\vec{\tau}(t)$, the unit vector $\hat{\xi}(t) = \vec{\xi}(t)/|\vec{\xi}|$ of a random force $\vec{\xi}(t)$, and its projection $\hat{\xi}_{\perp}(t)$ orthogonal to $\hat{e}(t)$ (cp. Eqs. (A.3) and (A.7)). The shaded area indicates a section of the unit disk around the particle's position, in the simulation box plane.

In order to solve the equations of motion (Eqs. (A.1) and (A.2)) numerically, they have to be discretized in timesteps of Δt , yielding

$$\vec{x}_i(t + \Delta t) = \vec{x}_i(t) + \Delta t v \hat{e}_i(t) \quad (\text{A.6})$$

$$\hat{e}_i(t + \Delta t) = \hat{e}_i(t) + \Delta t \left(\left(\hat{e}_i(t) \times \vec{\xi}(t) \right) \times \hat{e}_i(t) \right) \quad (\text{A.7})$$

after inserting Eq. (A.3). We can simplify the double cross product

$$\left(\hat{e}_i(t) \times \vec{\xi}(t) \right) \times \hat{e}_i(t) = |\vec{\xi}| \underbrace{\left(\hat{e}_i(t) \times \hat{\xi}(t) \right) \times \hat{e}_i(t)}_{=:\hat{\xi}_{\perp_i}(t)} \quad (\text{A.8})$$

through replacing the random force $\vec{\xi}(t) = |\vec{\xi}| \hat{\xi}(t)$ with its absolute value $|\vec{\xi}|$ and its unit vector $\hat{\xi}(t)$. The double cross product $\hat{\xi}_{\perp_i}(t)$ left over is nothing but $\vec{\xi}(t)$ projected orthogonal to $\hat{e}_i(t)$ then. The normalized random force $\hat{\xi}(t)$ however is a uniformly distributed random vector on the unit circle, and its absolute value $|\vec{\xi}|$ represents the strength of the random force.

Now only $|\vec{\xi}|$ is left to be discretized in time. Therefore, discretizing the Dirac delta with

$$\delta(t - t') \approx \begin{cases} \frac{1}{\Delta t} & \text{if } |t - t'| \leq \Delta t \\ 0 & \text{otherwise} \end{cases}, \quad (\text{A.9})$$

so that $\int_{-\infty}^{\infty} \delta(t - t') dt' = 1$ still holds, Eq. (A.5) becomes

$$\langle \vec{\xi}(t) \vec{\xi}(t') \rangle = \begin{cases} \frac{2D_r}{\Delta t} & \text{if } |t - t'| \leq \Delta t \\ 0 & \text{otherwise} \end{cases} \quad (\text{A.10})$$

$$\Rightarrow \langle \vec{\xi}(t) \vec{\xi}(t + \Delta t) \rangle = \frac{2D_r}{\Delta t} \quad (\text{A.11})$$

$$\Leftrightarrow |\vec{\xi}|^2 \underbrace{\langle \hat{\xi}(t) \hat{\xi}(t + \Delta t) \rangle}_{=1} = \frac{2D_r}{\Delta t} \quad (\text{A.12})$$

$$\Rightarrow |\vec{\xi}| = \sqrt{\frac{2D_r}{\Delta t}}. \quad (\text{A.13})$$

Using this together with Eq. (A.8), Eq. (A.7) becomes

$$\hat{e}_i(t + \Delta t) = \hat{e}_i(t) + \sqrt{2D_r \Delta t} \hat{\xi}_{\perp i}(t). \quad (\text{A.14})$$

Unfortunately, Eq. (A.14) does not ensure $|\hat{e}_i(t)| = 1$ for all times (see Fig. A.2). To compensate this, a Lagrangian correction term $\Delta t \alpha(t) \hat{e}(t)$ can be introduced, so that the set of discretized equations of motion finally reads:

$$\vec{x}_i(t + \Delta t) = \vec{x}_i(t) + \Delta t v \hat{e}_i(t) \quad (\text{A.15})$$

$$\hat{e}_i(t + \Delta t) = \hat{e}_i(t) + \sqrt{2D_r \Delta t} \hat{\xi}_{\perp i}(t) + \Delta t \alpha(t) \hat{e}_i(t), \quad (\text{A.16})$$

where $\alpha(t)$ is the Lagrangian multiplier, which has to be chosen such that $|\hat{e}_i(t)| = 1$ is satisfied at every iteration step.

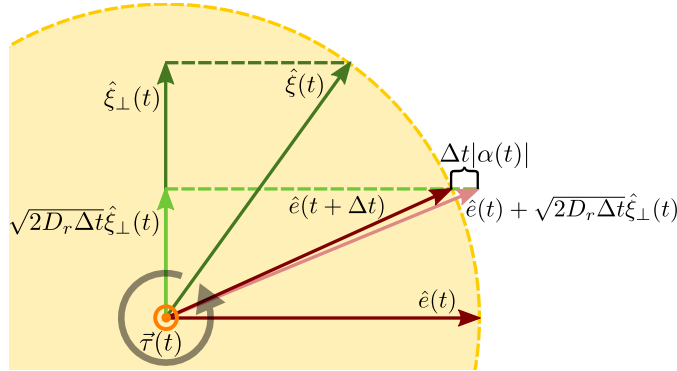


Figure A.2: Top down view of Fig. A.1. In addition to Fig. A.1, the terms of Eq. (A.16) are illustrated, showing how one time iteration step of length Δt rotates the particle's orientation from $\hat{e}(t)$ to $\hat{e}(t + \Delta t)$. Again, the shaded area indicates a section of the unit disk around the particle's position, in the simulation box plane.

B Mean Squared Interaction Distance

Equation (6.11) in Section 6.1 showed the need for a length scale describing the diffusion of food due to an exchange between ants with a given interaction radius R . In this chapter, we derive the ensemble averaged squared distance between pairs of interacting ants $\overline{r^2}(R)$ in a 1D finite system of length L . This quantity can serve as the squared length scale Δx^2 for Eq. (6.11).

The derivation can be split into two parts, depending on the size of R :

1. The ant's interaction range overlaps only with one system boundary or does not overlap with the boundaries: $R \in [0, L/2)$.
2. The ant's interaction range either overlaps with one or with both system boundaries: $R \in [L/2, L]$.

1. Case $R \in [0, L/2)$:

The average squared distance $\overline{r_f^2}$ of a point r in the interaction range $[-R, R] \subset \mathbb{R}$ (e.g. one ant) to the center of the interval $r = 0$ (e.g. the other ant) free of boundaries can be calculated as the mean of the uniform distribution $u(I)$ of points in the interval $I = [-R, R]$. The uniform distribution is

$$u(I) := \frac{1}{\int_I dr} = \frac{1}{|I|} = \frac{1}{2R}, \quad (\text{B.1})$$

where $|I| = 2R$ denotes the length of the interval.

Using this, the boundary free average squared distance can be calculated as

$$\overline{r_f^2} = \int_I r^2 u(I) dr = \frac{\int_{-R}^R r^2 dr}{\int_{-R}^R dr} = \frac{1}{2R} \int_{-R}^R r^2 dr = \frac{R^2}{3}. \quad (\text{B.2})$$

The same approach can be used to calculate the average squared distance $\overline{r_b^2}(s)$ of a point r in the truncated interaction range $[-s, R] \subset [-R, R]$ (e.g. one ant) to the original center of the interval at 0 (e.g. the other ant), when the interaction range overlaps with one system boundary. Without loss of generality, this boundary is put to the left in the calculation. Due to symmetry, the result remains the same

B Mean Squared Interaction Distance

for an overlap with the right system boundary.

$$\overline{r_b^2}(s) = \frac{1}{s+R} \int_{-s}^R r^2 dr = \frac{R^3 + s^3}{3(s+R)}. \quad (\text{B.3})$$

In order to calculate the system wide average over these average squared distances, the system interval $[0, L]$ needs to be split up into the following three regions:

1. The average squared distances resulting from interaction ranges overlapping with the left system boundary: $\frac{1}{R} \int_0^R \overline{r_b^2}(x) dx$.
2. The average squared distances resulting from non overlapping interaction ranges in the central region: $\frac{1}{L-2R} \int_R^{L-R} \overline{r_f^2} dx$.
3. The average squared distances resulting from interaction ranges overlapping with the right system boundary: $\frac{1}{R} \int_{L-R}^L \overline{r_b^2}(L-x) dx$.

These three regions can then be averaged using their lengths as weights to obtain the system wide average:

$$\overline{r^2} = \frac{1}{L} \left(\int_0^R \overline{r_b^2}(x) dx + \int_R^{L-R} \overline{r_f^2} dx + \int_{L-R}^L \overline{r_b^2}(L-x) dx \right). \quad (\text{B.4})$$

Due to the above mentioned symmetry of the system boundaries, the third integral can be rewritten to match the first one, so that

$$\overline{r^2} = \frac{1}{L} \left(2 \int_0^R \overline{r_b^2}(x) dx + \int_R^{L-R} \overline{r_f^2} dx \right). \quad (\text{B.5})$$

And with Eq. (B.2) and Eq. (B.3), the final expression for $R \in [0, L/2)$ becomes

$$\overline{r^2} = \frac{1}{L} \left(2 \int_0^R \frac{R^3 + x^3}{3(x+R)} dx + \int_R^{L-R} \frac{R^2}{3} dx \right) \quad (\text{B.6})$$

$$= \frac{1}{L} \left(\frac{5}{9} R^3 + \frac{1}{3} (L-2R) R^2 \right) \quad (\text{B.7})$$

$$= -\frac{1}{9} \frac{R^3}{L} + \frac{1}{3} R^2 \quad (\text{B.8})$$

2. Case $R \in [L/2, L]$:

This case needs an extra calculation for the average squared distance $\overline{r_{db}^2}(s)$ of a point r in the double truncated interaction range $[-s, L-s] \subset [-R, R]$ (e.g. one ant) to the original intervals center at 0 (e.g. the other ant), when the interaction range overlaps with both system boundaries.

The calculation of $\overline{r_{db}^2}(s)$, similar to those of $\overline{r_f^2}$ and $\overline{r_b^2}(s)$, is

$$\overline{r_{db}^2}(s) = \frac{1}{L} \int_{-s}^{L-s} r^2 dr = \frac{(L-s)^3 + s^3}{3L}. \quad (\text{B.9})$$

In order to also calculate the system wide average over these average squared distances for the case of $R \in [L/2, L]$, the system interval $[0, L]$ again needs to be split up into three regions (left, middle and right). The only differences are that the average squared distances calculated in the middle region now result from interaction ranges overlapping with both system boundaries, and a change in the region boundaries. To clarify, the three parts are:

1. The average squared distances resulting from interaction ranges overlapping with the left system boundary: $\frac{1}{L-R} \int_0^{L-R} \overline{r_b^2}(x) dx$.
2. The average squared distances resulting from interaction ranges overlapping with both system boundaries: $\frac{1}{2R-L} \int_{L-R}^R \overline{r_{db}^2}(x) dx$.
3. The average squared distances resulting from interaction ranges overlapping with the right system boundary: $\frac{1}{L-R} \int_R^L \overline{r_b^2}(L-x) dx$.

Again, using a weighted average, the analogous system wide average is

$$\overline{r^2} = \frac{1}{L} \left(\int_0^{L-R} \overline{r_b^2}(x) dx + \int_{L-R}^R \overline{r_{db}^2}(x) dx + \int_R^L \overline{r_b^2}(L-x) dx \right) \quad (\text{B.10})$$

$$= \frac{1}{L} \left(2 \int_0^{L-R} \overline{r_b^2}(x) dx + \int_{L-R}^R \overline{r_{db}^2}(x) dx \right). \quad (\text{B.11})$$

With Eq. (B.3) and Eq. (B.9), the final expression for $R \in [L/2, L]$ becomes

$$\overline{r^2} = \frac{1}{L} \left(2 \int_0^{L-R} \frac{R^2 + x^2}{2(x+R)} dx + \int_{L-R}^R \frac{(L-x)^2 + x^2}{2L} dx \right) \quad (\text{B.12})$$

$$= \frac{1}{18} L^2 - \frac{1}{3} LR + R^2 - \frac{5}{9} \frac{R^3}{L}. \quad (\text{B.13})$$

B Mean Squared Interaction Distance

Combined result

Putting both cases (Eqs. (B.8) and (B.13)) together in nondimensional terms ($\lambda = R/L$) finally gives the expression

$$\frac{\overline{r^2}}{L^2} = \begin{cases} -\frac{1}{9}\lambda^3 + \frac{1}{3}\lambda^2 & \text{if } \lambda \in [0, \frac{1}{2}) \\ -\frac{5}{9}\lambda^3 + \lambda^2 - \frac{1}{3}\lambda + \frac{1}{18} & \text{if } \lambda \in [\frac{1}{2}, 1]. \end{cases} \quad (\text{B.14})$$

C Solving the Diffusion Approximation

C.1 Food source as a boundary condition

The system solved in Section 6.2.1 is equivalent to

$$\frac{\partial \rho(x, t)}{\partial t} = D \frac{\partial^2 \rho(x, t)}{\partial^2 x}, \quad (\text{C.1})$$

with boundary and initial conditions

$$\rho(0, t) = \rho_{\max}, \quad \rho(2L, t) = \rho_{\max}, \quad (\text{C.2})$$

and

$$\rho(x, 0) = 0 \text{ for } x \in (0, 2L). \quad (\text{C.3})$$

Transforming $\rho(x, t) \rightarrow \rho'(x, t) = \rho_{\max} - \rho(x, t)$ turns the boundary and initial conditions into

$$\rho'(0, t) = 0, \quad \rho'(2L, t) = 0 \quad \text{and} \quad \rho'(x, 0) = \rho_{\max}. \quad (\text{C.4})$$

Solving the diffusion equation (Eq. (C.1)) with these boundary conditions is known as the problem of cooling of a rod and can be done through separation of variables. The solution reads

$$\rho'(x, t) = \frac{4\rho_{\max}}{\pi} \sum_{n=1}^{\infty} \frac{\sin\left(\frac{(2n-1)\pi x}{L}\right)}{2n-1} e^{-\left(\frac{(2n-1)\pi}{2L}\right)^2 Dt}. \quad (\text{C.5})$$

Transforming back to $\rho(x, t) = \rho_{\max} - \rho'(x, t)$ gives the solution used in Section 6.2.1:

$$\frac{\rho(x, t)}{\rho_{\max}} = 1 - \frac{4}{\pi} \sum_{n=1}^{\infty} \frac{\sin\left(\frac{(2n-1)\pi x}{L}\right)}{2n-1} e^{-\left(\frac{(2n-1)\pi}{2L}\right)^2 Dt}. \quad (\text{C.6})$$

Furthermore, a simple integration gives the average food density

$$\langle \rho(t) \rangle = \rho_{\max} \left(1 - \frac{8}{\pi^2} \sum_{n=1}^{\infty} \frac{1}{(2n-1)^2} e^{-(2n-1)^2 \frac{\pi^2}{4L^2} Dt} \right) \quad (\text{C.7})$$

and the mean squared food distance:

$$\overline{\text{MSD}}(t) = 1 + \frac{96}{\pi^4} \sum_{n=1}^{\infty} \frac{2 + \pi(-1)^n(2n-1)}{(2n-1)^4} e^{-(2n-1)^2 \frac{\pi^2}{4L^2} Dt}. \quad (\text{C.8})$$

C.2 Food source as a source term

In this section, we outline the derivation of Eq. (6.36) in Section 6.2.2. In this derivation, we assume that the system is infinite (as opposed to semi-infinite, as in Section 6.2.2), and that the source is at $x = 0$. The solution for the semi-infinite case can easily be obtained from the full system by considering only $x > 0$ and adjusting the normalization.

Dropping the tildes, the solution of the proposed diffusion equation (Eq. (6.31)) for $x \in (-\infty, \infty)$ reads:

$$\rho(x, t) = \frac{1}{\sqrt{4\pi}} \int_{-\infty}^{\infty} dx' \int_0^t dt' \frac{e^{-\frac{(x-x')^2}{4(t-t')} - t'}}{\sqrt{t-t'}} \delta(x') \quad (\text{C.9})$$

$$= \frac{1}{\sqrt{4\pi}} \int_0^t \frac{e^{-\frac{x^2}{4(t-t')} - t'}}{\sqrt{t-t'}} dt' \quad (\text{C.10})$$

$$= \frac{1}{\sqrt{4\pi}} \left[-\frac{\sqrt{\pi}}{2i} e^{-t} \left(e^{-ix} \left(1 + \operatorname{erf} \left(-\frac{x}{2\sqrt{t-t'}} + i\sqrt{t-t'} \right) \right) \right. \right. \\ \left. \left. + e^{ix} \left(-1 + \operatorname{erf} \left(\frac{x}{2\sqrt{t-t'}} + i\sqrt{t-t'} \right) \right) \right) \right]_0^t. \quad (\text{C.11})$$

The upper boundary ($t' = t$) of the time integral evaluates to zero for $x \geq 0$. For $x < 0$, it evaluates to

$$\sqrt{4\pi} e^{-t} \sin(x). \quad (\text{C.12})$$

The lower boundary ($t' = 0$) evaluates to

$$-\frac{\sqrt{\pi}}{2i}e^{-t} \left(e^{-ix} \left(1 + \operatorname{erf} \left(-\frac{x}{2\sqrt{t}} + i\sqrt{t} \right) \right) + e^{ix} \left(-1 + \operatorname{erf} \left(\frac{x}{2\sqrt{t}} + i\sqrt{t} \right) \right) \right). \quad (\text{C.13})$$

Through making use of $\operatorname{erfc}(z) := 1 - \operatorname{erf}(z)$ and denoting the complex conjugate of z with \bar{z} , the evaluated solution (Eq. (C.11)) can be concisely written as:

$$\rho(x, t) = e^{-t} \left[\sin(x)\Theta(-x) + \frac{1}{4i} (\bar{u} \operatorname{erfc}(\bar{w}) - u \operatorname{erfc}(w)) \right], \quad (\text{C.14})$$

where

$$u := e^{ix} \quad (\text{C.15})$$

and

$$w := \frac{x}{2\sqrt{t}} + i\sqrt{t}. \quad (\text{C.16})$$

Since

$$\bar{u} \operatorname{erfc}(\bar{w}) - u \operatorname{erfc}(w) = -2i \operatorname{Im}(u \operatorname{erfc}(w)), \quad (\text{C.17})$$

the solution finally becomes

$$\rho(x, t) = e^{-t} \left[\sin(x)\Theta(-x) - \frac{1}{2} \operatorname{Im} \left(e^{ix} \operatorname{erfc} \left(\frac{x}{2\sqrt{t}} + i\sqrt{t} \right) \right) \right]. \quad (\text{C.18})$$

The solution in the main text (Eq. (6.36)) can be obtained from this solution by dropping the $e^{-t} \sin(x)\Theta(-x)$ term, since $x \geq 0$. Note that Eq. (C.18), integrated over $x \in (-\infty, \infty)$ at $t \rightarrow \infty$ gives

$$\lim_{t \rightarrow \infty} \int_{-\infty}^{\infty} \rho(x, t) = 2f_{\max} \quad (\text{C.19})$$

in dimensional terms, which explains the factor 2 in Eqs. (6.28) and (6.30).

D Figures

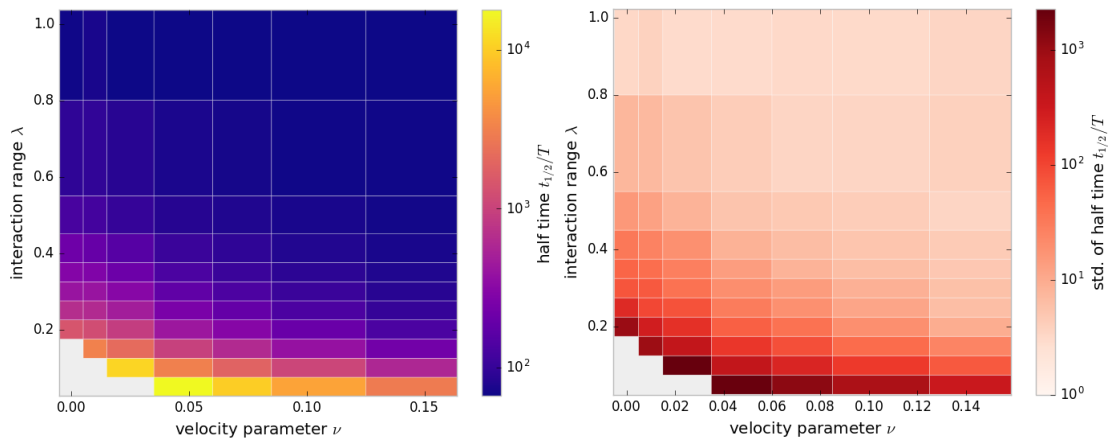
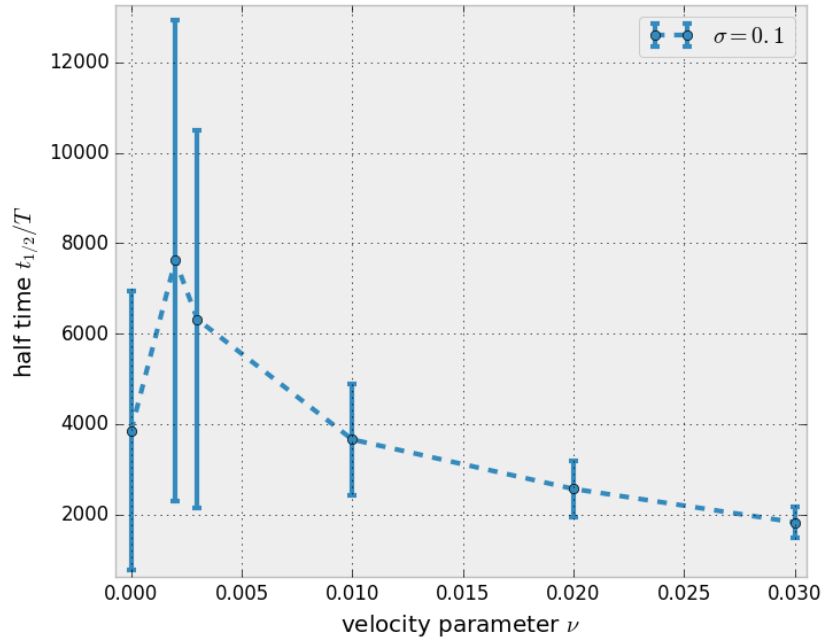


Figure D.1: Mean (left panel) and standard deviation (right panel) of the half-time $t_{1/2}/T$ (time until the colony is half full) as a function of the ant velocity parameter ν and the interaction range parameter λ , in units of the refractory period T . The food exchange ratio is fixed to $\sigma = 0.05$. Mean and standard deviation are calculated as an ensemble average over 100 independent simulation runs. The gray areas in the bottom left corner of both panels represent parameter values, for which no data was simulated. This is a closeup of Fig. 9.1.

D Figures

(a)



(b)

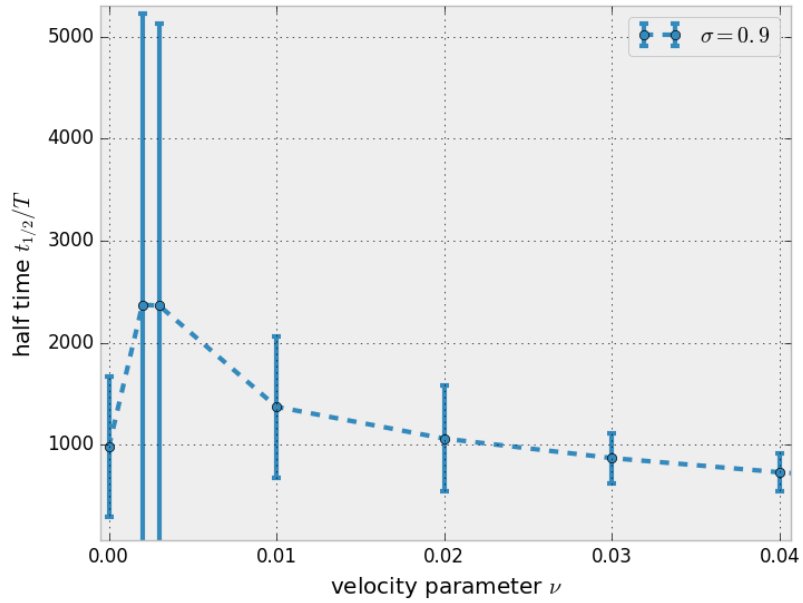


Figure D.2: Half-time $t_{1/2}$ in units of the refractory period T as a function of the ant velocity parameter ν with a food exchange ratio of (a) $\sigma = 0.1$ and (b) $\sigma = 0.9$. The interaction range parameter is fixed to $\lambda = 0.13$ and the number of ants is the usual $N = 100$.

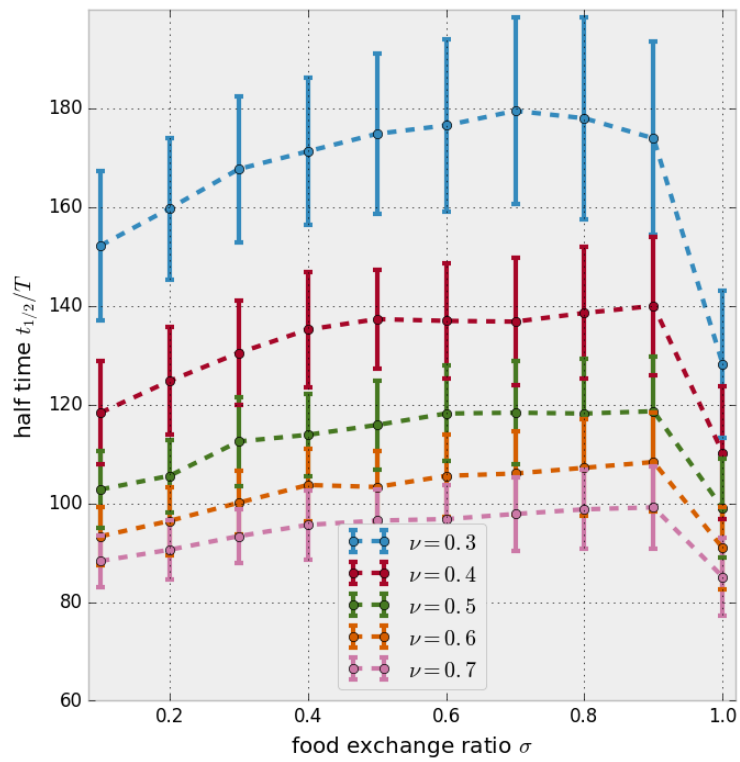


Figure D.3: Half-time $t_{1/2}$ in units of the refractory period T as a function of the food exchange ratio σ , varying the ant velocity parameter ν . The interaction range parameter is fixed to $\lambda = 0.13$. This shows the same data as Fig. 9.11.

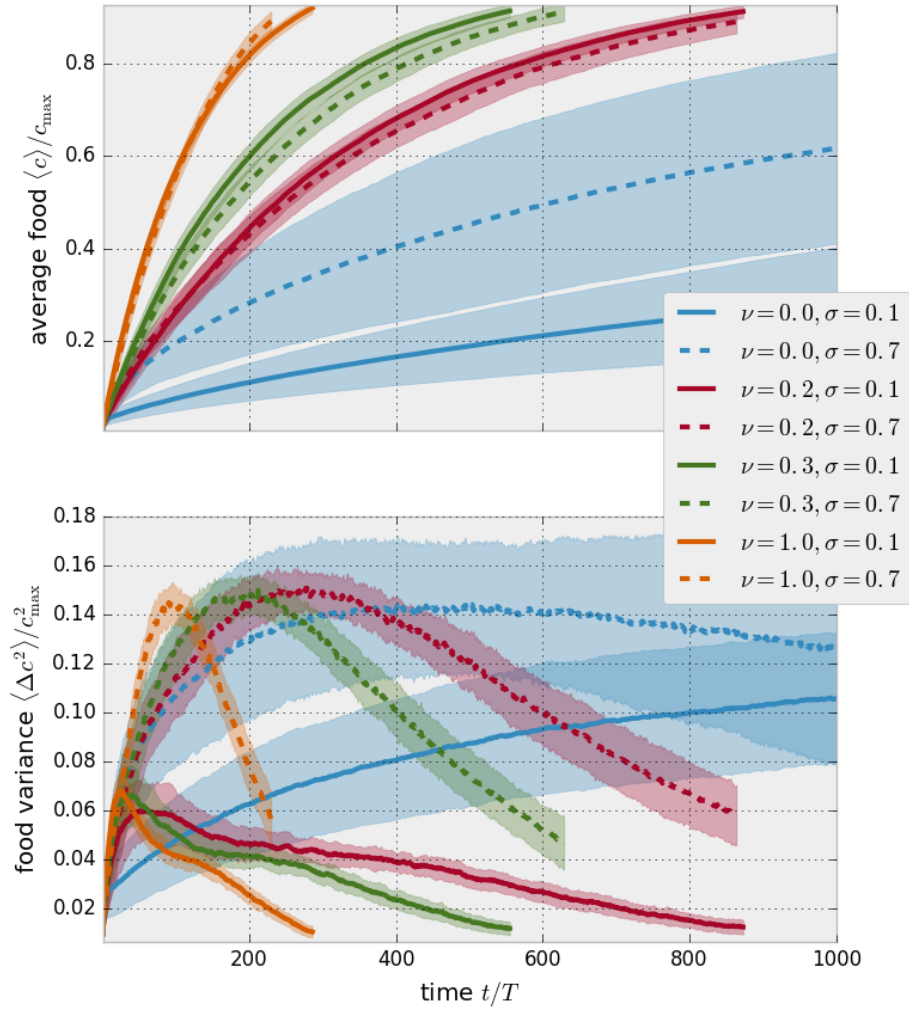


Figure D.4: Mean $\langle c(t) \rangle$ and variance $\langle \Delta c(t)^2 \rangle$ of the food concentration (in units of the carrying capacity c_{\max}) as a function of time (measured in units of the refractory period T) for various ant velocity parameters ν and food exchange ratios σ . The interaction range parameter is fixed to $\lambda = 0.13$.

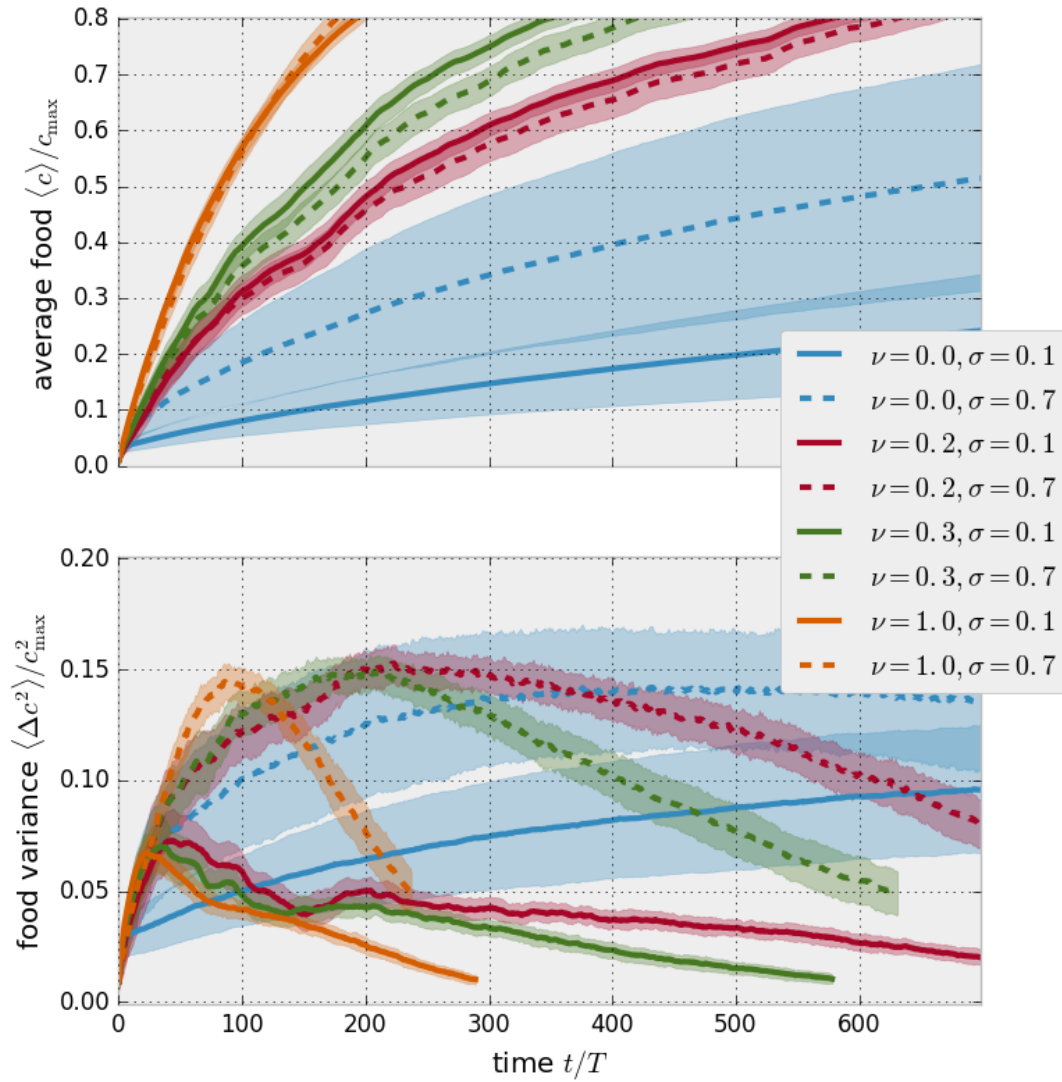


Figure D.5: Mean $\langle c(t) \rangle$ and variance $\langle \Delta c(t)^2 \rangle$ of the food concentration (in units of the carrying capacity c_{\max}) as a function of time (measured in units of the refractory period T) for various ant velocity parameters ν and food exchange ratios σ . The interaction range parameter is fixed to $\lambda = 0.13$. The data ensemble shown in this figure was obtained from 100 simulation runs with new food exchange random seeds for every run, but fixed motion random seed (cf. Section 9.2.3 for an explanation). See Fig. D.4 for comparison.

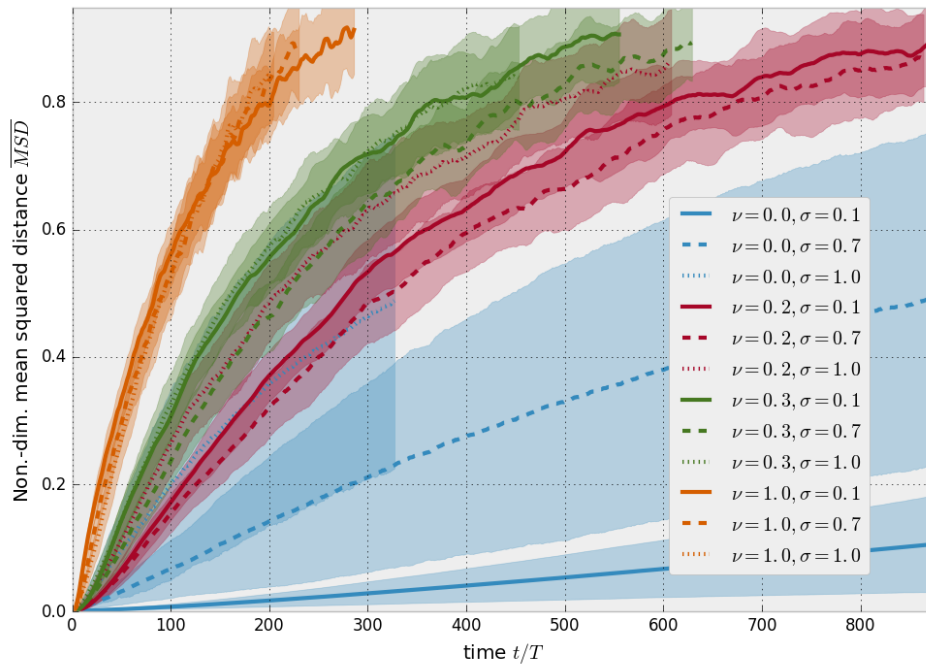


Figure D.6: Dimensionless mean squared food distance $\overline{MSD}(t)$ as a function of time (measured in units of the refractory period T) for various ant velocity parameters ν and food exchange ratios σ . The interaction range parameter is fixed to $\lambda = 0.13$.

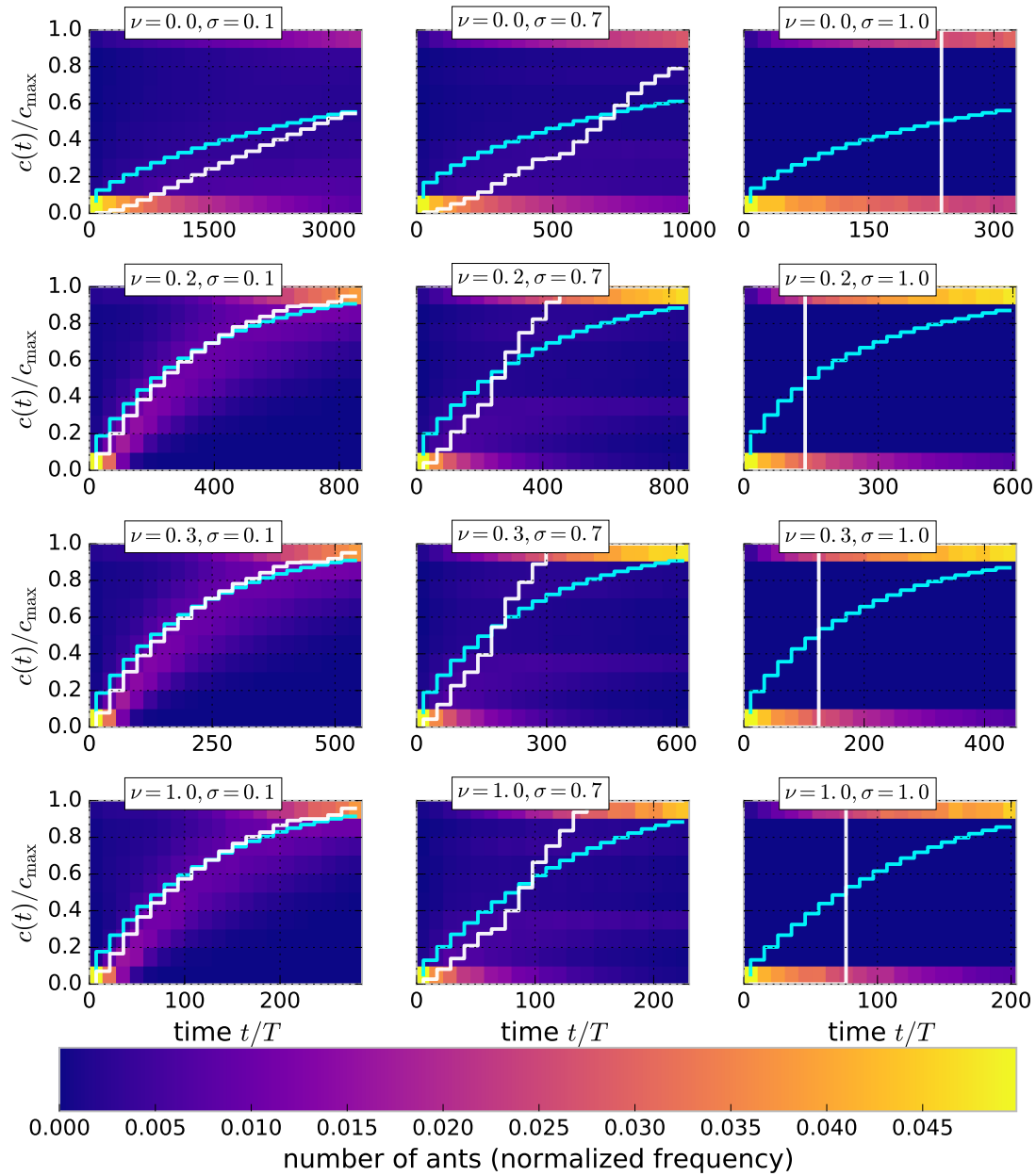


Figure D.7: Distribution of food $c(t)$ among ants (measured in units of the carrying capacity c_{\max}) as a function of time (measured in units of the refractory period T) varying the ant velocity parameter ν and the food exchange ratio σ . The interaction range parameter is fixed to $\lambda = 0.13$. The colored background shows a two-dimensional food concentration histogram, binned both in food and time dimension. The step-function lines show the mean (cyan) and median (white) of this histogram along the food axis for every time bin.

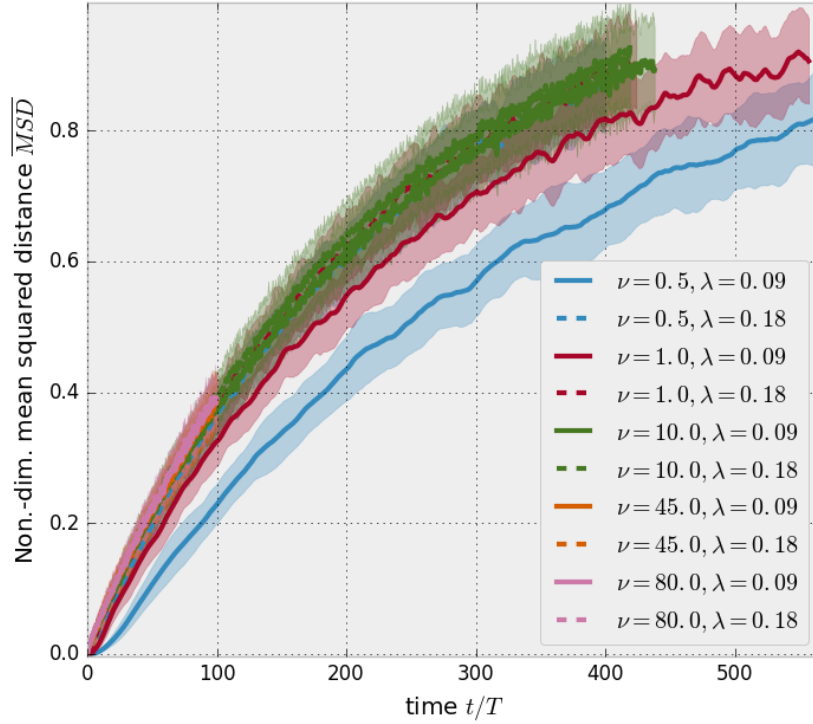


Figure D.8: Dimensionless mean squared food distance $\overline{MSD}(t)$ as a function of time (measured in units of the average ant refractory period \bar{T}_{ants}) for various ant velocity parameters ν and interaction range parameter λ values. The food exchange ratio is beta distributed with mean $\langle \sigma \rangle \approx 0.14$ and standard deviation $\langle \Delta \sigma^2 \rangle \approx 0.1$. The source refractory period is uniformly distributed with $\bar{T}_{\text{source}} = 2\bar{T}_{\text{ants}}$, $\delta_{T_{\text{source}}} = 1.4$, and $\delta_{T_{\text{source}}} = 0.7$. The carrying capacities are initialized using a uniform distribution with $\bar{c}_{\text{max}} = f_{\text{max}}/N$ and $\delta_{c_{\text{max}}} = 0.2$.

List of Figures

1.1	Examples of ant nests. Sources: https://commons.wikimedia.org/wiki/File:WeaverAntsNest.jpg (left), https://commons.wikimedia.org/wiki/File:Formica_rufa_nest_2.jpg (right)	9
1.2	Trophallaxis of Argentine ant <i>Linepithema humile</i> . Source: https://commons.wikimedia.org/wiki/File:LinepithemaHumile_1413.jpg	10
1.3	Social cooperation of weaver ants <i>Oecophylla</i> . Source: https://commons.wikimedia.org/wiki/File:Oecophylla.jpg (top), https://commons.wikimedia.org/wiki/File:SSL11903p.jpg (bottom) . .	11
2.1	Trophallaxis of carpenter ants <i>Camponotus</i> . Source: https://commons.wikimedia.org/wiki/File:Black-ants.jpg	17
2.2	Schematic drawing of the food exchange between two ants (trophallaxis)	18
2.3	Meat ants <i>Iridomyrmex purpureus</i> feeding. Source: https://commons.wikimedia.org/wiki/File:Meat_eater_ants_feeding_on_honey02.jpg	19
4.1	Illustration of the simulation model	32
5.1	Food concentration average and variance with system wide interaction range	53
5.2	Food concentration average and variance with intermediate interaction ranges	55
6.1	2D spatial food distribution	59
6.2	1D distribution of food in space and among ants	60
6.3	Analytic predictions of the spatial food distribution in the diffusive limit	66
6.4	Average food concentration in the diffusive limit	72
6.5	Mean squared food distance in the diffusive limit	73
6.6	Food concentration variance in the diffusive limit	74
6.7	Half-time in the diffusive limit	76
7.1	Total food comparison of simulation and master equation prediction .	85

List of Figures

7.2	Mean squared food distance comparison of simulation and master equation prediction	85
8.1	Distribution of food among individual ant (discrete space simulation)	91
9.1	Half-time as a function of ant velocity parameter and interaction range parameter (heat map)	94
9.2	Half-time as a function of ant velocity parameter and interaction range parameter (line scans)	95
9.3	Scaling relation of half-time and ant velocity	97
9.4	Scaling relation of half-time and interaction range parameter	99
9.5	Half-time in the slow motion limit with 500 ants	101
9.6	Half-time as a function of ant velocity parameter and food exchange ratio (heat map)	102
9.7	Food exchange ratio dependency of half-time without and with slow ant motion	103
9.8	Food exchange ratio dependency of half-time with medium fast and fast ant motion	104
9.9	Relative half-time change with food exchange ratio as a function of ant velocity parameter	105
9.10	Scaling relation of half-time and interaction range parameter	107
9.11	Half-time as a function of ant velocity parameter and food exchange ratio (heat map)	108
9.12	Food concentration average and variance of the heterogeneous case study	112
A.1	Rotational diffusion sketch	128
A.2	Discretized rotational diffusion sketch	129
D.1	Half-time as a function of ant velocity parameter and interaction range parameter (heat map closeup)	139
D.2	Half-time in the slow motion limit with 100 ants	140
D.3	Inverted food exchange ratio dependency of half-time	141
D.4	Food concentration average and variance for various ant velocity parameters and food exchange ratios	142
D.5	Food concentration average and variance for various ant velocity parameters and food exchange ratios (alternated simulation)	143
D.6	Mean squared food distance for various ant velocity parameters and food exchange ratios	144
D.7	Distribution of food among ants as a function of time for various ant velocity parameters and food exchange ratios	145

D.8 Mean squared food distance of the heterogeneous case study 146

Bibliography

- [1] E. O. Wilson, *Sociobiology : The new synthesis* (Belknap Press of Harvard University Press, Cambridge, Mass. , 1975).
- [2] B. Hölldobler and E. O. Wilson, *The ants* (Belknap Press of Harvard University Press, Cambridge, Mass. , 1990).
- [3] B. Hölldobler and E. O. Wilson, *The Superorganism: The Beauty, Elegance, and Strangeness of Insect Societies* (W. W. Norton & Company , 2008).
- [4] D. Grimaldi and M. S. Engel, *Evolution of the Insects* (Cambridge University Press , 2005).
- [5] B. Hölldobler, *Formica sanguinea (Formicidae) - Soliciting Food* (Encyclopaedia Cinematographica, related material of film no. E2013, IWF, Göttingen , 1973).
- [6] D. M. Gordon, *Ant encounters: interaction networks and colony behavior* (Princeton University Press , 2010).
- [7] E. O. Wilson, *The insect society* (Belknap Press of Harvard University Press, Cambridge, Mass. , 1971).
- [8] M. Dorigo, M. Birattari, and T. Stutzle, *Ant colony optimization*, IEEE Computational Intelligence Magazine **1**, 28 (2006).
- [9] M. Erthal, C. Peres Silva, and R. Ian Samuels, *Digestive enzymes of leaf-cutting ants, Acromyrmex subterraneus (Hymenoptera: Formicidae: Attini): distribution in the gut of adult workers and partial characterization*, Journal of Insect Physiology **50**, 881 (2004).
- [10] E. Greenwald, E. Segre, and O. Feinerman, *Ant trophallactic networks: simultaneous measurement of interaction patterns and food dissemination*, Scientific Reports **5**, 12496 (2015).
- [11] A. B. Sendova-Franks and N. R. Franks, *Spatial relationships within nests of the ant Leptothorax unifasciatus (Latr.) and their implications for the division of labour*, Animal Behaviour **50**, 121 (1995).

Bibliography

- [12] T. O. Richardson, L. Giuggioli, N. R. Franks, and A. B. Sendova-Franks, *Measuring site fidelity and spatial segregation within animal societies*, *Methods in Ecology and Evolution* (2017).
- [13] W. M. Wheeler, *A Study of Some Ant Larvæ, with a Consideration of the Origin and Meaning of the Social Habit among Insects*, *Proceedings of the American Philosophical Society* **57**, 293 (1918).
- [14] C. Sleigh, *Brave new worlds: trophallaxis and the origin of society in the early twentieth century.*, *Journal of History of the Behavioral Sciences* **38**, 133 (2002).
- [15] W. M. Wheeler, *Ants: their structure, development and behavior* (Columbia University Press, New York , 1910).
- [16] Mailleux, Deneubourg, and Detrain, *How do ants assess food volume?*, *Animal behaviour* **59**, 1061 (2000).
- [17] J. H. Hunt, *Trophallaxis and the evolution of eusocial Hymenoptera*, in M. D. Breed, C. D. Michener, and H. E. Evans (eds.), *Biology of social insects: Proc. IX Congress, IUSSI* (Westview Press, Boulder, Colo. , 1982).
- [18] W. T. Wcislo and V. H. Gonzalez, *Social and ecological contexts of trophallaxis in facultatively social sweat bees, *Megalopta genalis* and *M. ecuadoria* (Hymenoptera, Halictidae)*, *Insectes Sociaux* **53**, 220 (2006).
- [19] A. Buffin, D. Denis, G. Van Simaey, S. Goldman, and J.-L. Deneubourg, *Feeding and Stocking Up: Radio-Labelled Food Reveals Exchange Patterns in Ants*, *PLOS ONE* **4**, e5919 (2009).
- [20] G. S. Wilkinson, *Food Sharing in Vampire Bats*, *Scientific American* **262**, 76 (1990).
- [21] J. L. Gundermann, A. Horel, and C. Roland, *Mother-offspring food transfer in *Coelotes terrestris* (Araneae, Agelenidae)*, *Journal of Arachnology* **19**, 97 (1991).
- [22] B. A. Henderson, *Role of the Chick's Begging Behavior in the Regulation of Parental Feeding Behavior of *Larus glaucescens**, *The Condor* **77**, 488 (1975).
- [23] W. Goetsch, *Beiträge zur Bekämpfung von Ameisen-Staaten*, *Zeitschrift für Angewandte Entomologie* **27**, 273 (2009).
- [24] G. P. Markin, *Food distribution within laboratory colonies of the argentine ant, *Tridomyrmex humilis* (Mayr)*, *Insectes Sociaux* **17**, 127 (1970).

- [25] H. L. Nixon and C. R. Ribbands, *Food Transmission within the Honeybee Community*, Proceedings of the Royal Society B: Biological Sciences **140**, 43 (1952).
- [26] R. C. Pendelton and A. W. Grundmann, *Use of P32 in Tracing Some Insect-Plant Relationships of the Thistle, *Cirsium Undulatum**, Ecology **35**, 187 (1954).
- [27] D. L. Cassill, A. Stuy, and R. G. Buck, *Emergent Properties of Food Distribution Among Fire Ant Larvae*, Journal of Theoretical Biology **195**, 371 (1998).
- [28] A. Dussutour and S. J. Simpson, *Carbohydrate regulation in relation to colony growth in ants.*, Journal of Experimental Biology **211**, 2224 (2008).
- [29] A. A. Sorensen and S. B. Vinson, *Quantitative food distribution studies within laboratory colonies of the imported fire ant, *Solenopsis invicta* Buren*, Insectes Sociaux **0487**, 129 (1981).
- [30] D. I. Wallis, *Food-sharing behaviour of the ants *Formica sanguinea* and *Formica fusca**, Behaviour **17**, 17 (1961).
- [31] D. Cassill and W. Tschinkel, *Regulation of diet in the fire ant, *Solenopsis invicta**, Journal of Insect Behavior **12**, 307 (1999).
- [32] A. Dahbi, A. Hefetz, X. Cerdá, and A. Lenoir, *Trophallaxis Mediates Uniformity of Colony Odor in *Cataglyphis iberica* Ants (Hymenoptera, Formicidae)*, Journal of Insect Behavior **12**, 559 (1999).
- [33] C. Hamilton, B. T. Lejeune, and R. B. Rosengaus, *Trophallaxis and prophylaxis: social immunity in the carpenter ant *Camponotus pennsylvanicus**, Biology Letters **7**, 89 (2011).
- [34] A. Lenoir, *An informational analysis of antennal communication during trophallaxis in the ant *Myrmica Rubra* L.*, Behavioural Processes **7**, 27 (1982).
- [35] A. C. LeBoeuf, P. Waridel, C. S. Brent, A. N. Gonçalves, L. Menin, D. Ortiz, O. Riba-Grognuz, A. Koto, Z. G. Soares, E. Privman, E. A. Miska, R. Benton, and L. Keller, *Oral transfer of chemical cues, growth proteins and hormones in social insects*, eLife **5**, e20375 (2016).
- [36] W. M. Farina, *Food-exchange by foragers in the hive - a means of communication among honey bees?*, Behavioral Ecology and Sociobiology **38**, 59 (1996).
- [37] G. Nicolis and I. Prigogine, *Self-organization in nonequilibrium systems* (Wiley, New York , 1977).

Bibliography

- [38] H. Haken, *Synergetics* (Springer, Berlin, Heidelberg , 2004).
- [39] N. Razin, J.-P. Eckmann, and O. Feinerman, *Desert ants achieve reliable recruitment across noisy interactions*, *Journal of The Royal Society Interface* **10**, 20130079 (2013).
- [40] D. Charbonneau, B. Blonder, and A. Dornhaus, *Social Insects: A Model System for Network Dynamics*, in P. Holme and J. Saramäki (eds.), *Temporal Networks, Understanding Complex Systems*, 217–244 (Springer, Berlin, Heidelberg , 2013).
- [41] D. M. Gordon, *The Ecology of Collective Behavior*, *PLOS Biology* **12**, e1001805 (2014).
- [42] C. Hemelrijk, *Understanding social behaviour with the help of complexity science (invited article)*, *Ethology* **671**, 655 (2002).
- [43] E. Bonabeau, G. Theraulaz, J.-L. Deneubourg, S. Aron, and S. Camazine, *Self-organization in social insects*, *Trends in Ecology & Evolution* **12**, 188 (1997).
- [44] C. Detrain and J. L. Deneubourg, *Self-organized structures in a superorganism: do ants "behave" like molecules?*, *Physics of Life Reviews* **3**, 162 (2006).
- [45] D. M. Gordon, *The organization of work in social insect colonies*, *Complexity* **8**, 43 (2002).
- [46] S. N. Beshers and J. H. Fewell, *Models of division of labor in social insects.*, *Annual Review of Entomology* **46**, 413 (2001).
- [47] B. R. Johnson, *A self-organizing model for task allocation via frequent task quitting and random walks in the honeybee.*, *The American Naturalist* **174**, 537 (2009).
- [48] E. Ferrante, A. E. Turgut, E. Duéñez-Guzmán, M. Dorigo, and T. Wenseleers, *Evolution of Self-Organized Task Specialization in Robot Swarms*, *PLOS Computational Biology* **11**, e1004273 (2015).
- [49] M. C. Lanan, A. Dornhaus, E. I. Jones, A. Waser, and J. L. Bronstein, *The trail less traveled: individual decision-making and its effect on group behavior.*, *PLOS ONE* **7**, e47976 (2012).
- [50] R. Jeanson, J.-L. Deneubourg, A. Grimal, and G. Theraulaz, *Modulation of individual behavior and collective decision-making during aggregation site selection by the ant *Messor barbarus**, *Behavioral Ecology and Sociobiology* **55**, 388 (2004).

- [51] A. B. Kao, N. Miller, C. Torney, A. Hartnett, and I. D. Couzin, *Collective Learning and Optimal Consensus Decisions in Social Animal Groups.*, PLOS Computational Biology **10**, e1003762 (2014).
- [52] T. Bochynek and S. K. a. Robson, *Physical and Biological Determinants of Collective Behavioural Dynamics in Complex Systems: Pulling Chain Formation in the Nest-Weaving Ant *Oecophylla smaragdina*.*, PLOS ONE **9**, e95112 (2014).
- [53] H. V. D. Parunak, *"Go to the ant": Engineering principles from natural multi-agent systems*, Annals of Operations Research **75**, 69 (1997).
- [54] G. Recio, E. Martin, C. Estebanez, and Y. Saez, *AntBot: Ant Colonies for Video Games*, IEEE Transactions on Computational Intelligence and AI in Games **4**, 295 (2012).
- [55] E. Bonabeau, M. Dorigo, and G. Theraulaz, *Swarm intelligence: from natural to artificial systems* (Oxford University Press, New York , 1999).
- [56] J. M. Hereford, *Analysis of a new swarm search algorithm based on trophallaxis*, IEEE Congress on Evolutionary Computation 1–8 (2010).
- [57] E. Bonabeau, A. Sobkowski, G. Theraulaz, and J.-l. Deneubourg, *Adaptive Task Allocation Inspired by a Model of Division of Labor in Social Insects*, Biocomputing and Emergent Computation 36–45 (1997).
- [58] V. A. Cicirello and S. F. Smith, *Wasp-like agents for distributed factory coordination*, Autonomous Agents and Multi-Agent Systems **8**, 237 (2004).
- [59] H. Hamann and H. Worn, *A Space- and Time-Continuous Model of Self-Organizing Robot Swarms for Design Support*, in *First International Conference on Self-Adaptive and Self-Organizing Systems (SASO 2007)*, 23–23 (IEEE, Cambridge, Mass. , 2007).
- [60] T. Schmickl and K. Crailsheim, *Trophallaxis within a robotic swarm: bio-inspired communication among robots in a swarm*, Autonomous Robots **25**, 171 (2008).
- [61] T. D. Ngo and H. Schiøler, *Randomized Robot Trophallaxis*, in A. Lazinica (ed.), *Recent Advances in Multi-Robot Systems*, 197–232 (I-Tech Education and Publishing, Vienna, Austria , 2008).
- [62] M. Kubo and C. Melhuish, *Robot trophallaxis: Managing energy autonomy in multiple robots.*, Proceedings of Towards Autonomous Robotic Systems 77–84 (2004).

Bibliography

- [63] H. Duan, Q. Luo, and Y. Yu, *Trophallaxis network control approach to formation flight of multiple unmanned aerial vehicles*, Science China Technological Sciences **56**, 1066 (2013).
- [64] A. Schadschneider, D. Chowdhury, and K. Nishinari, *Stochastic transport in complex systems: from molecules to vehicles* (Elsevier , 2010).
- [65] J. Amudhavel, R. Ilamathi, D. Pradeepa, S. Ganesan, and B. Bhuvaneshwari, *Mathematical Modelling on Nutrient Transmission in a Colony of Leaf-Cutting Ants*, Indian Journal of Science and Technology **9** (2016).
- [66] A. B. Sendova-Franks, R. K. Hayward, B. Wulf, T. Klimek, R. James, R. Planqué, N. F. Britton, and N. R. Franks, *Emergency networking: famine relief in ant colonies*, Animal Behaviour **79**, 473 (2010).
- [67] A. Buffin, S. Goldman, and J. L. Deneubourg, *Collective regulatory stock management and spatiotemporal dynamics of the food flow in ants.*, FASEB journal: official publication of the Federation of American Societies for Experimental Biology **26**, 2725 (2012).
- [68] B. Blonder and A. Dornhaus, *Time-Ordered Networks Reveal Limitations to Information Flow in Ant Colonies*, PLOS ONE **6**, e20298 (2011).
- [69] H. W. Hethcote, *The Mathematics of Infectious Diseases*, SIAM Review **42**, 599 (2000).
- [70] A. Z. M. Shamsuddin, T. Ahsan, I. Rahman, and S. Momen, *Trophallaxis and energy optimization in swarms of robots*, in *19th International Conference on Computer and Information Technology (ICCIT)*, 490–495 (IEEE , 2016).
- [71] D. Naug, *Structure and resilience of the social network in an insect colony as a function of colony size*, Behavioral Ecology and Sociobiology **63**, 1023 (2009).
- [72] N. Pinter-Wollman, E. a. Hobson, J. E. Smith, a. J. Edelman, D. Shizuka, S. de Silva, J. S. Waters, S. D. Prager, T. Sasaki, G. Wittemyer, J. Fewell, and D. B. McDonald, *The dynamics of animal social networks: analytical, conceptual, and theoretical advances*, Behavioral Ecology **25**, 242 (2014).
- [73] J. H. Fewell, *Social Insect Networks*, Science **301**, 1867 (2003).
- [74] N. Pinter-Wollman, A. Bala, A. Merrell, J. Queirolo, M. C. Stumpe, S. Holmes, and D. M. Gordon, *Harvester ants use interactions to regulate forager activation and availability*, Animal Behaviour **86**, 197 (2013).
- [75] J. S. Waters and J. H. Fewell, *Information processing in social insect networks.*, PLOS ONE **7**, e40337 (2012).

- [76] P. Holme and J. Saramäki, *Temporal networks*, Physics Reports **519**, 97 (2012).
- [77] B. Blonder, T. W. Wey, A. Dornhaus, R. James, and A. Sih, *Temporal dynamics and network analysis*, Methods in Ecology and Evolution **3**, 958 (2012).
- [78] N. Pinter-Wollman, *Persistent variation in spatial behavior affects the structure and function of interaction networks*, Current Zoology **61**, 98 (2015).
- [79] M. González and H. Herrmann, *Scaling of the propagation of epidemics in a system of mobile agents*, Physica A: Statistical Mechanics and its Applications **340**, 741 (2004).
- [80] F. Peruani and G. J. Sibona, *Dynamics and Steady States in Excitable Mobile Agent Systems*, Physical Review Letters **100**, 168103 (2008).
- [81] F. Peruani and C. F. Lee, *Fluctuations and the role of collision duration in reaction-diffusion systems*, EPL **102**, 58001 (2013).
- [82] P. Romanczuk, M. Bär, W. Ebeling, B. Lindner, and L. Schimansky-Geier, *Active Brownian particles*, The European Physical Journal Special Topics **202**, 1 (2012).
- [83] J. M. C. Hutchinson and P. M. Waser, *Use, misuse and extensions of "ideal gas" models of animal encounter*, Biological Reviews **82**, 335 (2007).
- [84] E. Greenwald and O. Feinerman, *Private Communication* (2014).
- [85] D. F. Howard and W. R. Tschinkel, *The effect of colony size and starvation on food flow in the fire ant, Solenopsis invicta (Hymenoptera: Formicidae)*, Behavioral Ecology and Sociobiology **7**, 293 (1980).

Curriculum vitae

personal

name Johannes Gräwer
e-mail johannes.graewer@ds.mpg.de
date of birth January 10, 1988
place of birth Lüneburg, Germany

education

11/2013 - 06/2017 Max Planck Institute for Dynamics and Self-Organization
Göttingen,
PhD student in MPRG Physics of Biological Organization
(supervisor: Eleni Katifori) and Dep. Dynamics of Complex
Fluids (supervisor: Marco G. Mazza)

10/2012 - 10/2013 Max Planck Institute for Dynamics and Self-Organization
Göttingen,
M.Sc. student in MPRG Physics of Biological Organization
(supervisor: Eleni Katifori)

10/2011 - 11/2013 Georg-August-Universität Göttingen,
gaining the M.Sc. degree in Physics (grade: 1.1, study focus:
“Biophysics and Physics of Complex Systems”, thesis title:
“Architecture of dynamically adapting transport networks”,
supervisor: Eleni Katifori)

10/2008 - 09/2011 Georg-August-Universität Göttingen,
gaining the B.Sc. degree in in Physics (grade: 1.7, thesis
title: “Models of bacterial epidemic spread via fomites”,
supervisor: Reiner Kree)

teaching

- 08/2014 - 07/2015 Georg-August-Universität Göttingen / Max Planck Institute for Dynamics and Self-Organization Göttingen, supervising B.Sc. Thesis “Dynamics of Resource Dispersion in Interaction Networks” of Fabian Steuer
- 08/2014 - 09/2014 Göttingen Graduate School for Neurosciences, Biophysics, and Molecular Biosciences (GGNB), teaching “Introduction to Interactive Network Analysis and Visualization with Python”
- 05/2014 - 10/2014 Max Planck Institute for Dynamics and Self-Organization Göttingen, co-supervising internship of Aditya Tandon
- 04/2014 - 08/2014 Georg-August-Universität Göttingen / German Aerospace Center (DLR), assist in teaching “Experimental Fluid Dynamics”

work

- 10/2012 - 11/2013 German Aerospace Center (DLR), student assistant at DLR_School_Lab
- 07/2008 - 08/2008 Georg-August-Universität Göttingen, intern at II. Institute of Physics (supervisor: Arnulf Quadt)